THE UNIVERSITY OF CALGARY

TEMPERATURE EFFECTS IN CONCRETE BOX GIRDER BRIDGES

by

THOMAS N. SVEINSON

A THESIS

SUBMITTED TO THE FACULTY OF GRADUATE STUDIES

IN PARTIAL FULFILLMENT OF THE REQUIREMENTS FOR THE DEGREE OF

DOCTOR OF PHILOSOPHY IN CIVIL ENGINEERING

DEPARTMENT OF CIVIL ENGINEERING

CALGARY, ALBERTA
August, 2004

THE UNIVERSITY OF CALGARY

FACULTY OF GRADUATE STUDIES

The undersigned certify that they have read and recommend to the Faculty of Graduate Studies for acceptance, a thesis entitled "Temperature Effects in Concrete Box Girder Bridges", submitted by Thomas N. Sveinson in partial fulfillment of the requirements for the degree of Doctor of Philosophy in Civil Engineering.

Dr. W.H.Dilger (Supervisor)
Department of Civil Engineering

M. El-Badry

Dr. M Elbadry (Co-supervisor)
Department of Civil Engineering

Dr. M.A. Maes
Department of Civil Engineering

Dr. L. Sudak
Department of Mechanical Engineering

Dr. B. Massicotte (External Examiner)
Ecole Polytechnique de Montreal

Date Aug 27, 2004

ABSTRACT

An investigation into the thermal response of concrete box girder bridges is presented. It has been documented that structural damage can easily occur due to the effects of temperature. This investigation is concerned with the theoretical prediction of the temperature response in the bridge and comparison with the recorded data. Several cross sections along the bridge were modeled using the computer program FETAB, developed by Elbadry (1982). The input data for FETAB are: environmental data, including the maximum and minimum daily air temperature, diurnal solar radiation, the geometry of the cross section as well as the physical and thermal properties of the materials. FETAB computes the nodal temperatures, the nodal self-equilibrating stresses and the axial strain and curvatures about the two major axis of the cross section. Very good agreement between measured and recorded temperatures, as well as curvatures, was achieved. It was found that one of the most important pieces of data required for accurate temperature predictions was the appropriate value of the convection coefficients, which are dependent on the wind speed. It was determined that the wind speed varied significantly around the girder cross section, thus affecting the convection coefficients around the perimeter of the cross section. The predicted curvatures were compared to those calculated through the use of the recorded temperatures and input into the computer program SFrame for Windows in order to analyze the longitudinal behaviour of the bridge.

Two cross sections were then analyzed in the transverse direction using the computer program S-Frame for Windows. One cross section near a pier and the other at mid span between piers. The transverse bending moments in the girder walls were found to produce the relatively high stresses. This investigation revealed that the temperature differential through the thickness of the walls and the top and bottom slab of the box section can lead to significant bending moments/stresses when the frame action of the cross section is considered. These stresses, when added to the stresses due to self weight and truck wheel loading, increased the total bending stress by as much as 50% for a 14m deep cross section of the bridge and 24% for the shallower 4.5m cross section of the bridge.

In addition, this investigation revealed that there is a significant curvature due to temperature across the width of the cross section which, for the deeper 14m cross section, can have a higher value than the curvature resulting from temperature differentials through the depth of the cross section. However, due to the relatively high flexural stiffness of the cross section about the vertical axis, the transverse temperature differentials across the cross section were not critical when the frame behaviour of the bridge in the longitudinal direction was considered. It was found that the bending moments, due to temperature differentials through the depth, resulting from continuity in the bridge superstructure were of the same order of magnitude as those resulting from vehicle traffic, each of which are only a small portion of those resulting from self weight

The results of this thesis indicate the importance of considering the transverse bending moments due to a temperature differential in the walls of a concrete box girder bridge cross section. Currently, the Canadian Highway Bridge Design Code does not have clauses relating to concrete box sections. The *Precast Segmental Box Girder Bridge Manual (1978)* suggests that due to the temperature differential occurring through the depth of the section, the top slab will experience a higher temperature differential than the bottom slab and that this will lead to bending moments due to frame behaviour of the cross section. However, there is no mention of gradient effects through the individual parts of the cross section. Therefore, proposed new clauses for the Canadian Highway Bridge Design Code are included to aid the designer in considering the transverse bending moments which occur due to gradient effects through the individual parts of a concrete box girder section with one air cell.

ACKNOWLEDGEMENTS

I would like to take this opportunity to say thank you to Dr. W.H. Dilger for acting as my supervisor. His patience and guidance have made this journey both educational and enjoyable. I have taken so long in finally getting this thesis to print that he has indeed needed a good sense of humour to put up with me.

I would also like to thank Dr. M.M. Elbadry for acting as my co-supervisor. His guidance has been very much appreciated. In addition, I would like to thank Dr.s Maes and Sudak for reviewing this thesis.

I would like to extend a special thank you to Dr. B. Massicotte for acting as the external examiner for this thesis. The time he took in reviewing this thesis and his helpful comments were very much appreciated.

I gratefully acknowledge and appreciate the financial of the National Sciences and Research Council of Canada without whose support the many research projects involving the Confederation Bridge would not have been possible.

Finally, I would like to acknowledge and thank my wife, Karen, and family. The many hours I have spent working on this thesis have meant many hours away from them.

For Karen

John, Jennifer, Christine and Erik

Agnes, Norman and Carol

TABLE OF CONTENTS

LIST OF TABLES

LIST OF FIGURES

LIST OF SYMBOLS, ABBREVIATIONS AND NOMENCLATURE

a	=	absorptive coefficient
A	=	area
A_{ry}	=	reduced area for shear along y axis
A_{rz}	=	reduced area for shear along z axis
b_l	=	finite element edge length calculated by the computer from the nodal coordinates
[B]	=	matrix of finite element shape functions differentiated with respect to distance
c	=	specific heat
c_l	=	finite element edge length calculated by the computer from the nodal coordinates
[C]	=	capacitance matrix used for calculating transient heat flow
d	=	drop in temperature based on statistical return period
dT	=	difference in temperature across the thickness of a member
{d}	=	nodal displacement matrix
[d]	=	matrix of thermal heat conductivity
E	=	modulus of elasticity
E_c	=	modulus of elasticity of concrete
f_c'	=	28 day compressive strength of concrete
f(z)	=	mathematical function with respect to axis inside the brackets
{F}	=	nodal force matrix
$\{F^e\}$	=	nodal force matrix
h	=	heat convection coefficient
h1	=	cross section dimension
h2	=	cross section dimension
hbt	=	depth of blacktop (asphalt) on bridge deck

hd = depth of cross section

I = amount of solar radiation to reach the surface of the earth

I_y = moment of inertia about specified axis

I_z = moment of inertia about specified axis

J_x = torsional constant about the x axis

k = thermal conductivity

k_x = thermal conductivity along x axis

k_y = thermal conductivity along y axis

K_t = transmittance factor

L = length

M = bending moment

M_x = bending moment about the specified axis

M_y = bending moment about the specified axis

M_z = bending moment about the specified axis

M_t = mass term used in the computation of the Time Constant, Tco

M_{ox} = self equilibrating stress resultant due to curvature about the x axis

M_{oy} = self equilibrating stress resultant due to curvature about the y axis

n = number of exterior surfaces of a cross section, used for the computation of the Time Constant, Tco

n_x, n_y = direction cosines

N = axial force due to axial strain

N_o = self equilibrating stress resultant due to axial strain

N_1, N_2 = finite element shape function describing a unit displacement at the subscribed ordinate

$[N]$ = matrix of shape functions

q = quantity of heat flow

q_s = quantity of heat gain from the sun: solar radiation

q_c = quantity of heat gain/loss due to temperature difference between the air

		and the boundary surface
q_r	=	quantity of heat re-radiation from the boundary surface to the surrounding air
Q	=	quantity of heat
R	=	total solar radiation absorbed by a black body
S	=	empirical term used in the computation of the Time Constant, Tco
[S] =		stiffness matrix
$[S_c]$ =		heat conduction matrix
$[S_c^e]$ =		element heat conduction matrix
t	=	time
te	=	slab thickness used in the computation of the Time Constant, Tco
tk	=	finite element thickness
t_y	=	temperature at depth "y" in a cross section (Priestley temperature model)
t_y'	=	reduction in top surface temperature for deck slab directly over enclosed cells (Priestley temperature model)
T =		temperature
T_{ts}	=	temperature at the top surface of a concrete cross section (Priestley temperature model)
T_{top}	=	temperature at top fibre of a cross section
T_{bot}	=	temperature at bottom fibre of a cross section
TCo	=	time constant
{T}	=	nodal temperature matrix
V	=	statistical standard deviation
x,y,z	=	local axis Cartesian coordinates
X,Y,Z	=	global axis Cartesian coordinates
y_1,y_2	=	cross section dimension from neutral axis to side fibres
z_1,z_2	=	cross section dimension from neutral axis to top and bottom fibre

α_t	=	coefficient of thermal expansion
σ	=	Stress
δ	=	derivative of specified parameter
$\frac{\delta}{\delta t}$	=	derivative of specified parameter with respect to time
Δ	=	change in specified parameter
ψ_x	=	curvature about specified axis
ψ_y	=	curvature about specified axis
ψ_z	=	curvature about specified axis
ϑ	=	rotation
ϵ	=	Axial Strain
ρ	=	Material Density
[ ]	=	square brackets denote a square or rectangular matrix
{ }	=	curled brackets denote a single row or column matrix
$[\ ]^T$ or $\{\ \}^T$	=	the superscript T denotes a transposed matrix
$\int dv$	=	integral over the volume
$\int ds$	=	integral over the surface
——>>	=	double headed arrow indicates a couple about the axis depicted
——>	=	single headed arrow indicates a force or displacement along the axis depicted
ACI	=	American Concrete Institute
ASCE	=	American Society of Civil Engineers
ASTM	=	American Standard Testing and Materials
ATU	=	Alberta Transportation and Utilities
Cn	=	label of precast concrete segment on cantilevered side of pier
CAN	=	Canadian
CEB	=	Comtie Euro-International du Beton

CSA = Canadian Standards Association

E-W = East-West

FETAB = Finite Element Thermal Analysis of Bridges

Hn = label of precast concrete segment on hinged side of pier

Ld. Comb. No. = Load combination number

LRT = Light Rail Transit

Mn = bending moment at section n

NB = New Brunswick

N-S = North-South

NW = Northwest

OHBDC = Ontario Highway Bridge Design Code

PCA = Portland Cement Association

PCI = Precast Concrete Institute

PEI = Prince Edward Island

PTI = Post Tensioning Institute

PWC = Public Works Canada

Sn = cross section labelled n

SE = Southeast

SG = strain gauge

SSD = saturated surface dry

Pre. = predicted

Rec. = recorded

TC = thermocouple

x-trans. = translation in x direction

y-trans. = translation in y direction

z-trans. = translation in z direction

x-rot. = rotation about x axis

y-rot. = rotation about y axis

z-rot.	=	rotation about z axis
'-"	=	feet and inches
^{o}C	=	degrees Celcius
GPa	=	GigaPascal (pressure)
Hrs	=	hours (time)
J	=	Joule (energy)
kg	=	kilogram (mass)
km	=	kilometre (length
km/h	=	kilometres per hour (speed or velocity)
kN	=	kilo Newton (force)
K	=	Kelvin (absolute temperature)
MN	=	Mega Newton (force)
MPa	=	Mega Pascal (pressure)
N	=	Newton (force)
m	=	metre (length)
mm	=	millimetre (length)
s	=	second (time)
W	=	Watts (power)

CHAPTER ONE

INTRODUCTION

1.1 General Remarks

A wise man once commented, that the sole purpose of all education was to serve. It follows that if education has not been spent on serving our fellow creatures in some manner, then the education has been a waste. As a result, it is hoped that the research presented in this thesis will serve in a practical way to my fellow design engineers or researchers.

The effects of temperature on a given structure are often not critical at ultimate load levels. However, at service loads stresses due to temperature differences, across or through a cross section, may be high enough to cause cracking in concrete structures. In some cases the owner may not be concerned about large temperature movements or stresses, in other cases, where long-term durability is required, the owner will be very concerned about service level stresses and crack widths. One such structure is a bridge.

Unfortunately, the temperature response of most bridges is unknown. It is only when a new bridge is constructed, or an existing bridge is repaired, in conjunction with a research project, that thermocouples are installed on a bridge. This allows researchers to monitor the temperatures and resulting curvatures of a bridge structure. It is very fortunate, then, that researchers were given the opportunity to design and implement a comprehensive monitoring program on one of the largest bridge structures in the world; The Confederation Bridge from Prince Edward Island to New Brunswick, Canada.

In 1987, Public Works Canada (PWC), acting for the government of Canada, announced a competition to construct a bridge across the Northumberland Strait connecting the provinces of Prince Edward Island (PEI) and New Brunswick (NB), see Figure 1.1. The new bridge was to be located between Borden, PEI and Bayfield, NB and replace a government-operated ferry. Public Works Canada set out proposal guidelines that required the successful contractor(s) to design, build, finance, maintain, and operate the bridge for 35 years, at which time the ownership would then transfer to the government of Canada (Tadros, 1997).

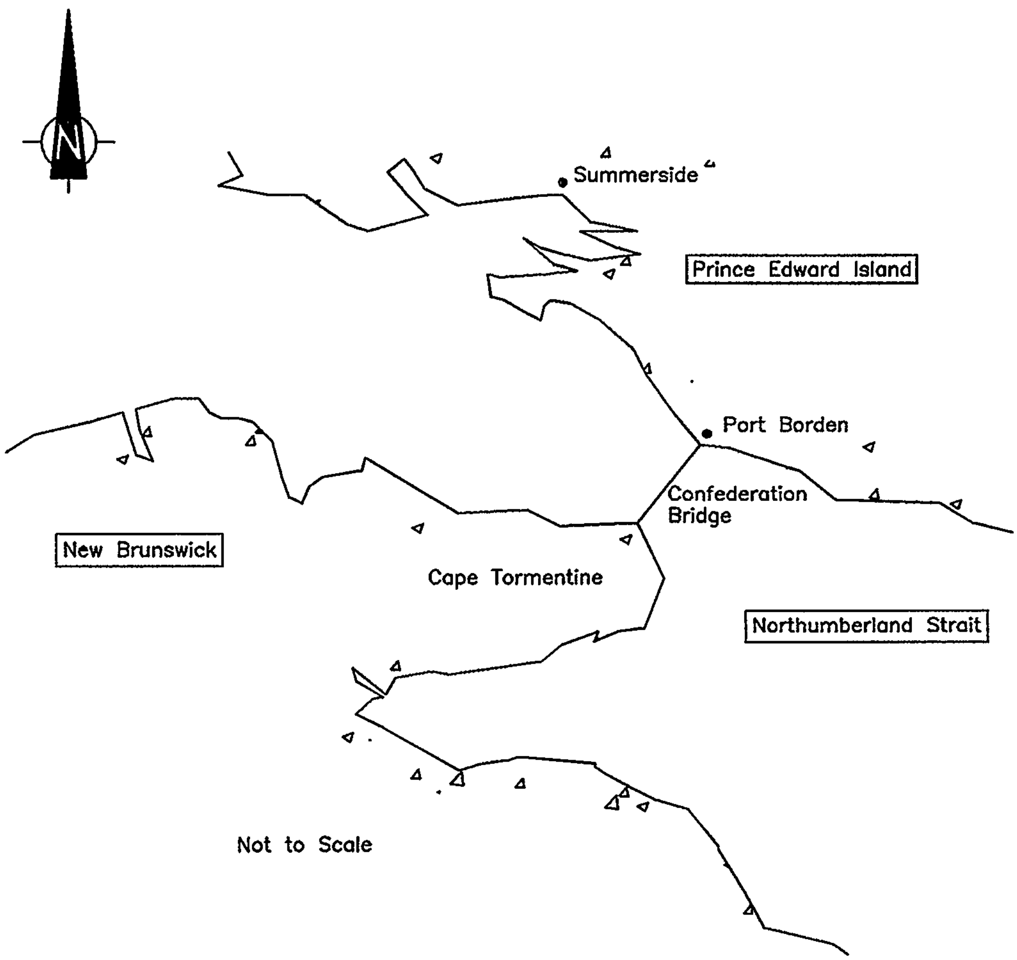

Figure 1.1 Location of Confederation Bridge

Several of the design guidelines set out by PWC differ from those found in the Canadian bridge design codes (CSA-S6, O.H.B.D.C) available at the time. Namely, the bridge would have a 100 year design life. This meant that new loads as well as new load and material resistance factors would need to be derived to maintain the target safety index of 4.0, typical of most bridge design codes.

As an indication of the importance of properly designing for the 100 year design life, the following needs to be considered. Alberta Infrastructure/ Alberta Transportation and Utilities (ATU) noted that the average life of standard bridges - those constructed with standard ATU precast concrete girders - was approximately 40 years and for major bridges - those constructed with more complex site specific girders - approximately 50 years. The estimated replacement cost of the provincial network of bridges in 1993 was 2-3 billion dollars. Imagine the cost to the provincial taxpayers if these bridges required substantial yearly maintenance or replacement before the average life expectancy (ATU, 1993, 1994). By comparison, the P.E.I. Bridge alone had a total construction cost of approximately one billion dollars.

The difficulty in deriving new loads and load factors for a 100year life cycle can not be overemphasized. Design loads for life cycles of 40 and 50 years are constantly evolving. Vehicle loads alone have substantially increased in only 30 years. The ice force exerted on bridge piers is an ever-evolving subject. Environmental loads are constantly being recorded and revised with each new design code edition.

Each year, hundreds of printed pages are generated on the topic of bridge performance. Catalogues of all bridge types and ages are compiled, along with rating systems for their overall performance (Dunker et al, 1990, 1992, 1993). The durability of concrete bridge decks is another topic with a never-ending list of references (ACI, 1991, 1992, 1994, PCA, 1995).

It becomes apparent that even after new loads and load factors are generated, through the use of probability and statistics, some measure of the bridge performance must be acquired. The required 100 year design life is more than double that usually used. Durability of the bridge, especially the concrete, is of prime importance.

Therefore, it is essential to monitor the bridge to observe if the design data generated was suitable for the 100 year-design life. The University of Calgary, in collaboration with the universities of Ottawa and Carleton, as member of the Canada wide Network for the Centres of Excellence in High Performance Concrete, initiated a monitoring program to record and interpret the behaviour of the P.E.I. Bridge over the course of its life cycle. Instruments were placed in two consecutive spans - one simple, and the other continuous - to monitor the short and long term performance. The following data is recorded for the use of researchers, (Cheung et al, 1997):

1) ice forces,
2) short and long-term deformations,
3) temperature variations and thermal strains,
4) traffic loads and load combinations,
5) vibrations due to wind, earthquake, and other transient load effects,
6) corrosion.

1.2 Background Comments

The work presented here concerns the analysis of the thermal response of the P.E.I. Northumberland Strait Bridge - commonly named The Confederation Bridge. An investigation concerning the structural response of a given load effect, whether it is from temperature or repeated truck over-load, becomes a durability problem. It is important to have an accurate prediction of the level of cracking that will occur in the structure.

Why is it important to analyse for temperature effects? In reviewing design drawings of early steel bridges, it is evident that designers did not consider the effects of temperature. However, these bridges were simply supported, truss type, structures held together with rivets. The use of rivets allows for sufficient shortening and elongation due to temperature fluctuations. This is because the holes punched in the steel members for the rivets are typically 3mm larger in diameter than the rivet. Also, these simply supported, truss type, structures contained short members which resulted in a large number of holes to accommodate the expansion or contraction due to temperature variations. Over time, designers have become aware of the economic advantages of designing for continuous structures. This leads to temperature stresses that are not present in simply supported structures. In concrete members this leads to cracking. In order to design for durability of concrete members there are two main considerations; cracking and water.

Concrete members deteriorate because water penetrates into the concrete and freezes and/or corrodes the steel reinforcement. Usually a concrete bridge deck slab is overlaid with an asphalt or a concrete wearing surface. In the past, the former has been the most popular, but, designers are slowly becoming aware of the fact that asphalt acts like a one-way sponge (Suprenant and Murray, 1993), as it allows water to seep through to the concrete deck, but will not let the moisture evaporate back through. Hence the water becomes trapped and must seep further down into the concrete deck, which may be cracked. A review of current bridge drawings reveals the importance of placing a sufficient number of drains in the concrete deck is not commonly known among design engineers. Such drains allow a good portion of the water, which migrates through the asphalt layer to be drained away without penetrating the concrete deck. A typical practice, recommended by Alberta Transportation and Utilities (ATU, Channon and Ramsay, 1992), is to have a 90mm asphalt topping placed over a 250mm thick structural slab spanning over either steel or concrete girders. Another practice is to have a 150mm concrete topping slab over precast concrete girders placed adjacent to each other. Unfortunately, it is also ATU policy, that when a concrete topping slab is used it is not mechanically connected to the rest of the structure (Skeet and Krivak, 1994). This, of course, allows the overlay slab to crack and de-bond from the supporting structure allowing more cracking and more water to enter the structure, accelerating the deterioration of the structure.

The above gives a brief rationale as to the importance of an accurate estimate of the degree of cracking, (Leonhardt et al, 1965, 1970 and 1979). It is known that temperature differentials can cause cracking in continuous concrete structures. If engineers are to design continuous bridges that are durable and do not require constant or costly repairs, then there must be a better understanding of the magnitude of temperature stresses; whether they act alone or in combination with other load cases.

Another reason for determining an appropriate temperature range is to avoid problems during construction. A curved steel box girder bridge, which was under construction in Calgary (in 1980), slid off its bearings and collapsed because the temperature rose suddenly and caused a higher curvature than the design engineers had foreseen.

The Confederation Bridge is constructed with a continuous precast concrete girder over two adjacent piers, with a simply supported drop-in precast section every second span. This type of design is beneficial for a number of design criteria, especially temperature. With rotation and expansion allowed at the supports of the drop-in spans, the stresses in the adjacent continuous spans will be greatly reduced.

Current bridge codes specify a maximum and minimum temperature as well as a maximum curvature for which the bridge is to be designed. Recent publications (Maes et al, 1992 and Li et al, 2003) have indicated that these temperatures and curvatures are not high enough, and that new higher values should be used in design. In particular, temperature measurements taken from the Calgary Light Rail Transit (LRT) bridge - constructed 1986 - across the Bow River display this fact. A visual inspection of the Calgary Bow River LRT bridge reveals an interesting characteristic. The bridge is situated such that the longitudinal axis is almost directly North-South (N-S). Hence the sides of the inverted concrete box girder face directly east and west. The early morning sun rises and shines on the east face. At this point the air is cool and moist. After mid-day, the sun shines directly on the west face of the bridge. At this point, the temperature is higher and the air is drier. As a result, the concrete on the west face of the bridge has deteriorated much more than the east-face. This would indicate that the temperature distribution across the section of the bridge is not constant. The deck temperature may be constant along the axis and across the section of the bridge, but the temperatures through the depth of the girders may be higher on one side of the bridge than the other. This would especially be true in a bridge situated East-West (E-W), in the Northern

Hemisphere, since the girders on the north side would rarely experience direct solar radiation. The bridge would tend to "bow" into the sun through the day. Whether the girders, deck, or bearings allow this movement is another question.

It has been stated in the literature that the absolute values of the maximum and minimum temperatures are of importance. In fact it is the shape of the temperature distribution throughout the depth that is of greater importance.

1.3 Objectives

The objectives for performing this investigation are:

1 To compare the measured and predicted temperature distributions for a cross section of the Confederation Bridge. There is a vast amount of temperature data recorded for the cross section S1, adjacent to a pier, and section S51, at mid span between piers. A data set of thermocouple readings for this cross section contains temperatures for an eighteen month period beginning in January 1998.

2 To determine the structural response for a given temperature distribution and attempt to compare it to measured values.

3 To reassess the thermal loads given in the Canadian Bridge Code in light of the results of the present study on a larger box girder. The maximum depth of the box girder in the Confederation Bridge is approximately 14m. In such a large structure it is reasonable to assume that the temperatures in the two webs will be different, leading to a transverse temperature gradient. It is hoped that a new proposal stressing the importance of transverse temperature distributions may be submitted.

1.4 Scope

As stated earlier, the work presented here concerns the analysis of the temperature effects on the Confederation Bridge and is aimed at proposing amendments for the design of temperature effects in the current CSA-S6 bridge design code. Factors that must be taken into account are discussed and described through the review of important literature. An analytical method was then adopted and implemented. Two existing computer programs were used. The first computer program, FETAB: Finite Element Thermal Analysis of Bridges, (Elbadry 1982), was used to generate temperature distributions for various cross sections of the bridge. These were compared with measured data selected from the large body of data recorded on the Confederation Bridge, (Li et al, 2003). The output from FETAB was then used to generate input to be implemented in the second computer program, SFRAME for Windows. The structural response from SFRAME was compared to measured data collected from the Confederation Bridge. This provided a comparison for the longitudinal temperature response.

Then, the structural response, due to temperature distributions in the transverse direction, was analyzed.

Next, the temperature distributions in the transverse direction were imposed on the cross sections and analyzed for frame behaviour. A deep section, located near the pier and the shallowest section, located at mid span, were modeled using SFRAME. Recorded temperature data was readily available specifically for these two sections. Therefore, the recorded temperature data was input directly into SFRAME.

The current edition of the Canadian Highway Bridge Design Code (CSA-S6-00) does not contain guidelines for the analysis of transverse temperature behaviour. Therefore a proposal is made for new guidelines to improve and clarify the current temperature loading criteria, with emphasis on the transverse temperature difference in the webs of a concrete box girder bridge.

CHAPTER TWO

LITERATURE REVIEW

2.1 Introduction

As with many topics in engineering, the design of bridges for thermal effects has undergone several changes. For early steel structures, temperature effects were simply ignored. Bridges were typically simply supported structures which allowed for sizeable movements. Eventually, longitudinal expansion and contraction were treated using an average rise and drop about an expected normal temperature. A linear relationship between the depth of the girder and the temperature was then used.

Over the past 30 years, there has been a growing awareness that the temperatures through the depth of a bridge girder are anything but linear. As a result, the self-equilibrating stress within the member and the bending stresses due to continuity of the structure can become very high.

Consider a simple rectangular section with a linear temperature variation from the top fibre to the bottom fibre. In an elastic material, plane sections remain plane. With a linear temperature distribution, the free strain due to temperature is linear. This is in agreement with the plane sections remain plane theorem, therefore no self-equilibrating stresses develop. However, if the temperature distribution is non-linear, stresses develop as plane sections are forced to remain plane, see Figure 2.1. Leonhardt (1965, 1970 and 1979) reviewed several bridges that were damaged due to the effects of temperature. Priestley (1972) noted that, engineers have understood the principles of thermal stressing for some time, it was not until the Newmarket Viaduct in Auckland, New Zealand, experienced damage due to temperature effects that researchers in New Zealand began to investigate the considerable stresses that can develop due to temperature differentials.

2.2 Temperature Distributions in Bridges

Before a proper design may be achieved, an accurate temperature distribution (ie: the variation of temperature through the depth of the bridge) must be obtained.

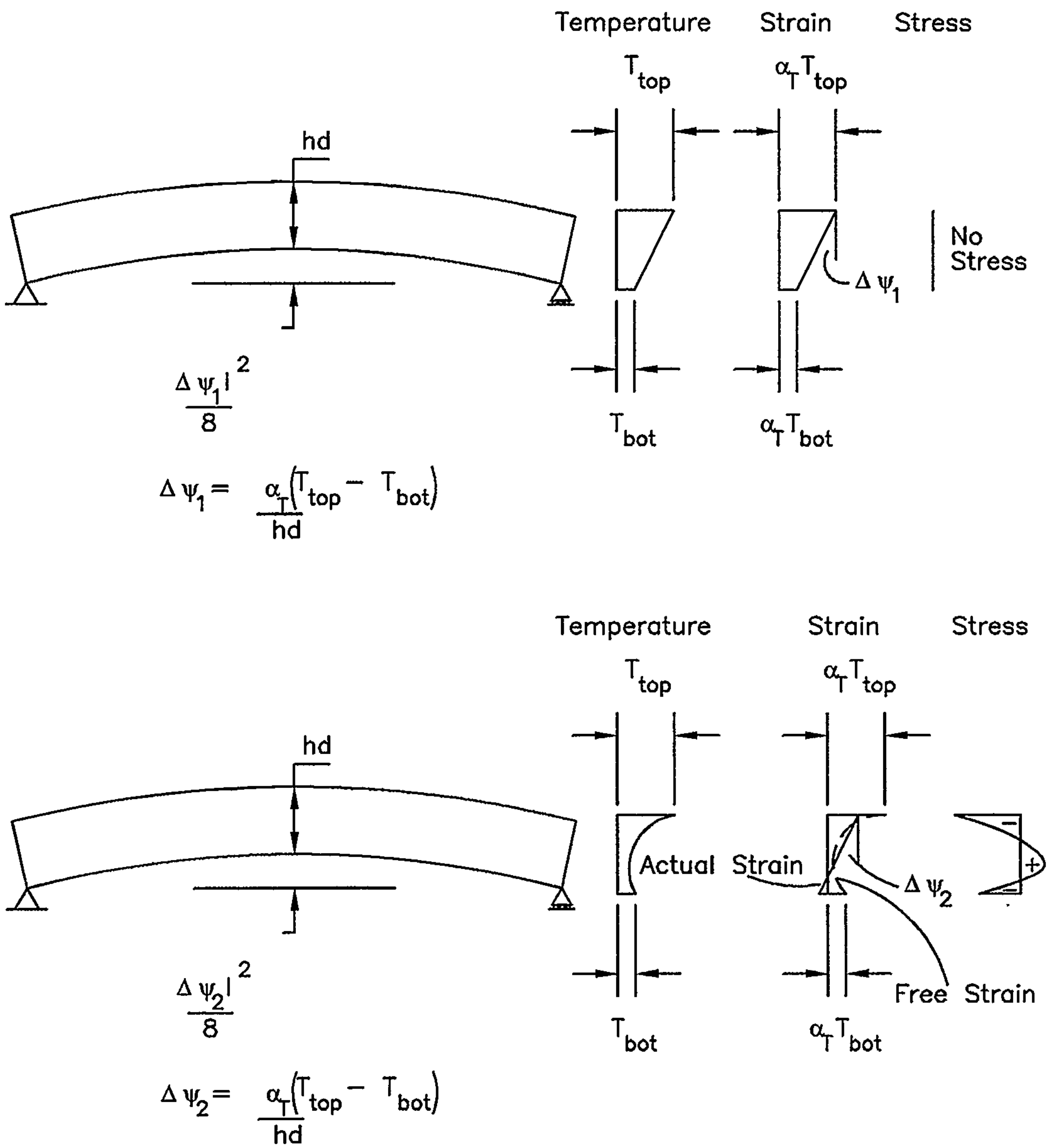

Figure 2.1 Deflection, strain and stresses in a simple beam due to a rise of temperature which varies linearly and non–linearly over the depth (Fig. 9.2 – Ghali, Favre and Elbadry)

Priestley (1972,1978) pointed out that temperature variations in bridges were at one time thought to be a simple or trivial matter. Longitudinal expansion and contraction were considered and accounted for, through the use of sliding bearings or flexible piers. However, after some prominent prestressed concrete box girder bridges in New Zealand started to show severe cracking due to temperature in the 1960's, researchers started to look into the matter more closely.

Priestley reviewed several temperature distributions. These included distributions with a constant temperature rise through the deck with no temperature rise in the girders or webs. Also, distributions with a linear temperature rise only in the slab, and then a series of polynomial equations, which modeled the temperature variations as a continuous function from the top of the deck slab to the bottom of soffit slab. Comparisons were then made of the residual stresses for each case.

The assumptions used by Priestley in computing this summary were as follows: first, that a plane section will remain plane; this is true for elastic materials. The assumption also holds for concrete, provided that shear deformations do not take place. Second, the temperature varies through the depth, but is constant across the section at each level. Priestley states that this assumption is only valid for special circumstances and that when the bridge is situated such that the solar radiation will cause a transverse temperature gradient it must also be taken into account.

The third assumption was that material properties were independent from temperature. This assumption is valid for normal temperature ranges (-30°C to 30°C). Sivakumaran and Dilger (1984) showed that at elevated temperatures (above 60 °C), the mechanical behaviour of concrete is altered. The fourth assumption is that the principle at of superposition is valid, which is typical of most engineering calculations in the elastic range.

After developing an analytical model based on the Fourier conduction equation, with boundary equations, to compute the thermal response, Priestley analyzed a series of seven bridge cross sections. This resulted in a recommended design thermal gradient, see Figure 2.2.

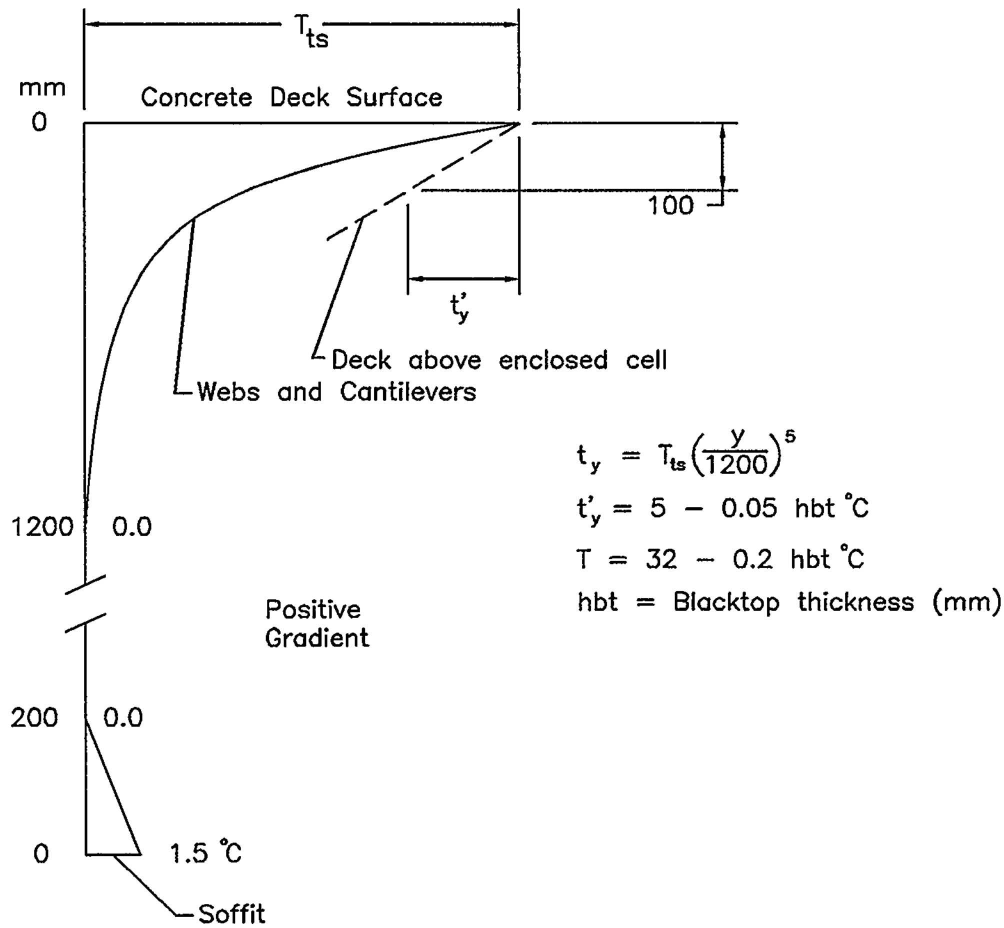

Figure 2.2 — New Zealand Design Temperature Distribution (Priestley, 1978)

2.3 Temperature Prediction Models

Several investigations have been put forward to develop analytical methods similar to Priestley's. Hambly (1978), Dilger and Ghali (1980), Churchward and Sokal (1981), Elbadry and Ghali (1983a, 1983b), Hirst and Dilger (1989), Moorty and Roeder (1992), Branco and Mendes (1993), Saetta, Scotta and Vitaliani (1995), Froli, Hariga and Nati (1996), and Silveira and Branco (2000), all presented analytical methods and parametric studies or comparisons with measured data.

Hambly (1978) presented simplified methods for computing the temperature distribution through concrete box girder bridge sections and then the resulting stresses. Hambly noted that the observed air temperatures inside the air cell of the concrete box sections changes by only approximately 1 to 2 °C on a daily basis. Therefore, for design purposes it is acceptable to assume that it is constant throughout the day. Hambly also noted, for cracked reinforced concrete sections, it may not be correct or accurate to superimpose the temperature stresses with live and dead loads. Each will result in a different level of cracking. Hambly proposed that the strains from each load case be calculated first, with the appropriate stiffness, and then added before computing the final stresses.

Dilger and Ghali (1980), followed by Elbadry and Ghali (1983a, 1983b), noted that many bridge designers recognize that temperature gradients through the depth of a bridge cross section are anything but linear, resulting in high stresses. However, there is little guidance in design codes as to how to accurately calculate them. Therefore, they presented a numerical method, using two-dimensional finite elements and taking into account environmental data, to compute the time-dependent temperature distribution through the bridge cross-section.

A review of the theory used in the development of this computational method was presented in Dilger and Ghali (1980), and is here summarized. Figure 2.3 has been reproduced from Ghali, Favre and Elbadry (2002) and shows the heat transfer actions/reactions which affect an exterior concrete member. When considering any

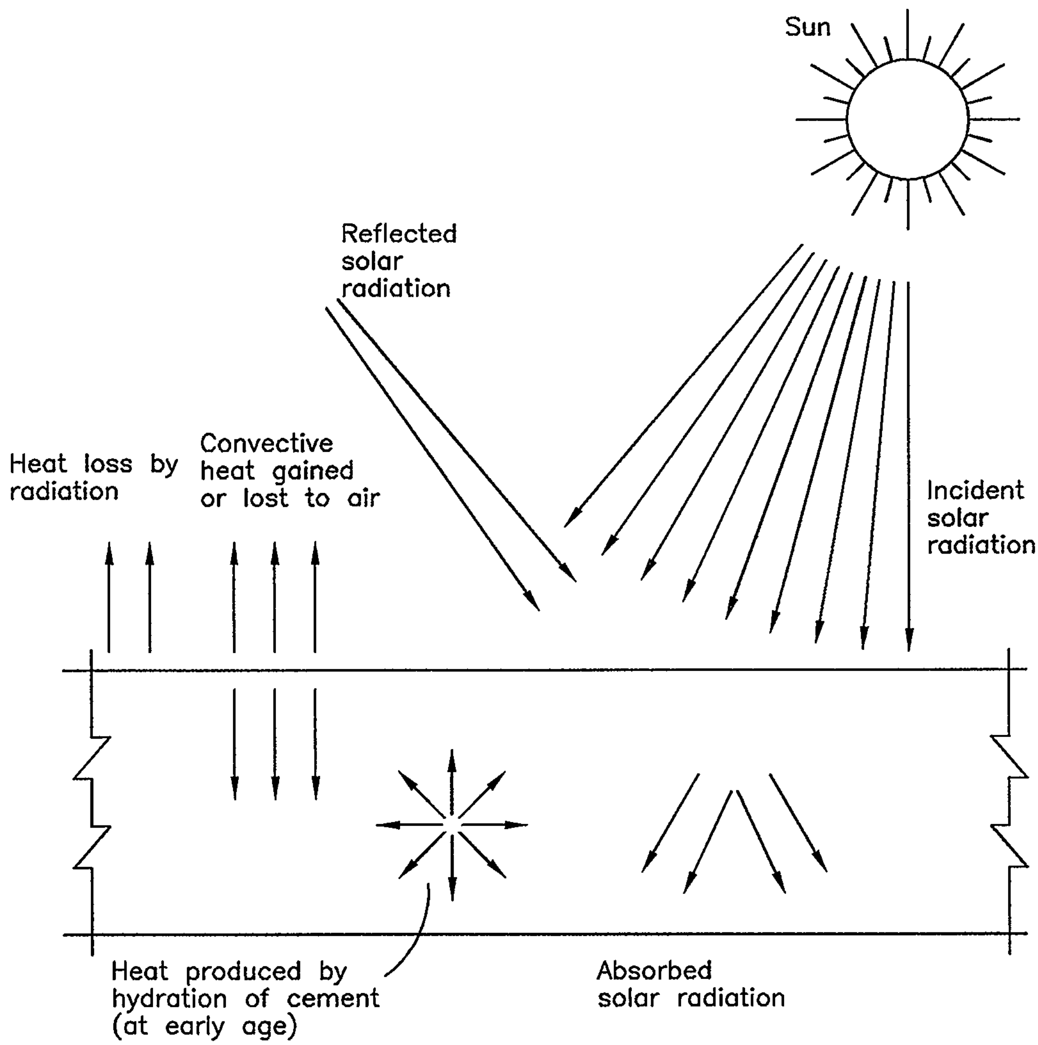

Figure 2.3 – Heat transfer process for a bridge
in daytime in summer
(Fig. 9.1 – Ghali, Favre and Elbadry)

exterior member exposed to solar radiation, a number of variables must be taken into account. Dilger and Ghali, list the following:

a) "Geometry of the cross section,

b) Thermal conductivity, specific heat and density of the material,

c) Nature and colour of the exposed surfaces, expressed on terms of solar radiation absorptivity, emissivity and convection coefficients,

d) Orientation of the bridge axis, latitude and altitude of the location,

e) Time of day and the season,

f) Diurnal variation of ambient air temperature and wind speed,

g) Degree of cloudiness and turbidity of the atmosphere."

Engineers are well aware of solar heat gain and loss during the summer and winter months. Regardless of whether a member is constructed of concrete or steel, the heat gain during

the day is greater than the heat loss at night - during the summer months. The opposite is true in the winter months. In order to compute the heat transfer process a number of partial differential

equations presented by Carslaw and Jaeger (1959) may be implemented:

$$\frac{\delta T}{\delta t}=\frac{k}{\rho c}\left[\frac{\delta^2 T}{\delta x^2}+\frac{\delta^2 T}{\delta y^2}+\frac{\delta^2 T}{\delta z^2}\right] \tag{2.1}$$

where,

T = Temperature

t = Time

k = Thermal conductivity

ρ = Material density

c = Specific heat

This is for three dimensional heat flow in a solid. For a bridge, it is a common and realistic assumption that the temperature along the length is constant. Therefore, equation 2.1 simplifies to:

$$\frac{\delta T}{\delta t} = \frac{k}{\rho c}\left[\frac{\delta^2 T}{\delta x^2} + \frac{\delta^2 T}{\delta y^2}\right]$$

(2.2)

To this equation Dilger and Ghali (1980) have added the term Q for the heat generated inside the body. Re-arranging equation 2.2:

$$\rho c \frac{\delta T}{\delta t} = k\left[\frac{\delta^2 T}{\delta x^2} + \frac{\delta^2 T}{\delta y^2}\right] + Q$$

(2.3)

At a member's boundary - surface - this equation changes slightly to account for the heat gain-loss over the surface of the boundary:

$$0 = \left[\frac{k\,\delta^2 T}{\delta x^2} n_x + \frac{k\,\delta^2 T}{\delta y^2} n_y\right] + q$$

(2.4)

This equation differs form Eq. 2.3 with the addition of direction cosines, n_x and n_y, normal to the boundary surface. The value of q, the heat transfer per unit area, is made up from three components:

$$q = q_s + q_c + q_r \qquad (2.5)$$

q_s = solar radiation - heat gain from the sun's ray,

q_c = convection - heat gain/loss due to the temperature difference between the air and the boundary surface, and

q_r, = re-radiation - heat from the boundary surface to the surrounding air.

Further derivations of q_s, q_c and q_r may be found in Dilger and Ghali (1980).

A bridge cross section is modelled as an assemblage of conduction finite elements. Boundary elements are added to take into account convection. Two types of analysis are possible. A *steady state analysis* computes the (self-equilibrating) eigenstresses for a given set of nodal temperatures while the *transient analysis* generates a new set of nodal temperatures for each time step. If desired, the (self-equilibrating) eigenstresses may be computed with each time step as well, provided that the temperature distribution is non-linear. Once these stresses have been computed the stress resultants may be calculated as follows:

$$\Delta N = \int\int \sigma_{restraint}\, \delta x\, \delta y \tag{2.6}$$

$$\Delta M_x = \int\int \sigma_{restraint}\, y\, \delta x\, \delta y \tag{2.7}$$

$$\Delta M_y = \int\int \sigma_{restraint}\, x\, \delta x\, \delta y \tag{2.8}$$

After applying and removing artificial restraint over the cross-section, the self-equilibrating stress results in a normal strain and a curvature about both the x and y axis.

$$\Delta \varepsilon_o = -\frac{\Delta N}{EA} \tag{2.9}$$

$$\Delta \psi_x = -\frac{\Delta M_x}{EI_x} \tag{2.10}$$

$$\Delta \psi_y = -\frac{\Delta M_y}{EI_y} \tag{2.11}$$

A more complete derivation of equations 2.6 to 2.11 may be found in Dilger and Ghali (1980)

Churchward and Sokol (1981) outline a research program undertaken by the Main Roads Department, Queensland and the University of Queensland, Australia. A constant depth (1500mm), double cell, post-tensioned concrete box girder bridge was instrumented with thermocouples at one cross section in order to record and monitor the thermal gradients which occur through the depth of the section. Two main types of deformations associated with temperature were noted. First, longitudinal expansion and contraction and second, vertical deflections caused by the temperature gradient through the depth of the section.

After monitoring the temperatures for a three year period, it was found that the temperature distribution in all webs (three for this bridge) were almost identical and the temperature distribution in the top flanges varied only slightly from the webs.

Churchward and Sokol reviewed design standards from New Zealand, Australia and Great Britain, as well as that proposed by Priestley. They noted that in each case the design standard specified the temperature gradient only. Missing was a temperature rise constant through the depth. To this, the gradient portion is added which usually affects the top 1000mm of a section, regardless of the overall depth.

The recorded data was analyzed using statistics and three different expressions were developed for the temperature gradient through the depth of the section. Curvatures were calculated from these temperature distributions, and comparisons made with the existing design relationships. It was found that the distribution proposed by Priestley gave the best estimate of curvature, and while their newly developed temperature distribution gave good estimates for the maximum temperatures, it underestimated the curvature. This lead Churchward and Sokol to their conclusion that an accurate relationship for temperature does not necessarily lead to accurate predictions of curvature.

It must be noted that the research was site specific and that the parameters used in design should also be generated by site specific data.

Hirst and Dilger (1989) describe a theoretical model for predicting the temperature distribution through a bridge cross section. The theoretical method utilizes the computer program FETAB developed at the University of Calgary by Elbadry (1982) using heat transfer theory. In order to obtain accurate results from the computational method, there is the question of initial conditions. It is common that a temperature analysis begin at dawn, when the daily temperature is at a minimum. However, there is the question of what should be input for the starting temperature.

Hirst and Dilger point out that the common practise of taking the average air temperature for the previous 24 hours may not be accurate. Concrete possesses a relatively large thermal mass, which means it takes a long time to heat up or cool down.

For thin slabs, taking the average air temperature for the previous 24 hour period may be an acceptable practise since the concrete can heat up and cool down relatively soon. However, with massive concrete sections the internal temperatures take longer to heat up and cool down. Therefore, the starting temperature can be higher than the previous days average air temperature.

Hirst and Dilger put forward the concept of a "time constant". From measured data, they observed the average bridge temperature at dawn corresponded to the air temperature a "time constant" before dawn. The time constant, TC, is computed as follows:

$$TCo = \frac{M_t}{S} \qquad (2.12)$$

where,

$M_t = t_e\, c\, \rho$

with,

t_e = slab thickness

c = specific heat of slab (J/kg °C)

ρ= density of slab

And S = 3600 h n

with,

h = surface convection heat transfer coefficient (W/m^2 °C)

n = number of external surfaces

n = 2 for single slab, but

n = 1 for a box girder as the interior surface is not counted.

It is noted that the time constant for large box girder bridges may be as much as 24 hours and effectively zero for steel sections. A thin slab may have a time constant of 2 hours.

The time constant approach was used with data from three bridges, one in Calgary, Canada, and two in South Australia. The bridge in Calgary is an upside-down concrete box girder meaning that the slabs cantilever from the bottom of the box rather the top, which is more conventional. This bridge supports LRT trains, with one on each side of the box. The two bridges in Australia are, a conventional concrete box girder section in Swanport, and a composite slab and steel girder bridge near Coober Pedy, South Australia. In each case the calculated temperatures were in close agreement with those measured on the actual bridges.

Moorty and Roeder (1992) presented an analytical method very similar to Dilger and Ghali (1980) for predicting the movements of composite I-girder bridge bearings. They noted that although the transverse deflections are smaller in magnitude than the longitudinal deflections, they are often more critical because the bearings may not accommodate the transverse movements. This makes it important to properly orientate the bearings, even more so for curved bridges. Moorty and Roeder also noted that due to the high thermal conductivity of the steel girders their temperature is governed by convection. The analytical method was shown to provide good agreement between predicted and recorded temperatures.

There is, however, a comparison with recorded data in Branco and Mendes (1993). Two concrete cross sections were analyzed. One concrete box girder (depth 2.6 m) and one solid slab girder (depth 1.07m) . Note that the box section is approximately half the size of the smallest cross section of the Confederation Bridge. The predicted temperatures were in good agreement with the recorded values. It should be noted that the predicted temperatures are in best agreement towards the bottom of the sections.

Saetta, Scotta and Vitaliani (1995) present a numerical method, again, very similar to Dilger and Ghali (1980). Two examples are presented to illustrate the comparison between predicted and recorded results. One for the Sa Stria Dam, Italy and another for a concrete box girder bridge (depth 1.2m), located in Italy. Of interest here is the box girder section example, for which the top and bottom slab had a thickness of 200mm and the webs had a thickness of 500mm. Temperature comparisons are shown through the symmetrical axis of the bridge (ie: through the top slab and the bottom slab. The temperatures predicted for the bottom slab are in good agreement with the recorded values, while the top slab temperatures seem to vary by as much as 7-8°C. There are no comparisons for the temperatures in the webs. As well, there are no comparisons between predicted and recorded curvatures.

Froli, Hariga, Orlandini and Nati (1996) presented research comparing the predicted thermal behaviour of a prestressed concrete box girder bridge with the measured values. Similar to the Confederation Bridge, thermocouples were embedded at several locations in various cross sections of a concrete bridge. The analytical method presented is very similar to Dilger and Ghali (1980). And in fact uses the theoretical method presented by Ghali and Elbadry (1983) for computing the air temperature inside the concrete box girder. They noted that there are two methods of considering the air in the girder cell. The first is to treat the heat transfer as strictly conduction through still air (Ghali and Elbadry), while the other method considers predominantly convective heat flow in the air volume. The first method is significant for small air volumes and the second for large air volumes.

Comparing the predicted and measured temperatures a maximum difference of 3°C was observed. Therefore the analysis was deemed satisfactory. These temperature predictions were then converted into temperature gradients (ie: curvatures) and were in general found to be satisfactory.

Silveira, Branco and Castanheta (2000) presented a analytical method similar to Dilger and Ghali (1980) complete with statistical analysis for the temperature distribution. Dilger and Ghali (1980), incorporated a sine relationship for the temperature. Now, Silveira, Branco and Castanheta present a statistical analysis based on choosing upper and lower characteristic values for the extreme temperature distributions to be expected for the life cycle of the bridge. The researchers noted that the self-equilibrating stresses should not be ignored as they are the only stresses present in a statically determinate structure. However, the maximum value of the self-equilibrating stresses does not necessarily occur at the same moment as the maximum curvature due to an extreme temperature distribution. Concluding that the maximum stresses will occur on either the top or bottom fibre of the bridge section, another statistical analysis is presented to predict maximum and minimum values for the self-equilibrating stresses. However, the research presented does not contain a direct comparison between predicted and recorded data.

2.4 Comparisons of Field Data with Prediction Models

Dilger et al (1981) documented field measurements of the Muskwa River Bridge in northern British Columbia, Canada, see Figure 2.4. Although the bridge is a concrete deck with twin steel box girders, it serves as an interesting comparison to a concrete box girder bridge.

The temperature data for this bridge was gathered during construction and while in-use. In cross section the bridge has an 8 inch (0.20 m) thick reinforced concrete slab, 37 feet (11.28 m) wide. Two steel box girders are spaced 9'-6" (2.90 m) apart and 9 inches (0.23 m) off centre. The east box has an over hang of 6'-0" (1.83 m), while the west box has an overhang of 4'-6" (1.37 m). Each box section is 8'-6"(2.59 m) wide. The steel box girder sections are tapered from approximately 8'-0" (2.44 m) deep at midspan to approximately 12'-6" (3.81 m) deep over the piers.

The most interesting temperature data was reported on March 20, 1976. This day presents more or less the maximum variation between morning low temperature and afternoon high temperature. The authors are careful to point out that the daily maximum and minimum are not seasonal maximum. Only the daily temperature change is a maximum. As such, the morning low temperature on this date was -18°C and the afternoon high temperature was -4.4°C. The temperature of the concrete deck slab remained relatively constant throughout the day at -9°C (noon), while the temperature of the steel box rose from -1°C (noon) to 32°C (2:30 p.m.). This creates a maximum temperature differential of 42°C. This high temperature in the steel was due to solar radiation on the dark brown (rusty) steel box girder.

Dilger et al (1983) followed up the measurements taken on the Muskwa with a paper detailing an analytical method for computing the temperature distribution across a bridge cross section.

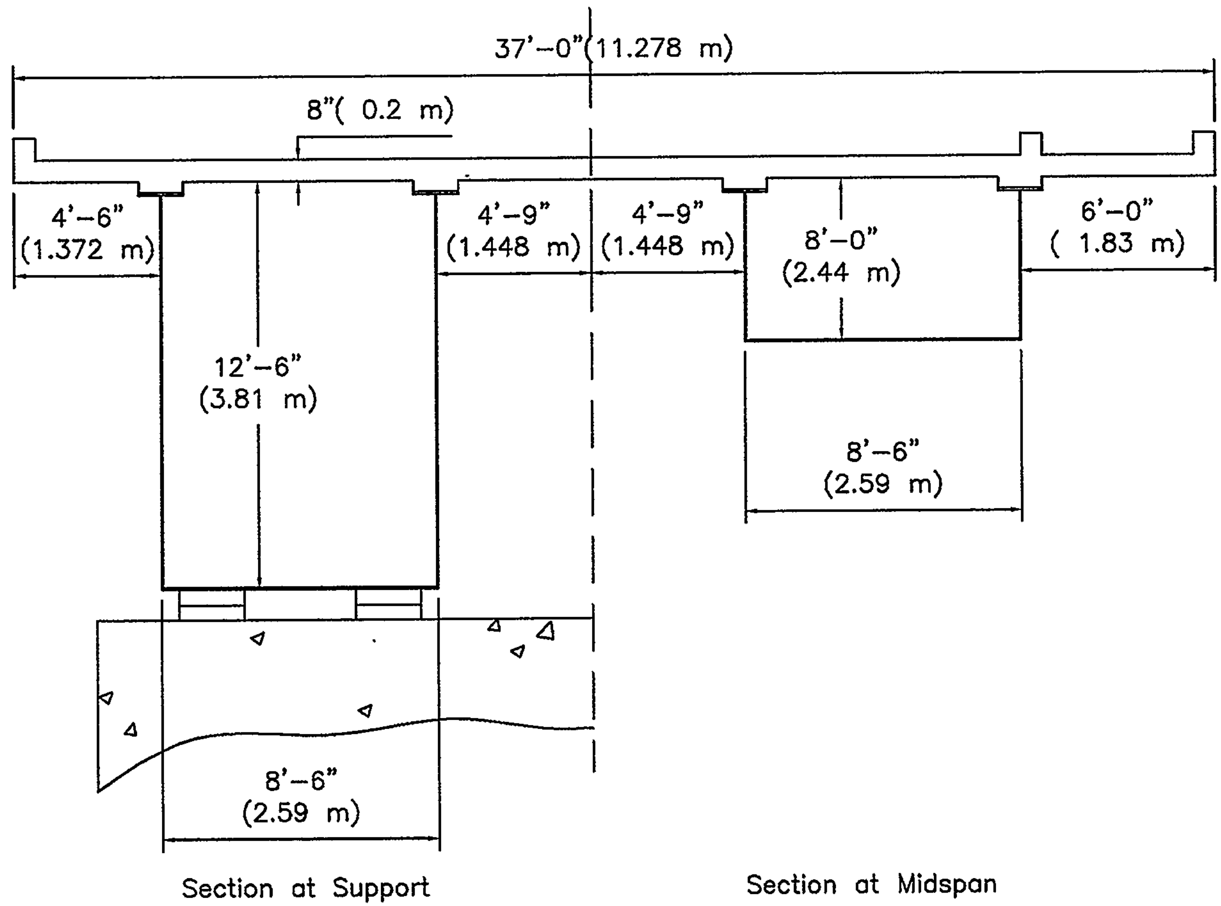

Schematic – Not to Scale

Figure 2.4 – Muskwa Bridge Cross Section

Dilger et al point out that temperature gradients across the cross section of a closed box can lead to stresses high enough to cause structural damage. In addition, reference is made to a composite concrete slab and steel box girder bridge that rolled off its bearings and collapsed during construction, due to un-foreseen temperature gradients.

To properly design a structure, the engineer must have the proper loads to apply to the structure. Therefore, after explaining the analytical method, a parametric study is then presented to show the affect of the many variables.

Molesini and Massicotte (1993) and Massicotte and El-Alam (1996) each reported on a monitoring program on the Grand-Mere Bridge in Quebec, Canada. This bridge is a three span precast concrete box girder with a cross section depth varying from 2.90m at mid span of the centre span to 9.75m at the two continuous supports, with a maximum interior span of 181.36m. Some time after construction the bridge started showing signs of distress. In conjunction with the repair measures that were implemented, thermocouples were installed on two cross sections of the bridge. The resulting thermocouple temperatures were compared to those predicted with a customized version of the computer program FETAB, which was designated FETAB-2. Very close agreement between the measured and predicted temperatures was reported. The measured and predicted temperatures on the top slab of the concrete box girder section differ by only 1-4°C, while the temperatures on two walls of the differ by only 1-2°C. It is important to note that each Molesini and Massicotte (1993) and Massicotte and El-Alam (1996) found that the behaviour of the bridge could modelled accurately with the use of FETAB, which assumes that the longitudinal temperature distribution along the bridge axis is constant.

2.5 Temperature Design Data - Current Canadian Design Code

One common complaint of practising engineers that is alluded to in the literature is that design codes tend to be rather vague in details concerning the exact method of design (Ghali, Favre and Elbadry, 2002). Although design codes go to great lengths to state maximum and minimum values for loads or stresses, the proper method of dealing with a particular load case is often left to the designer. To illustrate this point, excerpts from the new Canadian bridge code are reproduced for the reader.

2.5.1 CSA/CAN-S6-00 (2000) Temperature Design Data

The following is a excerpt from CAN/CSA-S6-00 (2000) concerning the design for temperature:

"3.9.4.1. Temperature Range

The temperature range shall be the difference between the maximum and minimum effective temperatures, as given in Table 3.9.4.1 for the type of structure. The temperature range shall be modified in accordance with the depth of the superstructure as indicated in Figure 3.9.4.1. The maximum and minimum daily mean temperature shall be taken from Appendix A3.1.

Table 3.9.4.1 Maximum and Minimum Effective Temperatures

Superstructure type	*Maximum effective temperature*	*Minimum effective*
Type A	*25°C above maximum daily mean temperature*	*15°C below minimum daily mean*
Type B	*20°C above maximum daily mean temperature*	*5°C below minimum daily mean*
Type C	*10°C above maximum daily mean temperature*	*5°C below minimum daily mean*

Type A superstructures include steel beam, box, or truss systems with steel decks, and truss systems that are above the deck.

Type B superstructures include steel beam, box, or deck truss systems *with concrete decks.*

Type C superstructures include concrete systems with concrete decks.

Figure 3.9.4.1. is unchanged from OHBDC (1992). See Figure 2.5. for modifications to the maximum and minimum temperatures.

3.9.4.2 Effective Construction Temperature

In the absence of more site specific data, an effective construction temperature of 15°C shall be assumed for design. This temperature shall be used to determine the effective temperature ranges to be used in the calculation of expansion and contraction.

For Type C structures that are cast-in-place, the heat generated by cement hydration may cause the concrete temperature to be above the effective construction temperature at the time of initial set. This shall be considered as a possibility. If more precise data are not available, it shall be assumed that concrete cools by 25°C from its initial set to the effective construction temperature.

3.9.4.4.1. Thermal Gradient Effects

The effects of thermal gradients through the depth shall be considered in the design of Type A, B, and C structures.

A thermal gradient is positive when the top surface of the superstructure is warmer than the bottom surface.

Values of temperature differentials are given for Type A and Type C structures in Figure 3.9.4.4. For winter conditions, positive and negative differentials shall be considered. For summer conditions, only positive differentials shall be considered.

For composite and non-composite Type B structures, a positive temperature differential decreasing linearly by 30°C from the top to the bottom of the deck slab shall be considered. The temperature shall be

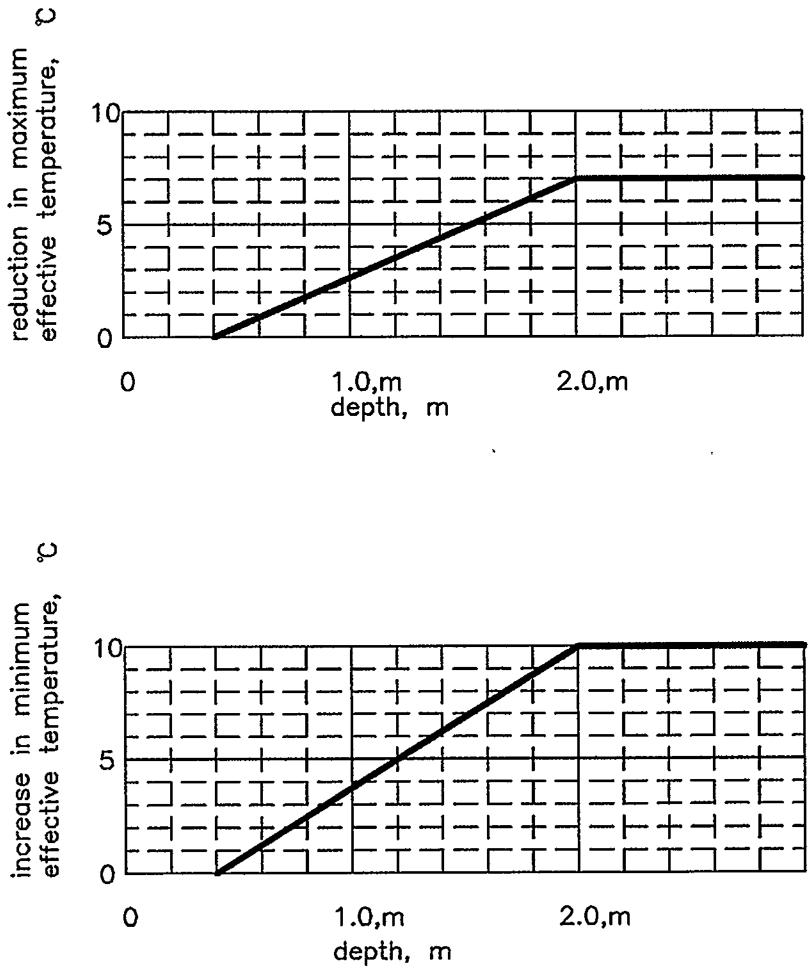

Figure 2.5 – Modifications to Maximum and Minimum Effective Temperature O.H.B.D.C 1992 and Figure 3.9.4.1 from CAN/CSA–S6–00

assumed to remain constant throughout the beam or truss below the slab. Negative differentials need not be considered.
Allowances shall be made for the stresses and deformations induced when the coefficients of expansion of the materials used in the structure differ."

See Figure 2.6 for Figure 3.9.4.4 which again was also part of the OHBDC (1992) and is unchanged for CAN/CSA-S6-00.

Note that in none of these codes is a specified temperature gradient similar to that proposed by Priestley. Hence, in none of these codes are the self-equilibrating stresses taken into account.

2.6 ACI - Box Girder Bridge Design

Over the years, the American Concrete Institute (ACI) has published several design handbooks as a guide for practising engineers. One such publication, Degenkolb (1977) summaries 30 years of experience in the design and construction of concrete box girder bridges, both prestressed and/or conventionally reinforced. Degenkolb summarizes several design considerations and points out that the transverse temperature gradients through the cross section of the bridge are typically more significant than the temperature gradient through the depth. Temperature gradients through the depth of a member cause translations and rotations and the accompanying forces may be greatly reduced in magnitude through the installation of expansion joints and rotating bearings. However, the transverse temperature gradients can cause very serious longitudinal cracking in the girder webs. In box girder bridges the air temperature inside the box can be very different from the outside air temperature causing significant curvatures in the girder webs. Adding to this the fact that the temperature distribution across the girder webs may vary from one side of the bridge to the other it becomes apparent that very significant stresses could develop. To minimize the transverse temperature stresses, Degenkolb recommends using girder webs as thin as possible so as to increase their flexibility and reduce stresses.

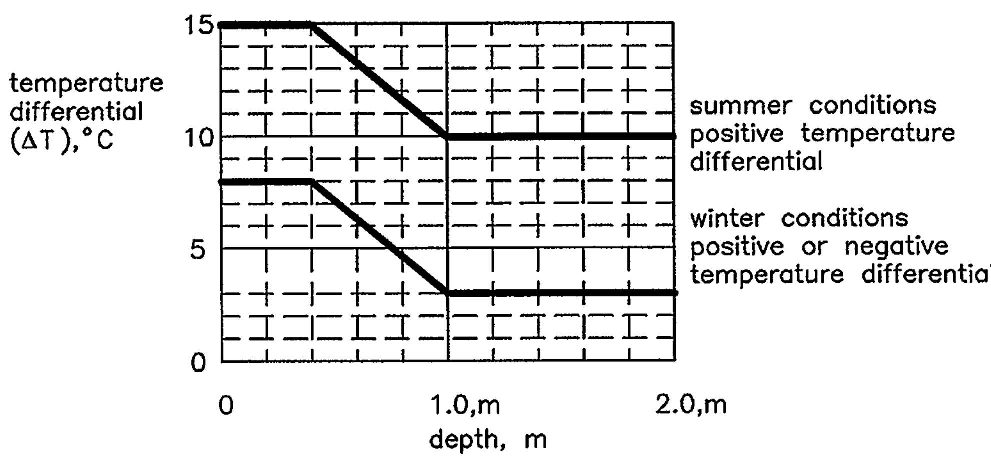

Figure 2.6 – Temperature Differentials for Type A and C Superstructures O.H.B.D.C 1992 and Figure 3.9.4.4 from CAN/CSA–S6–00

2.7 PCI-PTI Design Recommendations for Precast Segmental Box Girder Bridges

Precast Segmental Box Girder Bridge Manual (1978) is a joint publication by the Precast/Prestressed Concrete Institute and the Post-Tensioning Institute. It is a very detailed design manual and also points out the potentially significant effects of transverse temperature gradients. Three items stand out in particular and are here reproduced for the reader:

"1. *At sections near the supports, the relatively thin top slab may cool much more rapidly than the thicker bottom slab. This will cause tensile stresses around the exterior of the cross section.*

2. *With strong and prolonged sun radiation on the bridges surface, the air in the interior of a hollow box girder may become heated to over 100 °F (38 °C). When the outer air temperature difference between the interior and outer air produces transverse flexural moments in the webs and slabs which cause tensile stresses around the exterior of the cross section.*

3. *Thick concrete elements exposed to intense sun radiation are subject to substantial tensile stresses when the exterior surfaces cool due to the lag in response of the interior concrete to the temperature change."*

It is also pointed out that the transverse temperature effects become even more significant when they are combined with the transverse prestressing forces in the slab.

2.8 ACI-ASCE Bridge Design Criteria

Analysis and Design of Reinforced Concrete Bridge Structures (1988) is a joint publication by the American Concrete Institute and the American Society of Civil Engineers. In this publication the recommended temperature distribution is taken from Priestley. There is no mention of transverse temperature gradients nor of their effects. However, as an alternative to the Priestley temperature distribution, one derived from heat flow equations using site specific temperature data is mentioned.

2.9 Confederation Bridge Temperature Design Data

The following is an excerpt concerning the Temperature design criteria used in the design of the Confederation Bridge (MacGregor et al, 1997):

"2.6. Temperature

2.6.1 Design criteria

The design criteria specified the maximum effective temperature to be 5°C above the 2 ½ % dry bulb temperature in July, and the minimum effective temperature as 3°C above the 1 % dry bulb temperature in January. Assuming an ambient temperature of 15°C at the time that closure is made between the cantilevers and the drop-in spans, the design temperature drop was as specified 34°C, and the design temperature rise as 17°C. Vertical thermal gradients were also specified for the superstructure.

2.6.2. Statistical distributions of temperature loads

2.6.2.1. 100-year temperature drop: Records of daily average temperatures for 46 years in Summerside were analyzed. Due to the large thermal mass of the superstructure, it was assumed that the temperature of the structure would be related to the 3-day average minimum temperatures. Extrapolating the data to 100-years, the mean annual coldest three-day temperature was -19.21°C with a standard deviation of 1.07°C.

It was assumed that the bridge would be made continuous at night at an average temperature of +15°C with a standard deviation of 3°C. Based on the data from Maes et al (1992) it was assumed that the minimum bridge temperature would be about 4°C above the lowest three-day average minimum temperature. Thus, the extreme 100-year temperature *drop from that at closure would be +15 - (-19.21 + 4) = 30.2°C with a standard deviation of 3.19°C. The distribution of the 100-year temperature drop was d = 30.2/34 = 0.888 and V = 0.106.*

2.6.2.2. Temperature drop for serviceability calculations: In the derivation of the cracking load criteria, the design temperature drop for load calculations where temperature was a principal load was the three-day temperature drop, which is equalled or exceeded 100 times in the 100-year life of the structure. The average temperatures for the 35 consecutive three-day periods between December 1 and mid-March the following year were calculated from the daily average temperatures from Summerside, P.E.I., over 46 years between 1941 and 1991. Forty-six of these *were equal to or less than -15.9°C. It was further assumed that the standard deviation of this value would be the same as that of the mean annual three-day average minimum temperature for 100 years, or 1.07°C.*

The temperature drop that was equalled or exceeded 100 times in 100 years was +15 - (-15.9 + 4) = 26.9°C. The standard deviation was 3.19°C. This distribution was taken as normal with d = 26.9/34 = 0.79 and V = 0.118.

When temperature is a companion load in a serviceability limit states load combination, the appropriate temperature is the average winter temperature. From *the data for 1980, which was a colder-than-average year, the mean temperature during the three and a half winter months was -7.03°C with a standard deviation of 4.2°C. Assuming the bridge was made continuous at +15°C, the mean temperature drop was 22.3°C with a standard deviation of 5.16°C, giving d = 0.659 and V = 0.231."*

Note that data published in the commentary to the National Building Code of Canada

(1990) lists the January 2 ½ % temperature in Summerside, P.E.I as -20°C and the July 2 ½ % temperature as 27°C. For comparison, the same values for Calgary, Alberta are -31°C and 29°C, respectively. The temperature distributions used in the design are shown in Figure 2.7. These distributions were taken from the design working drawings, drawing no. M-GN001 (90% submission).

2.10 Conclusions

After reviewing the material presented the following conclusions may be drawn.

1) The comment made by Ghali, Favre and Elbadry (2002) about design codes leaving out the finer details as to the correct method of design is well founded.

2) Mathematical models for the temperature distribution may be factual with regard to temperature, but it is equally important to yield accurate estimates for the resulting curvature. It has been stated by several researchers, that obtaining accurate estimates for both temperature and curvature at the same time can be a difficult task. Simply predicting the temperature distribution of concrete sections can prove difficult enough. It may be observed that the prediction models that reported the closest comparisons between theoretical and measured data were based on a composite section with a concrete slab and either steel I-girders or box section. This results from the relatively high thermal conductivity of steel compared to concrete. The steel rapidly heats up to a uniform temperature and cools down quickly. Concrete sections are slow to heat up and slow to cool. In addition, the temperature through the thickness of the concrete web/wall is not uniform.

3) The temperature gradient proposed by Priestley is generally considered to be one of the better estimates for the actual temperature distribution and resulting curvatures. However, it must be remembered that this is for only one hour of the day. Although researchers appear to agree this temperature distribution yields a maximum curvature to be used in design, the self-equilibrating stresses resulting from this temperature distribution will not be critical.

Temperature Variation (T)

Temperature range as per CAN/CSA–S6–88
Assumed temperature at erection: 15 ℃
Temperature rise: 17 ℃
Temperature fall: –34 ℃
Temperature differentials in superstructure

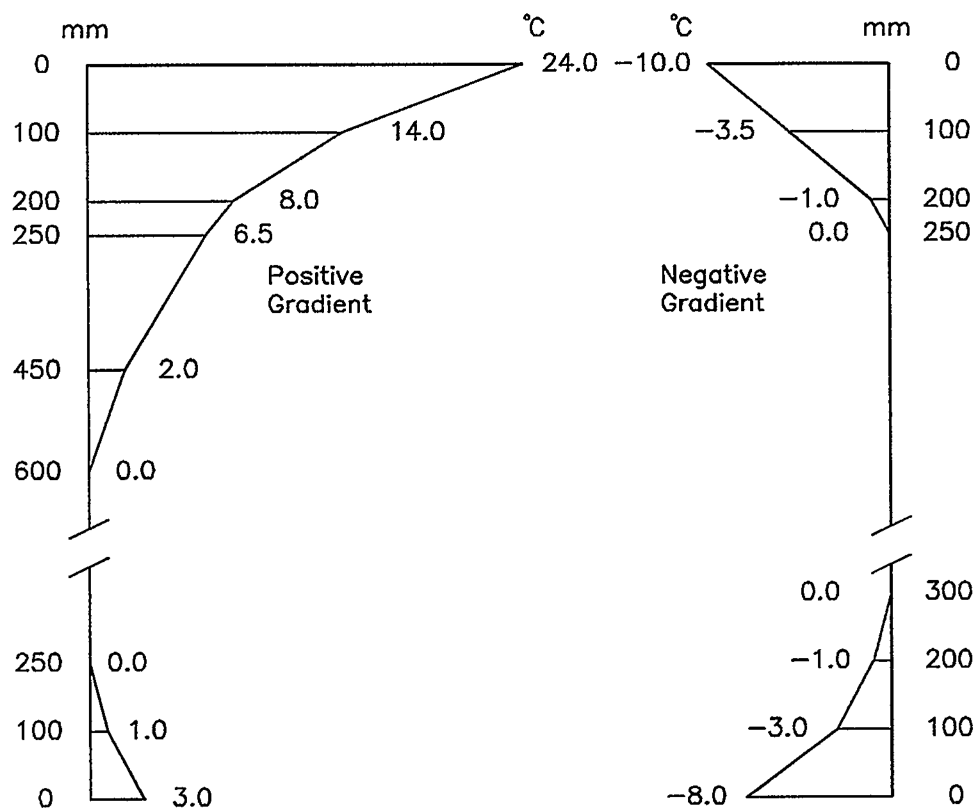

Temperature Design data taken from drawing number M–GN001 Rev. 0
Main Spans Design General Notes
The Northumberland Strait Crossing Project

Figure 2.7 – Temperature Design Data

4) Researchers readily admit that the temperature distribution across a section at any elevation is not linear, yet Canadian design codes recommend this assumption. According to the Canadian Highway Bridge Code, CSA-S6-00, a linear temperature distribution is to be assumed for a given type of structure. Then, a curvature is obtained for charts relating temperature difference to the depth of the structure. This curvature is about the horizontal axis through the cross-section. There is no mention of a curvature about the vertical axis.

5) Design aids produced for the practising engineer warn against transverse temperature gradients. It is recommended that thin flexible webs be used in concrete box girder sections to reduce the bending stresses resulting from such temperature distributions. However, temperature gradients for the webs/slab of the box girder - for transverse affects - are not given. Temperature gradients to be used in design through the depth of a member are also linear. Hence, there are no self-equilibrating stresses. Since it is known that the temperature distribution across a section is not linear it is doubtful that it would be linear across the box girder wall - when it is known to vary significantly through the depth of the top slab.

6) When reviewing the temperature gradients recommended by researchers it may be puzzling to view the temperature gradient used in the design of the Confederation Bridge. In Priestley's non-linear temperature distribution the gradient extends to a depth of 1.2m. Here the design engineers chose a gradient which extends a depth of only 0.6m for summer conditions and only 0.25m for winter conditions. However, the research presented by Molesini and Massicotte (1993) and Massicotte and El-Alam (1996) on the Grand-Mere Bridge shows that the non-linear temperature distribution extends approximately 0.6m for both the 9.75m deep section and the 2.9m deep section.

The transverse temperature affects have apparently been ignored in the design of the Confederation Bridge, as there is no mention of them on the contract drawings.

7) It is interesting to note that the design engineers for the Confederation Bridge used a Priestley type of design gradient, which results in self-equilibrating stresses, for the design of curvatures. However, the value of the self-equilibrating stresses, resulting from this design gradient, can not be said to be a worst case loading. The self-equilibrating stresses, resulting from the Priestley type design gradient, along the top surface of the girder have a compressive value of about 10% of the 28 day compressive strength.

This is true when the top fibre temperature is higher than the internal fibres. However, as the top fibre temperature cools faster than the internal temperatures tensile stresses develop in the top fibre. Concrete bridge design engineers should be more concerned with concrete tensile stresses than low level compressive stresses.

8) After reading the enclosed excerpts from CAN/CSA-S6-00 along with the data presented by Dilger et al (1981,1983) one becomes aware of how little up to date information is, at times, contained in design codes. In clause 3.9.4.4.1 *Thermal Gradients,* CAN/CSA-S6-00 states that for composite type B structures (steel girder and concrete deck) negative differentials (where the top surface is colder than the bottom surface) need not be considered.

In Dilger et al (1981,1983) the data recorded from the Muskwa Bridge clearly display a very large negative differential. On the day in March 1976 that the data was presented a temperature differential of approximately 42°C was recorded. It must be remembered that this temperature differential was negative. The top surface of the concrete deck was -9°C while the steel girder was +32°C.

One example of the dangers of not considering a negative temperature differential occurred in Calgary. Although it has not been documented in published literature, a case study has been presented as part of an annual seminar on the design of steel bridges (Steel Bridges, 1994, 2001). At the end of these seminar's, a slide presentation of construction failures outlines the cause of the failure and how it could have been prevented. The bridge in question is a three span composite concrete deck with steel box girder. One unusual feature of this structure was that one side of the concrete deck cantilevered farther than the other. In addition, the end supports had two bearings while the two interior supports had only one bearing. Further to this was the fact that none of the bearing locations had restraining devices for uplift.

Calgary, Alberta, is located fairly close to the eastern slopes of the Rocky Mountains and is therefore subject to Chinook winds. The concrete deck was poured in fairly normal winter weather conditions. However, a Chinook happened to arrive. Steel and concrete have very different thermal masses which results in steel heating up and cooling down faster than concrete. As expected, the steel girder warmed up faster than the concrete deck resulting in a negative temperature differential. Since no provision for uplift was present, the ends of the exterior spans lifted. This left the bridge supported by the two single interior bearings. As mentioned, the concrete deck imposed an eccentric load on the structure. If the two interior supports had two bearings each the structure may have stayed in place. However, each support had only one bearing and as a result the bridge simply rolled to one side and off the supports. Luckily the steel girder was able to be salvaged and construction continued after the steel girder was repaired and re-installed on it's supports.

One other reason for considering a negative temperature differential in both summer and winter is that in a continuous beam the continuity stresses result in tension all along the top surface of the structure. This should be of importance to every bridge engineer, yet the CAN/CSA-S6-00 design code states that engineers need not consider a negative temperature differential.

CHAPTER THREE
COMPUTATIONAL METHODS UTILIZED

3.1 Introduction

In the previous chapter it was conveyed that in order to obtain an accurate estimate of the temperature effects on a structure, an accurate estimate of the temperature distribution throughout the structure must first be obtained. Since it would be almost impossible and very cost prohibitive to monitor enough cross sections throughout a bridge structure to obtain sufficient data for input into a structural analysis computer program, it is necessary to model bridge cross-sections on the computer in order to obtain curvatures due to thermal effects. These curvatures may then be input into a structural analysis computer program to obtain deformations and stresses.

As shown in the previous chapter, many researchers have developed analytical methods, based on Fourier's Law (Carslaw and Jaeger, 1959). These methods produce accurate results for both temperature distribution and curvature. One such analysis method was developed by Elbadry and Ghali (1983a, 1983b) at the University of Calgary (1982), and implemented in the computer program FETAB: Finite Element Thermal Analysis of Bridges. The curvatures that are generated from this computer analysis may then be used as input for a structural analysis computer program. In order that the effects of a transverse temperature gradient that may be incorporated a three-dimensional structural analysis program must be used. For this type of analysis the computer program SFRAME for Windows was purchased.

3.2 FETAB: Finite Element Thermal Analysis of Bridges

As mentioned above, the computer program FETAB was developed at the University of Calgary in the early 1980's (Elbadry and Ghali (1983a, 1983b) and Elbadry and Ghali (1984) for the analysis of concrete bridge cross sections. The temperature distribution along the longitudinal axis of the bridge is assumed to be constant. Therefore, for a bridge of constant cross section, only one cross section needs to be modeled. As with any computer analysis, it is imperative that the assumptions made in the development of the analysis method are understood prior to its implementation, otherwise incorrect results could be obtained. Therefore, at this time a brief review of the theory used in the development of the computer program FETAB will be presented.

3.2.1 FETAB Development

It is stated in the user's manual for the programs FETAB (Elbadry and Ghali, 1984) that the thermal stresses in a cross section continuously vary with time unless the ambient temperature is more or less constant for several days. From this it follows that the temperature distribution at any given point in a cross section varies with time, so that temperature imposes a transient load on the structure. However, the loading frequency would be very low – approximately one cycle per minute. Granted, the change in temperature from minute to minute is very small. Therefore, for computer use, it is sufficient to calculate the temperature distribution and the accompanying stresses at intervals no smaller than one hour.

The finite element method can be a very powerful mathematical tool and was used in the development of the program FETAB. It was mentioned in the previous section that the first assumption used was that the temperature distribution along the longitudinal axis of the bridge is assumed to be constant. Figure 3.1 displays the coordinate system assumed in the development of FETAB. The basic equations used in the development of the programs FETAB have already been presented in Chapter 2.

It becomes apparent that when these equations are applied to an actual structure a set of simultaneous equations result with nodal temperatures as the unknown quantity. For computer solutions, the set of simultaneous equations is generated after the structure is modeled as an assemblage of nodes and elements. The total number of equations to be solved is governed by the total number of nodes and the degrees of freedom assumed at each node. This set of simultaneous equations is best partitioned in matrix form. Engineers, when using external gravity loads, typically solve the equations in the well

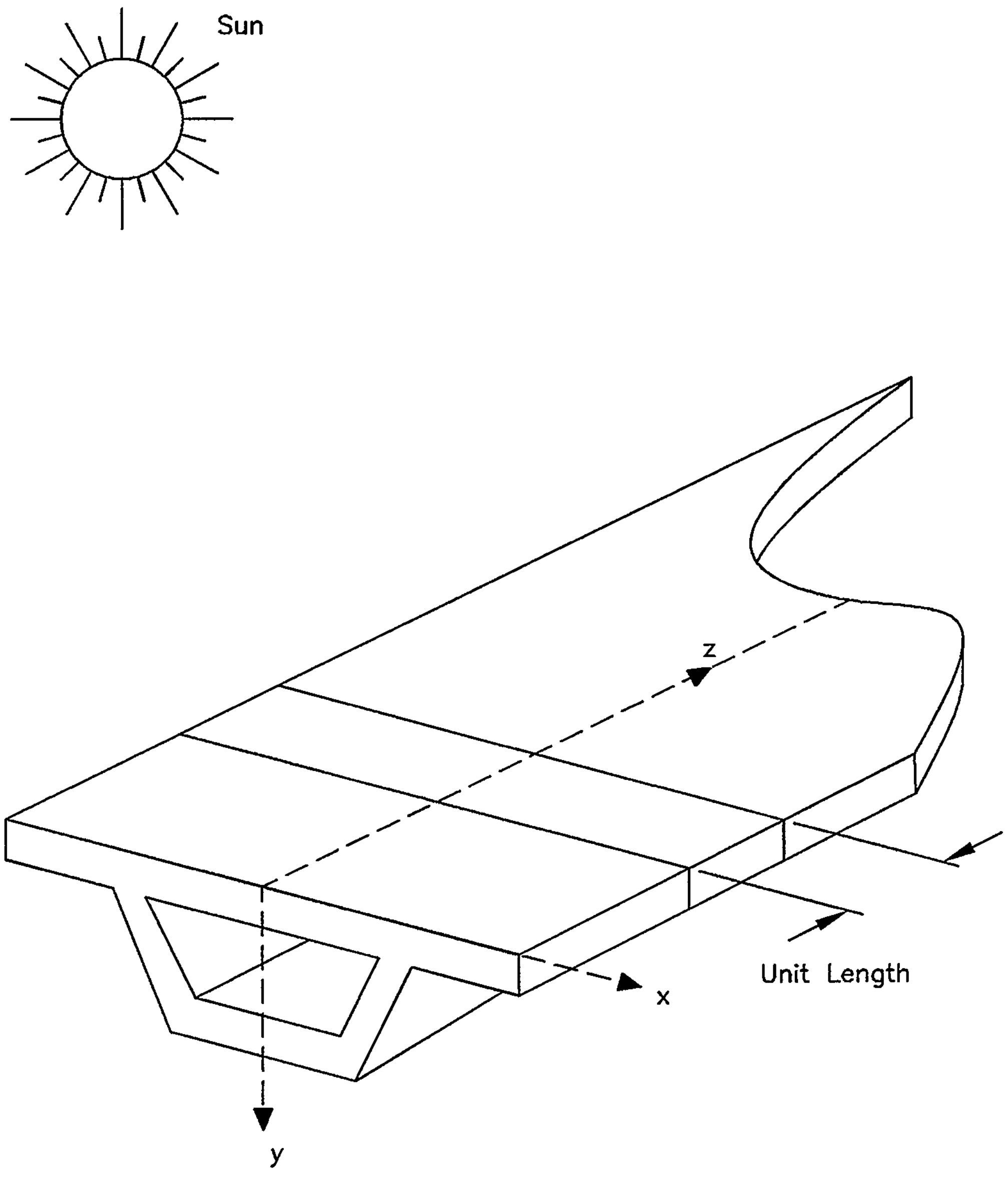

Figure 3.1 — FETAB Coordinate system

known form

$$[S]\{d\} = \{F\} \tag{3.1}$$

where,

[S] = the stiffness matrix of the structure

{d} = the unknown nodal displacements of the structures

{F} = the given forcing function

It should not come as a surprise that temperature loading may be considered in a similar manner:

$$[S_c]\{T\} = \{F\} \tag{3.2}$$

where,

$[S_c]$ = the heat conduction matrix of the structure

{T} = the unknown nodal temperatures of the structure

{F} = the forcing function - amount of heat flow at a given node

As per equation 2.5, the vector {F} becomes the sum of:

q_s = heat gain from solar radiation,

q_c = heat gain or loss due to and caused by the temperature difference between the air and the boundary surface, and

q_r = heat loss due to re-radiation from the boundary surface to the surrounding air.

The approach taken to generate the conduction matrix is similar to that of the stiffness matrix for gravity loads. Each element is assumed to have a given shape function. For temperature it may be shown that a linear shape function gives the best results.

For heat conduction the following equation applies:

$$[S_c^e] = -\int [B]^T\,[d]\,[B]\,dv \tag{3.3}$$

where,

$$[d] = \begin{bmatrix} k_x & 0 \\ 0 & k_y \end{bmatrix}, \text{ and}$$

[B] is derived by differentiating the shape functions.

The heat transfer equations must be modified for convection at any boundary surface as follows.

$$[S_c^e] = \int [N]^T h\, [N]\, ds \tag{3.4}$$

It is easier to visualize the computational method involved through the use of a simple example. Figure 3.2 shows a steel bar extending from a surface. The bar is made up of four single degree of freedom elements. It is assumed that the temperature at the connected end of the bar is 80°C and the surrounding air temperature is 20°C. Assuming that each element has the following linear shape functions:

$$[N_1] = [1 - x/L] \text{ and } [N_2] = [\, x/L] \tag{3.5}$$

After the conduction and convection components are summed the element conduction matrix becomes:

$$[S_c^e] = \begin{bmatrix} 6.667 & -5.333 & 0 & 0 & 0 \\ -5.333 & 13.333 & -5.333 & 0 & 0 \\ 0 & -5.333 & 13.333 & -5.333 & 0 \\ 0 & 0 & -5.333 & 13.333 & -5.333 \\ 0 & 0 & 0 & -5.333 & 7.066 \end{bmatrix} \frac{W}{{}^{o}C}$$

A more complete derivation of the conduction matrix is found in Appendix A.

The force vector for each element, $\{F^e\}$, may be computed by:

$$\{F^e\} = -\int [N]^T Q\, dv + \int [N]^T q\, ds - \int [N]^T T_a h\, ds \tag{3.6}$$

where,

Q = the quantity of heat generated within the body per second per unit volume .

q = heat flux = the quantity of heat per second per unit area.

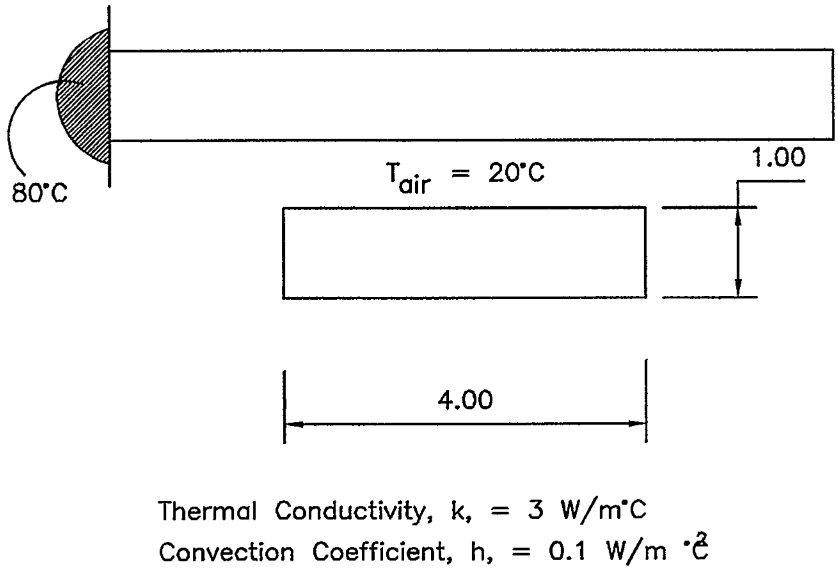

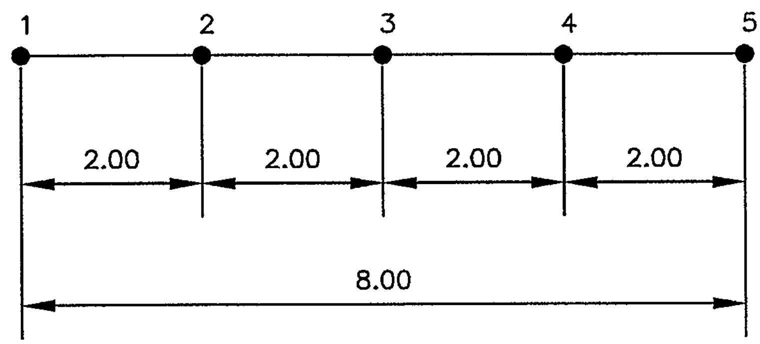

(a) – Five nodes, Four Elements

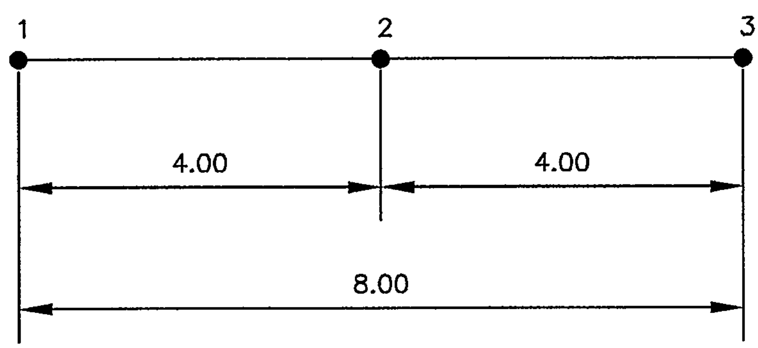

(b) – Three nodes, Two Elements

Figure 3.2 – Heat Transfer Example

h = the convection coefficient = the quantity of heat per second per unit area per unit temperature difference between surface area and heat.

It is important to note that heat flux and convection (the second and third terms) cannot occur over the same boundary area at the same time.

From this it may be shown that the final $\{F^e\}$ matrix becomes,

$$\{F^e\} = \{20 \;\; 40 \;\; 40 \;\; 40 \;\; 28\}^T \, W$$

now,

$$[S_c^e]\,\{T\} = \{F^e\} \tag{3.7}$$

Since it is known that $T_1 = 80°C$, eq. 3.2 may be reduced to,

$$\begin{bmatrix} -5.333 & 13.333 & -5.333 & 0 & 0 \\ 0 & -5.333 & 13.333 & -5.333 & 0 \\ 0 & 0 & -5.333 & 13.333 & -5.333 \\ 0 & 0 & 0 & -5.333 & 7.066 \end{bmatrix} \frac{W}{{}^oC} \begin{Bmatrix} T_2 \\ T_3 \\ T_4 \\ T_5 \end{Bmatrix} = \begin{Bmatrix} 493.333 \\ 40 \\ 40 \\ 28 \end{Bmatrix} W$$

which may be solved to obtain:

$$\{\,T\,\} = \{\,80,\; 53.95,\; 39.87,\; 32.81,\; 30.27\,\}°C$$

This example may be re-worked with two elements and three nodes instead of four elements and five nodes, see Figure 3.2, which results in,

$$\{\,T\,\} = \{\,80,\; 38.6,\; 29.18\,\}°C$$

Note that with half the number of nodes and elements a satisfactory level of accuracy is still obtained. In addition, this example may be re-worked using different shape functions. However, after using second and third order equations and even exponential functions, the linear shape function still gives the best results.

To model a bridge cross section, the computer program FETAB uses an assemblage of quadrilateral and/or triangular elements, see Figure 3.3. Hence, the conduction matrix must be determined in both x and y directions. Again, the convection matrix is determined for each boundary surface and added to the conduction matrix. In order to illustrate this procedure the previous example will again be presented. For ease of computation, two rectangular elements will be used to model the steel bar, see Figure 3.4.

The conduction and convection matrices, again, are summed. Then this new

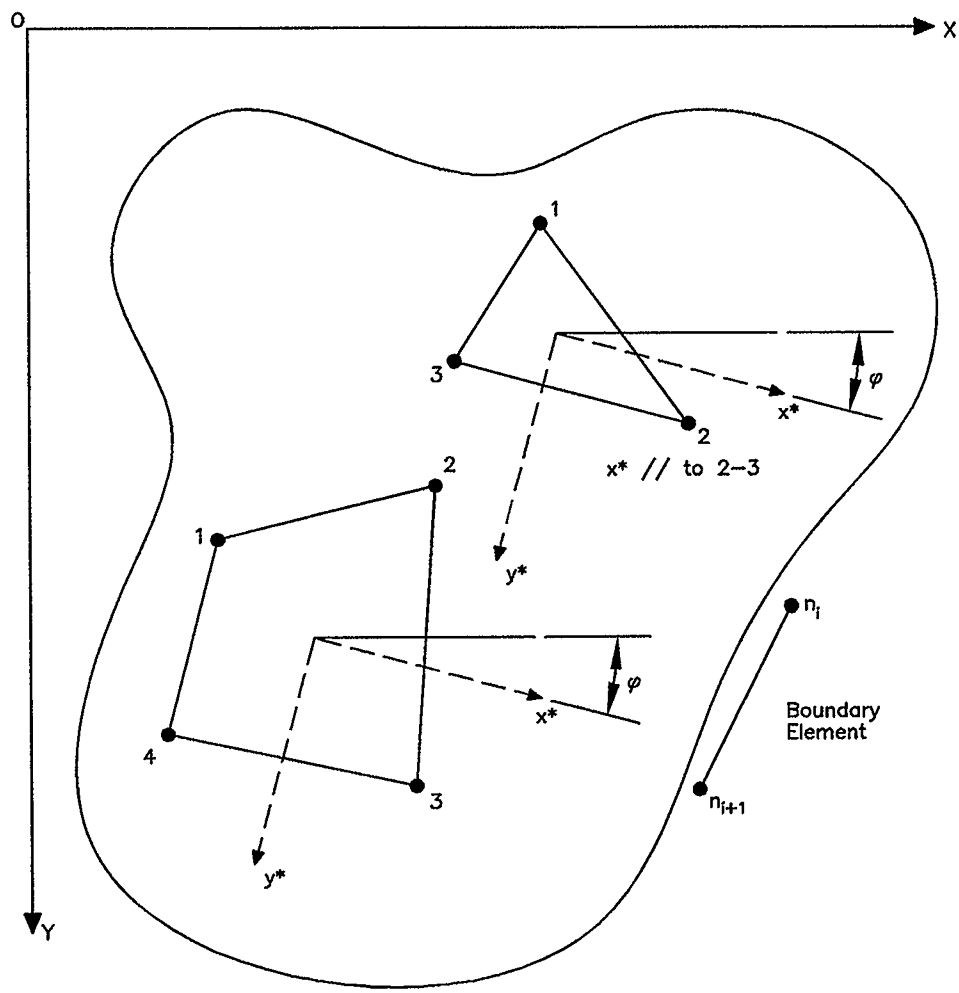

x*, y* Local Axis Corresponding to k' and k'
Note: For concrete $k'_x = k'_y$
X, Y Gobal Axis
φ = Orthotrophy Orientation of Element

Figure 3.3 – FETAB Element Types

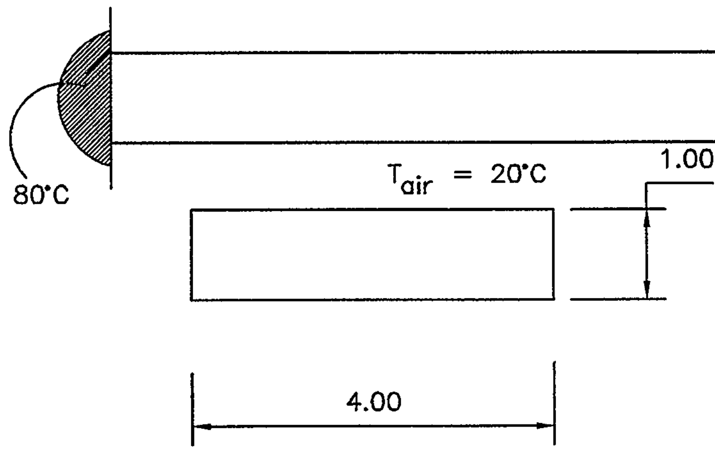

Thermal Conductivity, k, = 3 W/m°C
Convection Coefficient, h, = 0.1 W/m^2°C

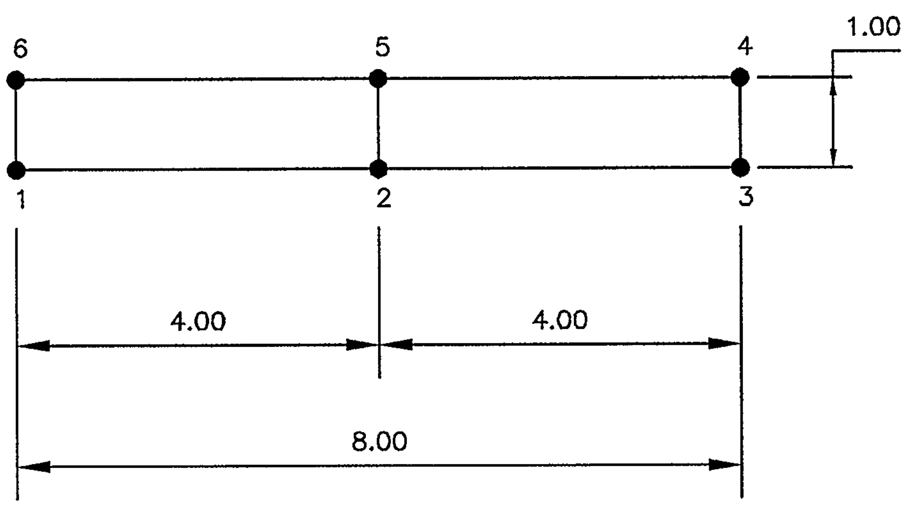

Six Nodes, Two elements

Figure 3.4 — Heat Transfer Example

conduction matrix must now be modified for the boundary surfaces around each element by a convection matrix. The convection matrix, which accounts for the boundary surfaces, depends on the shape function selected and may be determined by equation 3.4. Integrating this equation over the surface of each element will result in six matrices, one for each surface. The first element, 1256, has four surfaces exposed to the air while the second, 2345, has five surfaces. The resulting convection matrix is found in Appendix A.

The loading vector (forcing function) is determined in a similar manner. Going back to equation 3.6:

$$\{F^e\} = -\int [N]^T Q \, dv + \int [N]^T q \, ds - \int [N]^T T_a \, h \, ds \qquad (3.6)$$

Here, the first two terms are zero. After integrating the third term six vectors are obtained, one for each surface. As with the convection matrices there are four surfaces for element one and five for element two. The resulting load vector becomes:

$$\{F^e\} = \{\ 20, 40, 24, 24, 40, 20\}^T \,^\circ C$$

now equation 3.7 may be solved,

$$[S_c^e]\ \{T\} = \{F^e\} \qquad (3.7)$$

knowing that $T_1 = T_2 = 80^\circ C$ the equation 3.7 may be reduced and solved:

$$\{T\} = \{\ 80, 38.62, 29.18, 29.18, 38.62, 80\ \}^T \,^\circ C$$

which is the same as the result for two bar elements.

This example has been computed for steady state conditions. If a transient heat transfer problem is required, which is the purpose for developing a computer program such as FETAB, then an added term must be incorporated into equation 3.7.

$$[C] \frac{\delta}{\delta t} \{T\} + [S_c^e]\ \{T\} = \{F^e\} \qquad (3.8)$$

where $\delta/\delta t$ is of course a derivative with respect to time, and [C] is a capacitance matrix

$$[C] = \int \rho \, c \, [N]^T [N] \, dv \qquad (3.9)$$

where ρ = density and

c = specific heat

In order to perform a transient analysis, initial temperatures are assumed. Environmental data is required, such as the location (latitude and elevation), maximum and minimum daily temperatures and orientation of the bridge axis. For the program FETAB, the starting time is specified, and from the environmental data a set a initial temperatures are computed. On the second time step the term [C] $\delta\{T\}/\delta t$ is determined by the difference between the initial temperatures and those newly calculated. After the analysis has been performed for three days (72 hours) the nodal temperatures have usually stabilized.

For each time step, if desired, the nodal temperatures and self-equilibrating "Eigen" stresses are printed out along with the stress resultants, N_o, M_{ox}, M_{oy} and resulting longitudinal strain and curvatures.

This completes a brief summary of the important points in the development of the program FETAB.

3.3 SFRAME for Windows

After a cross section of the structure has been modeled using the program FETAB and the desired strains and curvatures have been obtained, the engineer may use this output in a frame analysis. The analysis of a Plane Frame with a few degrees of freedom by hand is manageable. However, to analyze a structure of sizable magnitude, especially a Space Frame of some size, with many degrees of freedom the use of a computer is necessary. The use a of Space Frame computer program is necessary when the temperature distribution across a section is not constant such that ΔM_y has a magnitude other than zero. This will result in deformations in all three directions.

In order to model the structural response of the Confederation Bridge the standard version of the computer program SFRAME for Windows, by Softek Services Ltd., was used. There are three versions of the program SFRAME: the standard, the enterprise and the professional editions. The standard edition performs a linear elastic analysis, while the other two editions of the program perform a variety of other features including dynamic, vibration, buckling and moving load analysis. This program performs a three dimensional structural analysis, which assists in determining the structural response due to temperature distributions through the depth and in the transverse direction.

3.4 Computer Model for the Confederation Bridge Structure

3.4.1 Description of the Confederation Bridge

The main portion of the Confederation Bridge is made up of 46 consecutive spans; each span being 250m in length. Every second span contains a drop in section with simply supported ends. Hence the structural behaviour of the bridge may be modelled by analyzing one span as a portal frame complete with cantilever spans of 95m to either side, see Figure 3.5.

3.4.2 Description of the Computer Model

The bridge is constructed with tapered precast concrete elements to form a haunched girder. In addition, the pier columns are constructed using precast concrete sections. As shown in Figure 3.5, eight girder segments are centred about a pier section. On one side they are labelled H1 to H8 to signify "hinged", the other side are labelled C1 to C8 to signify "continuous". The continuous side segments are joined by a 52m long drop-in section. This section is grouted in place with a 1.5m cast-in-place joint making the drop-in section continuous with the adjacent sections. Similarly, the hinged side segments are joined with a drop-in section supported by bearing seats cast against the H8 sections.

Figure 3.6 shows the dimensions of segments C1 to C8. Note that the segments H1 to H8, for all intensive purposes, are mirror images of segments C1 to C8. Note that in this figure there are cross section marks, S1 and S5, for each end of the segment. These cross section labels shown indicate the position of nodes used in the final computer model. It is important to note that the nodes are located at the neutral axis of

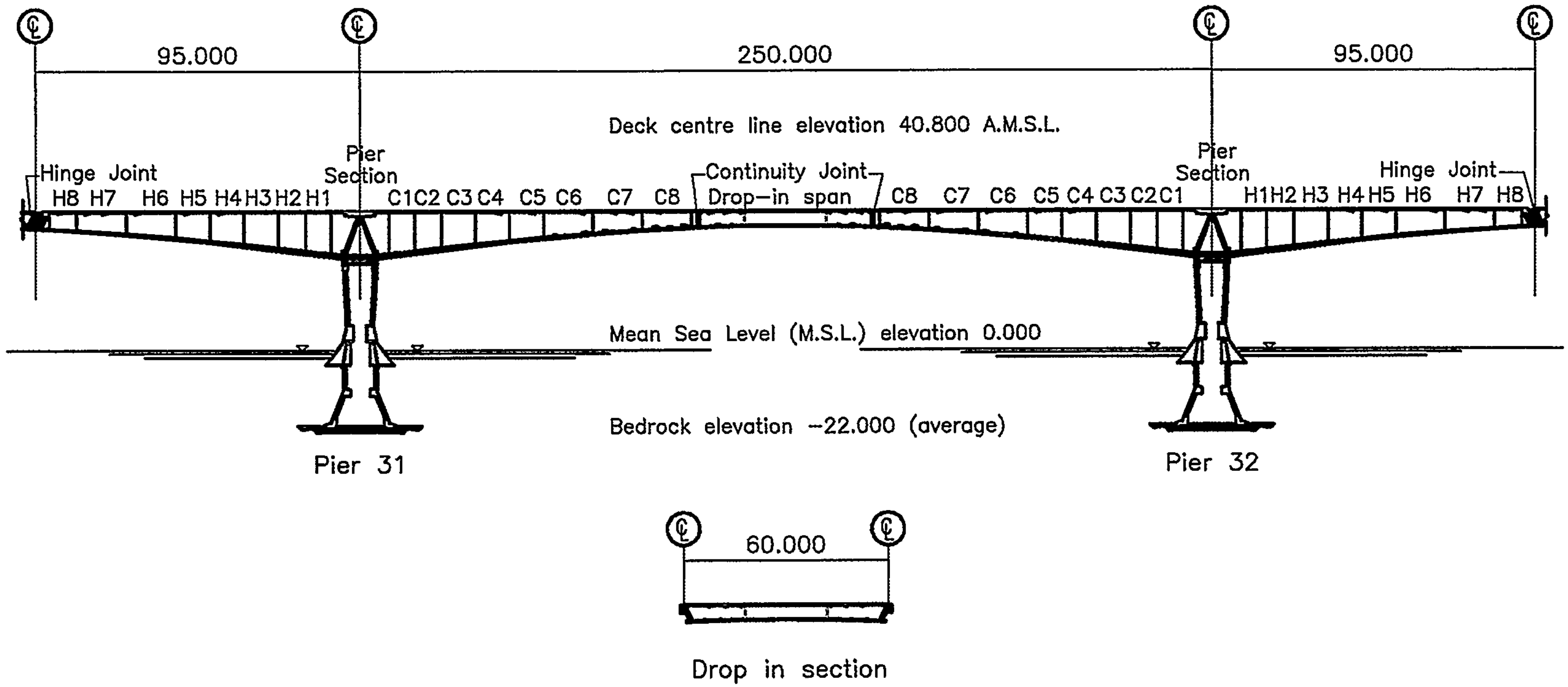

All dimensions are m

Figure 3.5 General Arrangement

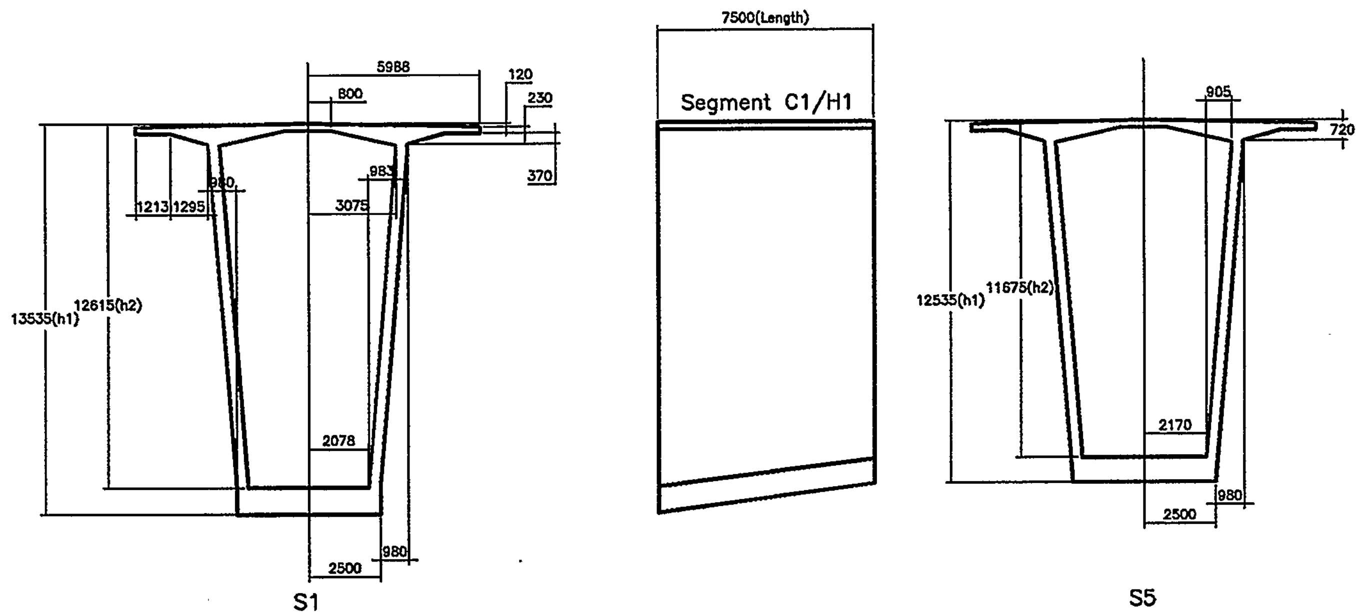

Segment		Deep End		Shallow End		
Segment	Length	h1	h2	h1	h2	Wall thickness
C2/H2	8000	12535	11675	11525	10730	400
C3/H3	10000	11525	11675	10325	9610	400
C4/H4	10000	10325	9610	9215	8580	400
C5/H5	10000	9215	8580	8200	7645	350
C6/H6	14500	8200	7645	6915	6475	350
C7/H7	14500	6915	6475	5870	4830	350
C8	14500	5870	4830	5094	4774	350
H8	10000	5870	4830	4951	4485	350
Pier section	17000	13990	13037	13525	12615	400
Drop in span	60000	5152	4832	4500	4180	300

Figure 3.6 Precast Concrete box Girder Segments. Dimensions in mm.

each cross section.

Figures 3.7 displays a view of the pier column, which is supported by a conical foundation cast into a trench dug in the strait's bedrock. On top of the footing section sits an ice shield, shaped like an antique cattle scoop on a train locomotive, designed to break the ice by allowing it to act as a *ice wedge* in the middle of the strait. The top of the ice shield section is again circular, upon which is mounted the pier column extending to the under side of the longitudinal bridge girder. The pier column tapers and changes shape. The lower end is circular to fit the top of the ice shield, while the upper end is rectangular to match the pier template on the under side of the main girder.

Figure 3.8 shows a section through the upper portion of the ice shield and footing, complete with a table containing the dimensions of each section. The pier column bears on top of the ice shield. It changes shape from the top of the ice shield, which is circular with an outer diameter of 8000 mm and an inner diameter of 3800 mm, to the under side of the girder at the pier section, which is rectangular in shape. The top of the pier column, directly under the girder, measures 5190 mm by 10,000 mm, see Figure 3.9.

Before any analysis can begin, the section properties of each segment must first be obtained. Therefore a computer program was written, for which all significant dimensions were input, to calculate the gross area, shear areas, torsional constant and moments of inertia. A similar computer program was written to calculate the section properties for the footing sections and the pier shaft sections. To model the structural behaviour of the pier shaft, the ice shield portion of the shaft has been neglected. This part of the section, although vital to break up the ice forces in the strait, offers little to the over all structural rigidity of the pier.

This completes the sections contained in the main girder. The remaining two portions of the bridge are the hinged drop-in section and the continuous drop-in section. Table 3.1 contains the cross section properties for the many sections used to model the girders, the pier column and the footings.

Referring again to Figure 3.5, it is important to mention that nodes for the main

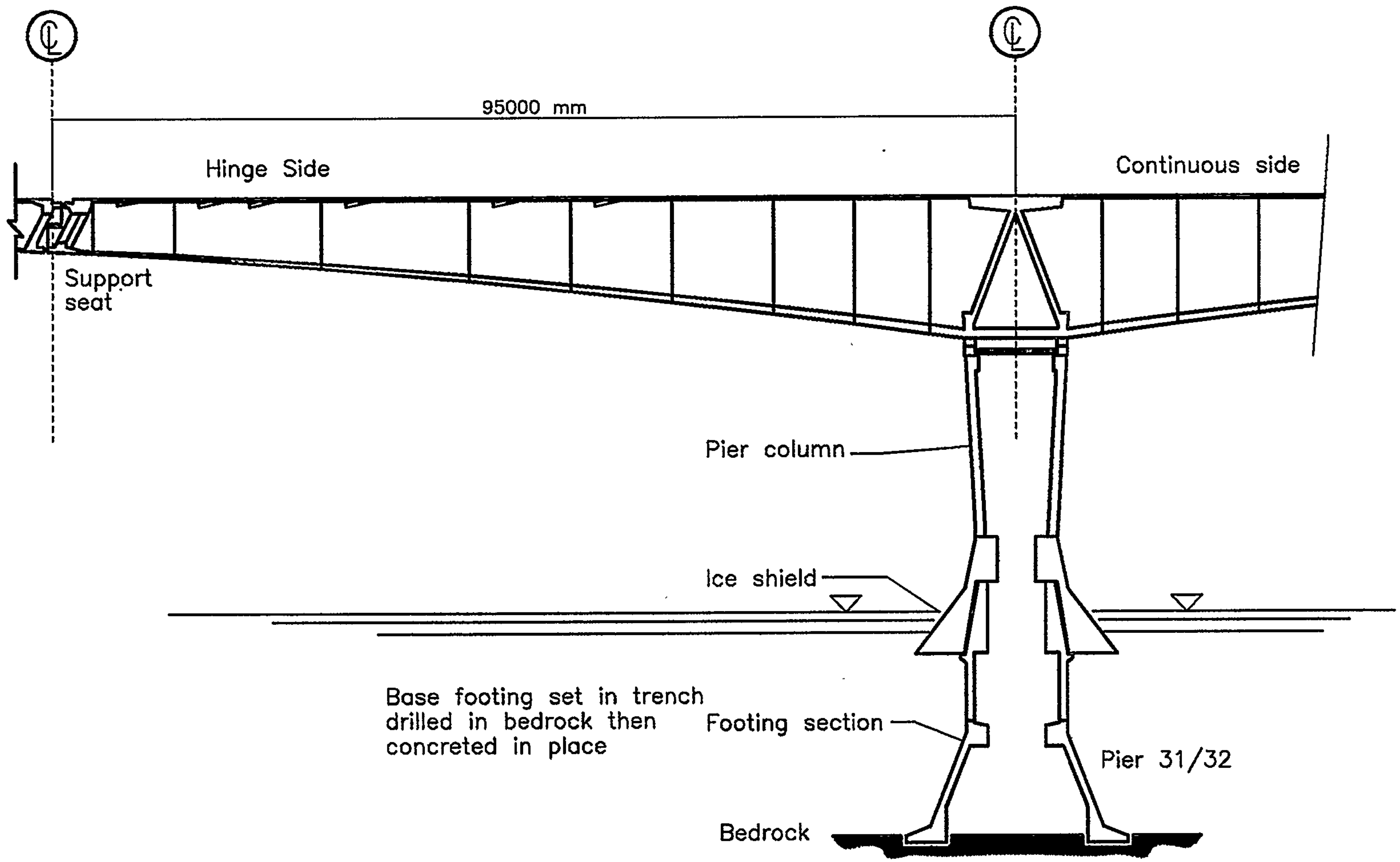

Figure 3.7 Pier Column

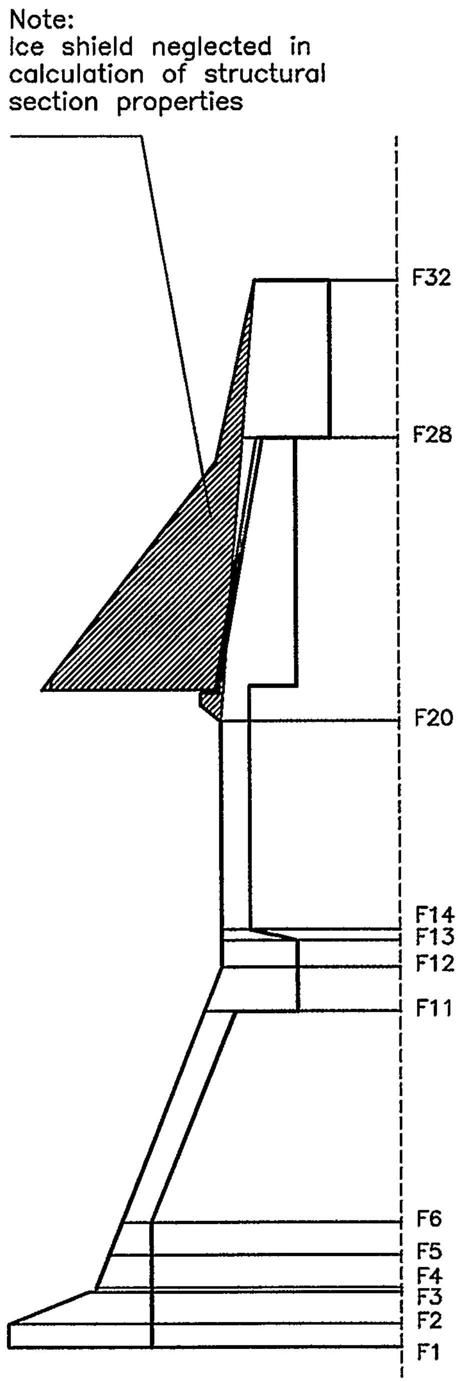

Footing Section	Outside radius (mm)	Inside radius (mm)
F1	11000	7000
F2	11000	7000
F3	8750	7000
F4	8545	7000
F5	8187	7000
F6	7824	7000
F11	5491	2875
F12	5000	2875
F13	5000	2875
F14	5000	4200
F20	5000	4200
F28	4355	1900
F32	4000	1900

Figure 3.8 Footing Upper Sections for Computer Model

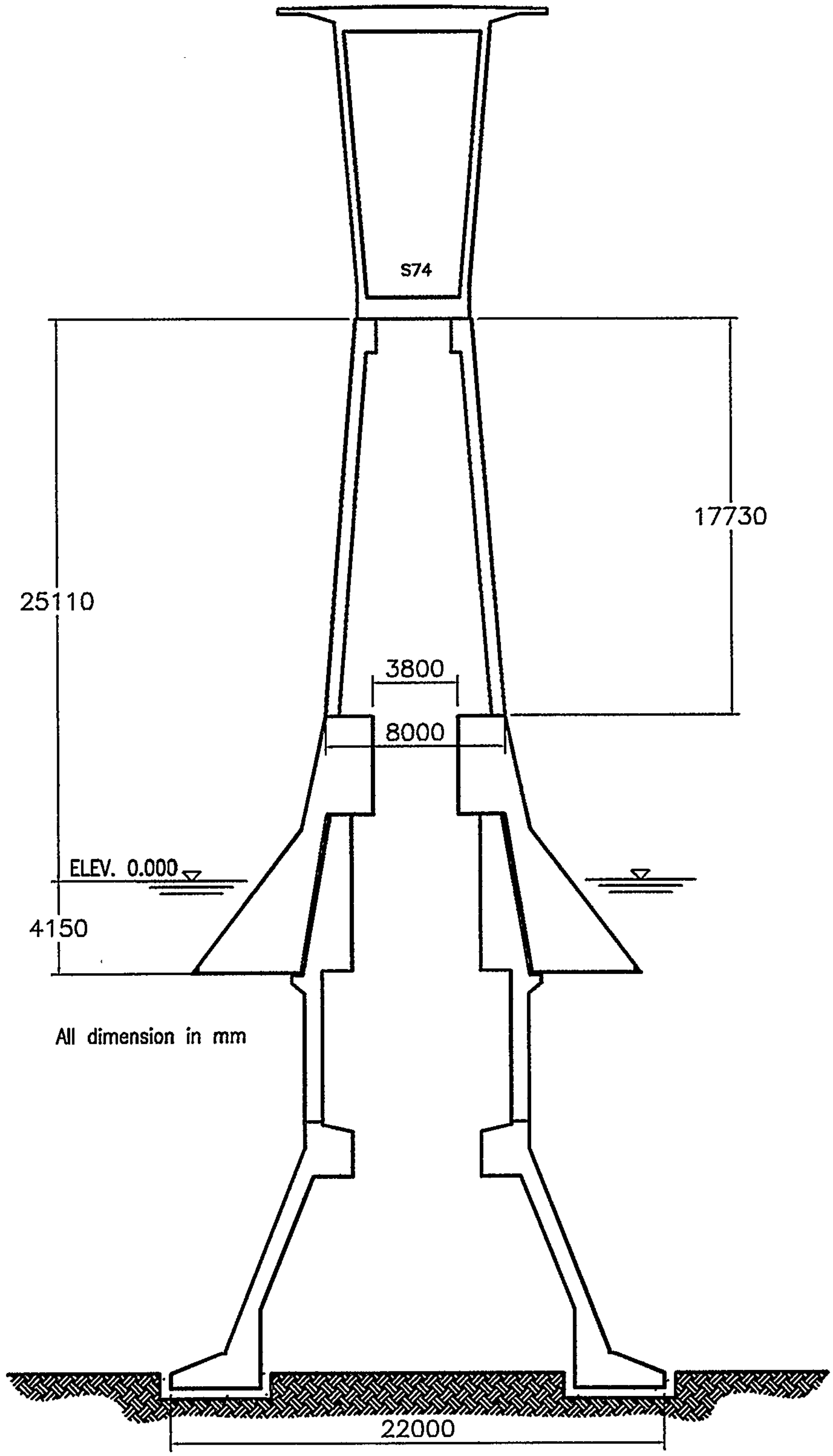

Figure 3.9 Pier Shaft Along Bridge Axis

Section	Area	Zbar	Ary	Arz	Jx	Iy	Iz
	m2	m	m2	m2	m4	m4	m4
S1	20.000	6.770	7.350	26.500	224.000	509.000	145.000
S2	19.400	6.600	7.350	26.000	219.000	481.000	141.000
S3	19.000	6.450	7.350	25.500	214.000	458.000	138.000
S4	18.600	6.310	7.350	25.100	209.000	435.000	135.000
S5	17.900	6.080	7.050	24.600	204.000	405.000	132.000
S6	17.700	5.960	7.050	24.100	198.000	385.000	130.000
S7	17.500	5.830	7.050	23.600	192.000	367.000	128.000
S8	17.000	5.620	6.730	23.100	186.000	341.000	126.000
S9	16.800	5.500	6.730	22.600	180.000	324.000	125.000
S10	16.600	5.350	6.730	22.000	174.000	304.000	123.000
S11	15.900	5.090	6.330	21.400	166.000	276.000	120.000
S12	15.700	4.950	6.330	20.800	159.000	258.000	119.000
S13	15.500	4.810	6.330	20.200	153.000	241.000	117.000
S14	15.300	4.680	6.330	19.700	147.000	226.000	115.000
S15	15.100	4.550	6.330	19.200	141.000	211.000	114.000
S16	14.500	4.300	5.930	18.600	134.000	190.000	111.000
S17	14.300	4.170	5.930	18.100	128.000	177.000	109.000
S18	14.100	4.050	5.930	17.600	123.000	186.000	108.000
S19	13.900	3.940	5.930	17.100	118.000	155.000	106.000
S20	13.700	3.820	5.930	16.600	112.000	145.000	105.000
S21	13.100	3.590	5.530	16.100	106.000	129.000	102.000
S22	12.900	3.470	5.530	15.600	101.000	119.000	101.000
S23	12.700	3.360	5.530	15.100	95.700	110.000	99.200
S24	12.500	3.240	5.530	14.600	90.700	102.000	97.600
S25	12.400	3.120	5.530	14.100	85.700	93.600	96.100
S26	11.600	2.850	4.950	13.600	78.700	79.300	93.200
S27	11.400	2.760	4.950	13.100	74.900	73.700	91.900
S28	11.300	2.670	4.950	12.700	71.100	68.400	90.700
S29	10.500	2.400	4.350	12.300	63.900	56.700	88.000
S30	10.200	2.290	4.350	11.900	60.600	51.800	86.200

Table 3.1 - Section Properties

S31	10.100	2.210	4.350	11.500	57.100	47.700	85.000
S32	9.990	2.160	4.350	11.300	55.300	45.500	84.300
S33	9.910	2.120	4.350	11.100	53.500	43.400	83.700
S34	9.830	2.080	4.350	10.900	51.700	41.400	83.000
S35	9.750	2.030	4.350	10.600	49.900	39.500	82.400
S36	9.670	1.990	4.350	10.400	48.200	37.600	81.700
S37	9.590	1.940	4.350	10.200	46.400	35.700	81.100
S38	9.510	1.900	4.350	9.980	44.700	33.900	80.500
S39	9.460	1.870	4.350	9.820	43.500	43.600	80.000
S40	9.400	1.840	4.350	9.680	42.300	31.400	79.500
S41	9.350	1.810	4.350	9.530	41.200	30.300	79.100
S42	9.300	1.780	4.350	9.400	40.200	29.300	78.700
S43	9.260	1.760	4.350	9.290	39.300	28.500	78.400
S44	9.220	1.740	4.350	9.180	38.500	27.700	78.100
S45	9.180	1.720	4.350	9.080	37.800	27.000	77.800
S46	9.160	1.710	4.350	9.020	37.300	26.500	77.600
S47	0.914	1.690	4.350	8.950	36.800	26.000	77.400
S48	9.110	1.680	4.350	8.890	36.300	25.600	77.200
S49	9.110	1.680	4.350	8.870	36.200	25.500	77.100
S50	9.100	1.670	4.350	8.840	36.000	25.300	77.100
S51	9.090	1.670	4.350	8.820	35.900	25.100	77.000
S52	9.990	2.160	4.350	11.300	55.200	45.500	84.300
S53	9.910	2.120	4.350	11.100	53.400	43.300	83.600
S54	9.830	2.070	4.350	10.800	51.500	41.300	83.000
S55	9.740	2.030	4.350	10.600	49.700	39.300	82.300
S56	16.800	2.130	6.740	8.680	92.900	51.900	11.100
S57	8.170	1.370	2.480	2.550	4.500	4.550	31.300
S58	14.600	0.894	7.980	1.840	4.650	6.710	139.000
S59	9.560	1.920	4.350	10.100	45.600	34.800	80.800
S60	9.490	1.890	4.350	9.910	44.100	33.300	80.200
S61	9.420	1.850	4.350	9.740	42.800	31.900	79.700
S62	9.370	1.820	4.350	9.600	41.700	30.800	79.300

Table 3.1 - Section Properties

S63	9.310	1.790	4.350	9.430	40.400	29.500	78.800
S64	9.260	1.760	4.350	9.300	39.400	28.600	78.400
S65	9.220	1.740	4.350	9.170	38.500	27.600	78.000
S66	9.180	1.720	4.350	9.070	37.700	26.900	77.700
S67	9.150	1.700	4.350	9.000	37.200	26.400	77.500
S68	9.130	1.690	4.350	8.940	36.700	26.000	77.400
S69	9.110	1.680	4.350	8.880	36.300	25.600	77.200
S70	9.100	1.680	4.350	8.860	36.200	25.400	77.100
S71	9.100	1.670	4.350	8.840	36.000	25.300	77.100
S72	9.100	1.690	4.400	8.820	36.200	25.400	76.900
S73	20.400	6.910	7.350	27.000	229.000	534.000	147.000
S74	25.200	6.980	9.580	27.400	324.000	703.000	167.000
S75	26.400	7.140	10.600	27.400	345.000	733.000	171.000
S76	27.900	7.320	11.800	27.400	364.000	764.000	175.000
Pier TMP	22.200	0.000	9.450	12.700	194.000	287.000	82.000
P1	26.800	0.000	11.200	15.700	215.000	318.000	92.500
P2	30.800	0.000	10.900	18.500	274.000	348.000	121.000
P3	20.200	0.000	9.150	9.730	239.000	260.000	103.000
P4	22.700	0.000	8.710	13.100	189.000	242.000	81.500
P5	19.800	0.000	8.270	7.760	292.000	242.000	126.000
P6	19.700	0.000	7.830	6.780	310.000	232.000	137.000
P7	19.500	0.000	7.390	5.790	322.000	222.000	146.000
P8	19.300	0.000	6.950	4.800	327.000	211.000	155.000
P9	19.100	0.000	6.500	3.820	325.000	199.000	161.000
P10	19.000	0.000	6.060	2.830	317.000	188.000	165.000
P11	18.800	0.000	5.620	1.840	302.000	177.000	168.000
F1	226.000	0.000	189.000	189.000	19,200.000	9,610.000	9,610.000
F2	226.000	0.000	189.000	189.000	19,200.000	9,610.000	9,610.000
F3	86.600	0.000	72.200	72.200	5,440.000	2,720.000	2,720.000
F4	86.600	0.000	72.200	72.200	5,440.000	2,720.000	2,720.000
F5	56.600	0.000	47.200	47.200	3,290.000	1,640.000	1,640.000
F6	38.400	0.000	32.000	32.000	2,120.000	1,060.000	1,060.000

Table 3.1 - Section Properties

F7	36.300	0.000	30.200	30.200	1,750.000	877.000	877.000
F8	34.200	0.000	28.500	28.500	1,440.000	7,190.000	7,190.000
F9	32.000	0.000	26.700	26.700	1,160.000	579.000	579.000
F10	29.800	0.000	24.800	24.800	915.000	458.000	458.000
F11	68.800	0.000	57.300	57.300	132.000	660.000	660.000
F12	52.600	0.000	43.800	43.800	874.000	437.000	437.000
F13	52.600	0.000	43.800	43.800	874.000	437.000	437.000
F14	23.100	0.000	19.300	19.300	493.000	247.000	247.000
F15	23.100	0.000	19.300	19.300	493.000	247.000	247.000
F16	23.100	0.000	19.300	19.300	493.000	247.000	247.000
F17	23.100	0.000	19.300	19.300	493.000	247.000	247.000
F18	23.100	0.000	19.300	19.300	493.000	247.000	247.000
F19	23.100	0.000	19.300	19.300	493.000	247.000	247.000
F20	23.100	0.000	19.300	19.300	493.000	247.000	247.000
F21	50.100	0.000	41.700	41.700	812.000	406.000	406.000
F22	47.600	0.000	39.700	39.700	754.000	377.000	377.000
F23	45.200	0.000	37.600	37.600	698.000	349.000	349.000
F24	42.800	0.000	35.600	35.600	644.000	322.000	322.000
F25	40.400	0.000	33.700	33.700	594.000	297.000	297.000
F26	38.100	0.000	31.800	31.800	546.000	273.000	273.000
F27	35.800	0.000	29.900	29.900	500.000	250.000	250.000
F28	48.200	0.000	40.200	40.200	545.000	272.000	272.000
F29	45.800	0.000	38.200	38.200	500.000	250.000	250.000
F30	43.500	0.000	36.200	36.200	458.000	229.000	229.000
F31	41.200	0.000	34.300	34.300	419.000	209.000	209.000
F32	38.900	0.000	32.400	32.400	382.000	191.000	191.000

Table 3.1 - Section Properties

girder were placed at the cross sections neutral axis, thus properly representing the geometry of the tapered cross sections. Figure 3.10 contains a line drawing through the nodes showing the arched geometry, the global axis and the local axis. In the global coordinate system the X axis was taken as the centreline of the top slab of the box girder section, the Y and Z global axis follow using the right hand rule with the positive direction of the Z axis being vertical towards the sky. Table 3.2 contains the coordinates for all nodes used in the computer model.

3.5 Computer Model for the Confederation Bridge Cross Sections

With the structural properties of the Confederation Bridge modeled using the computer program SFRAME, it is necessary to generate load vectors. SFRAME, like many structural computer programs, analyzes for a linear temperature variation through the depth of a member, in either the 'y' or 'z' local axis. However, as discussed earlier, the temperature variation through the depth or across a member is normally non-linear. For the Confederation Bridge the situation is complicated further due to the variable depth of cross section.

The computer program FETAB uses an assemblage of finite elements to model a cross section. A transient analysis may be performed, from which hourly nodal temperatures and self equilibrating "eigen" stresses are tabulated. In addition, the longitudinal strains and curvatures are tabulated each hour. Therefore, in order to obtain curvatures for input into the computer programs SFRAME, a number of cross sections must be modeled so that the variable cross section depth is taken into account.

As shown in Figure 3.5, the Bridge is symmetrical about the centreline of the piers. The continuous side segments C1 to C7 are virtually the same as the hinge side segments H1 to H7. This reduces the number of cross sections that need to be modeled. Nodes for the structural behaviour were chosen at the segment boundaries and at the anchor block locations for the post-tensioned cables. Therefore it is sufficient to choose the cross sections at the segment boundaries to model with FETAB. Figure 3.11 contains cross sections utilized with FETAB, while Table 3.3 contains a listing of the

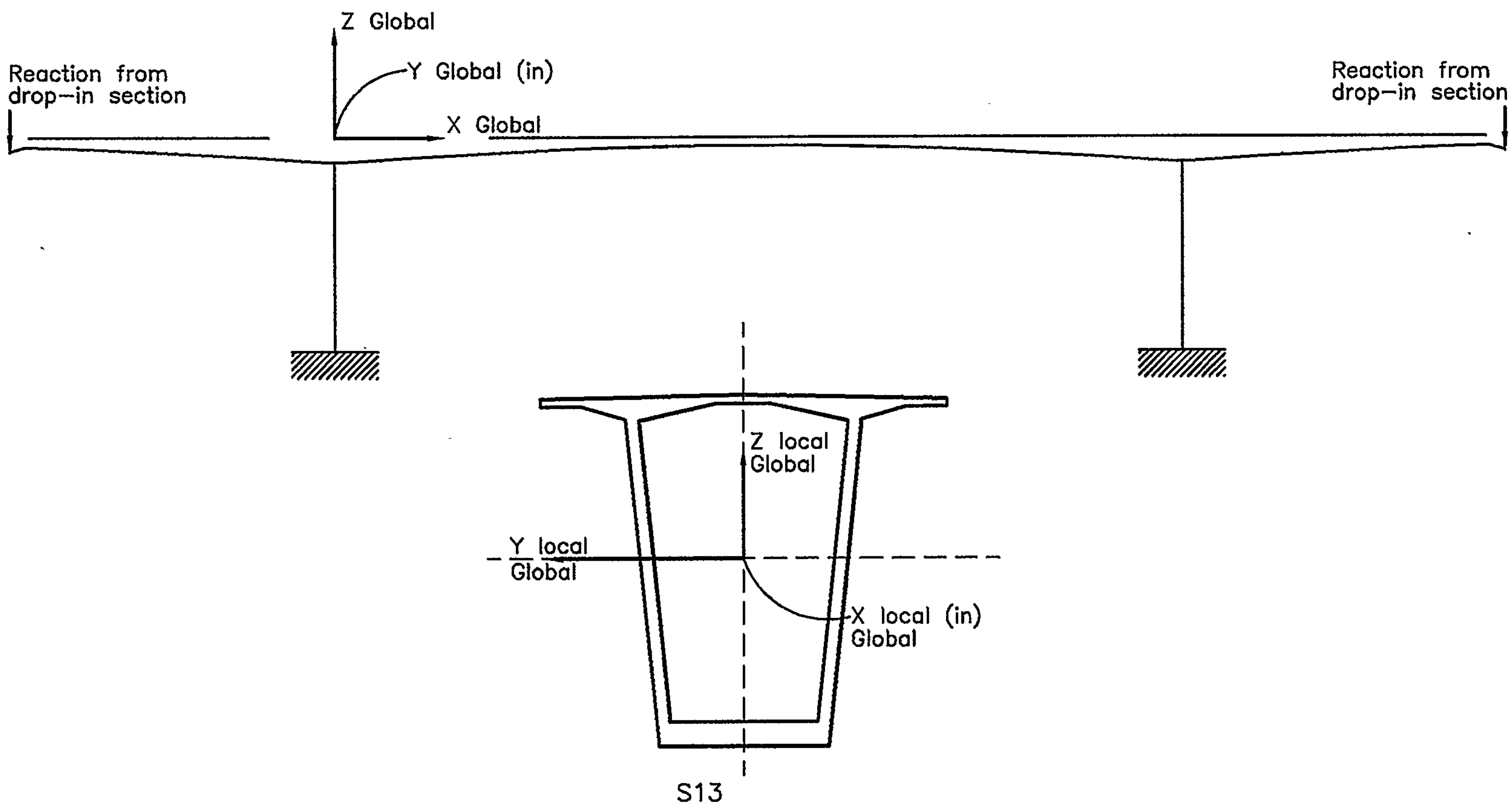

Figure 3.10 Computer model with global and local axis

Node	X(m)	Y(m)	Z(m)	Node	X(m)	Y(m)	Z(m)
1	-95.00	0	-4.125	45	112.40	0	-1.719
2	-93.00	0	-2.133	46	114.50	0	-1.706
3	-91.00	0	-2.026	47	125.00	0	-1.668
4	-89.00	0	-2.072	48	135.50	0	-1.706
5	-83.00	0	-2.208	49	137.60	0	-1.719
6	-80.10	0	-2.293	50	139.70	0	-1.739
7	-74.30	0	-2.666	51	141.80	0	-1.76
8	-68.50	0	-2.847	52	143.90	0	-1.782
9	-65.60	0	-3.124	53	146.00	0	-1.809
10	-54.00	0	-3.588	54	148.10	0	-1.838
11	-51.50	0	-3.818	55	150.30	0	-1.867
12	-44.00	0	-4.172	56	152.50	0	-1.899
13	-41.50	0	-4.301	57	154.40	0	-1.943
14	-34.00	0	-4.809	58	158.60	0	-2.031
15	-24.00	0	-5.499	59	160.70	0	-2.075
16	-16.00	0	-6.082	60	162.80	0	-2.119
17	-8.50	0	-6.766	61	167.00	0	-2.208
18	-4.50	0	-6.975	62	169.90	0	-2.293
19	0.00	0	-7.319	63	175.70	0	-2.666
20	4.50	0	-6.975	64	181.50	0	-2.847
21	8.50	0	-6.766	65	184.40	0	-3.124
22	16.00	0	-6.082	66	196.00	0	-3.588
23	24.00	0	-5.499	67	198.50	0	-3.818
24	34.00	0	-4.809	68	206.00	0	-4.172
25	41.50	0	-4.301	69	208.50	0	-4.301
26	44.00	0	-4.172	70	216.00	0	-4.809
27	51.50	0	-3.818	71	226.00	0	-5.499
28	54.00	0	-3.588	72	234.00	0	-6.082
29	65.60	0	-3.124	73	241.50	0	-6.766
30	68.50	0	-2.847	74	245.50	0	-6.975
31	74.30	0	-2.666	75	250.00	0	-7.319
32	80.10	0	-2.293	76	254.50	0	-6.975
33	83.00	0	-2.208	77	258.50	0	-6.766
34	87.20	0	-2.119	78	266.00	0	-6.082
35	89.30	0	-2.075	79	274.00	0	-5.499
36	91.40	0	-2.031	80	284.00	0	-4.809
37	95.60	0	-1.943	81	291.50	0	-4.301
38	97.50	0	-1.899	82	294.00	0	-4.172
39	99.70	0	-1.867	83	301.50	0	-3.818
40	101.90	0	-1.838	84	304.00	0	-3.588
41	104.00	0	-1.809	85	315.60	0	-3.124
42	106.10	0	-1.782	86	318.50	0	-2.847
43	108.20	0	-1.76	87	324.30	0	-2.666
44	110.30	0	-1.739	88	330.10	0	-2.293

Table 3.2 - Nodal Coordinates

Node	X(m)	Y(m)	Z(m)
89	333.00	0	-2.208
90	339.00	0	-2.072
91	341.00	0	-2.026
92	343.00	0	-2.133
93	345.00	0	-4.125
94	0.00	0	-13.99
95	0.00	0	-15.69
96	0.00	0	-19.17
97	0.00	0	-22.794
98	0.00	0	-26.346
99	0.00	0	-29.898
100	0.00	0	-33.45
101	0.00	0	-37.85
102	0.00	0	-45.85
103	0.00	0	-51.705
104	0.00	0	-52.015
105	0.00	0	-52.767
106	0.00	0	-54.015
107	0.00	0	-59.945
108	0.00	0	-60.869
109	0.00	0	-61.794
110	0.00	0	-61.9
111	0.00	0	-62.8
112	0.00	0	-63.45
113	250.00	0	-13.99
114	250.00	0	-15.69
115	250.00	0	-19.17
116	250.00	0	-22.794
117	250.00	0	-26.346
118	250.00	0	-29.898
119	250.00	0	-33.45
120	250.00	0	-37.85
121	250.00	0	-45.85
122	250.00	0	-51.705
123	250.00	0	-52.015
124	250.00	0	-52.767
125	250.00	0	-54.015
126	250.00	0	-59.945
127	250.00	0	-60.869
128	250.00	0	-61.794
129	250.00	0	-61.9
130	250.00	0	-62.8
131	250.00	0	-63.45

Table 3.2 - Nodal Coordinates

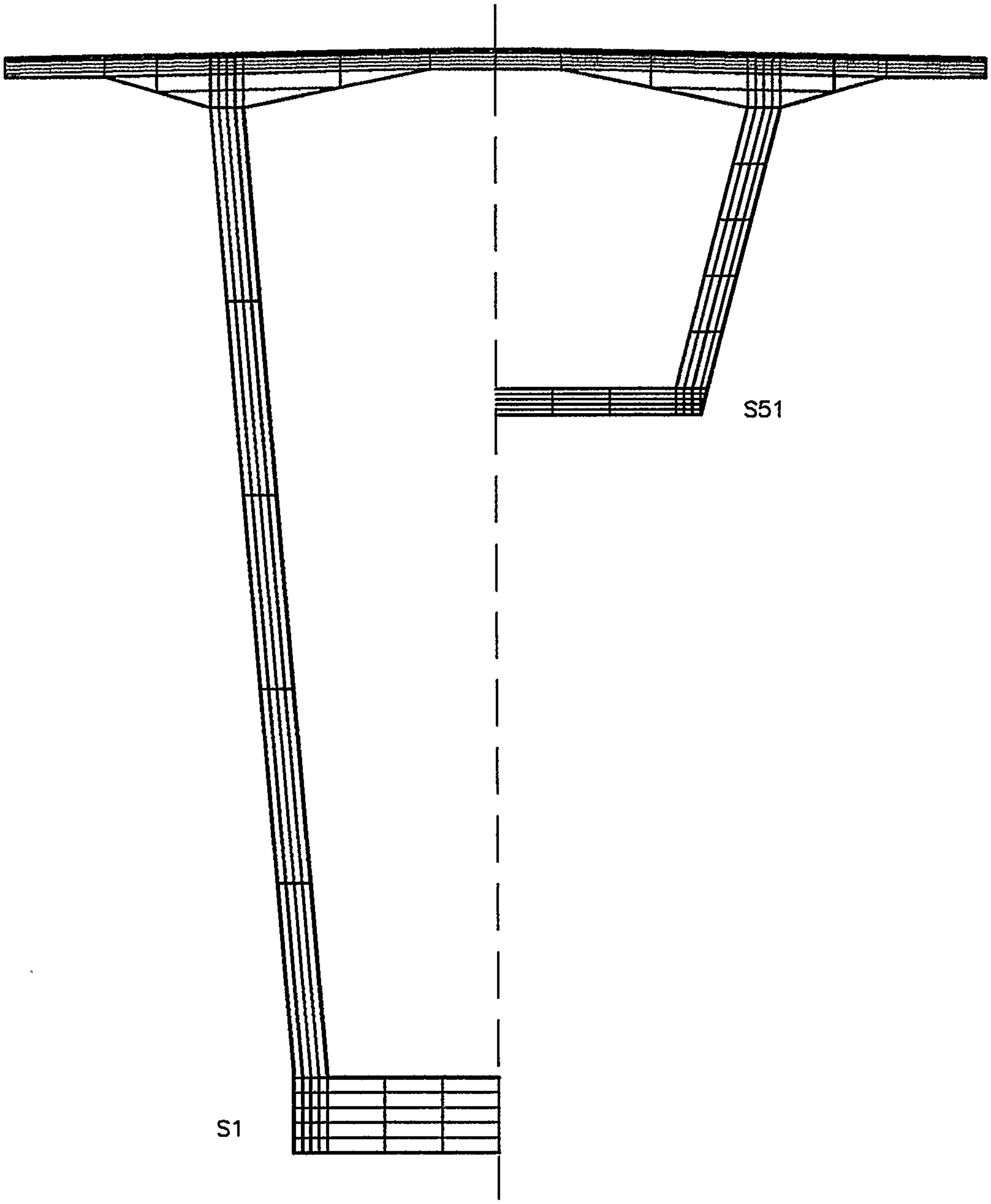

Figure 3.11 FETAB mesh for Section S1 and S51.
FETAB meshs for Sections S5, S9, S13, S17, S21,
S26, S31, S35, S38 and S45 (not shown)
correspond to the boundaries between the precast segments

Node	Section	Fetab	Node	Section	Fetab	Node	Section	Fetab
1	57	51	44	44	45	87	28	31
2	56	51	45	45	45	88	30	31
3	55	51	46	46	45	89	31	31
4	54	51	47	51	51	90	54	51
5	31	31	48	46	45	91	55	51
6	30	31	49	45	45	92	56	51
7	28	31	50	44	45	93	57	51
8	26	26	51	43	45			
9	25	26	52	42	45			
10	21	21	53	41	38			
11	20	21	54	40	38			
12	17	17	55	39	38			
13	16	17	56	38	38			
14	13	13	57	37	38			
15	9	9	58	35	38			
16	5	5	59	34	31			
17	1	1	60	33	31			
18	74	1	61	31	31			
19	76	1	62	30	31			
20	74	1	63	28	31			
21	1	1	64	26	26			
22	5	5	65	25	26			
23	9	9	66	21	21			
24	13	13	67	20	21			
25	16	17	68	17	17			
26	17	17	69	16	17			
27	20	21	70	13	13			
28	21	21	71	9	9			
29	25	26	72	5	5			
30	26	26	73	1	1			
31	28	31	74	74	1			
32	30	31	75	76	1			
33	31	31	76	74	1			
34	33	31	77	1	1			
35	34	31	78	5	5			
36	35	38	79	9	9			
37	37	38	80	13	13			
38	38	38	81	16	17			
39	39	38	82	17	17			
40	40	38	83	20	21			
41	41	38	84	21	21			
42	42	45	85	25	26			
43	43	45	86	26	26			

Table 3.3 - Nodal Sections

actual cross sections at a particular node and the corresponding FETAB cross section used for that node for the temperature analysis.

Once the cross sections have been modeled, comparisons may be made between the computer results from FETAB and available recorded temperature data to estimate the accuracy of the computer models for the locations where thermocouples and strain gauges had been embedded in selected cross sections of the bridge

3.6 Manipulation of FETAB Output for Input into SFRAME

For each hour, the computer program FETAB will calculate the nodal temperatures, the nodal self-equilibrating stresses, the artificial restraining forces N_o, M_x and M_y, and the corresponding axial strain, ε_o, at the neutral axis and the curvatures, ψ_x and ψ_y, about the principle coordinates. This information must be manipulated so that it may be incorporated by the computer program SFRAME.

The artificial restraining forces N_o, M_x and M_y, must be renamed to suit the coordinate system used by SFRAME. The axial force and strain, N_o and ε_o, act along the global/local x axis. The bending moments M_x and M_y, and the corresponding curvatures ψ_x and ψ_y, act about the global/local y and z axis respectively. As noted earlier, the temperature model used by the program SFRAME assumes a linear temperature difference between the top fibre to the bottom fibre. Therefore, the axial strain and curvatures must be manipulated. Figure 3.12(a) shows a typical cross section of the Confederation Bridge, with a predicted temperature distribution (b). It must be noted that the temperatures contained in this distribution are total values, meaning that they may be separated into two portions, Figure 3.12(c). A constant reference temperature combined with a variable temperature. Bridge codes treat the reference temperature as the temperature at the time of construction, to which the gradient portion is to be superimposed. For the purposes of analysis, the temperature distribution shown in Figure 3.12(b) may be manipulated into the temperature distribution shown in Figure 3.12(e) as follows,

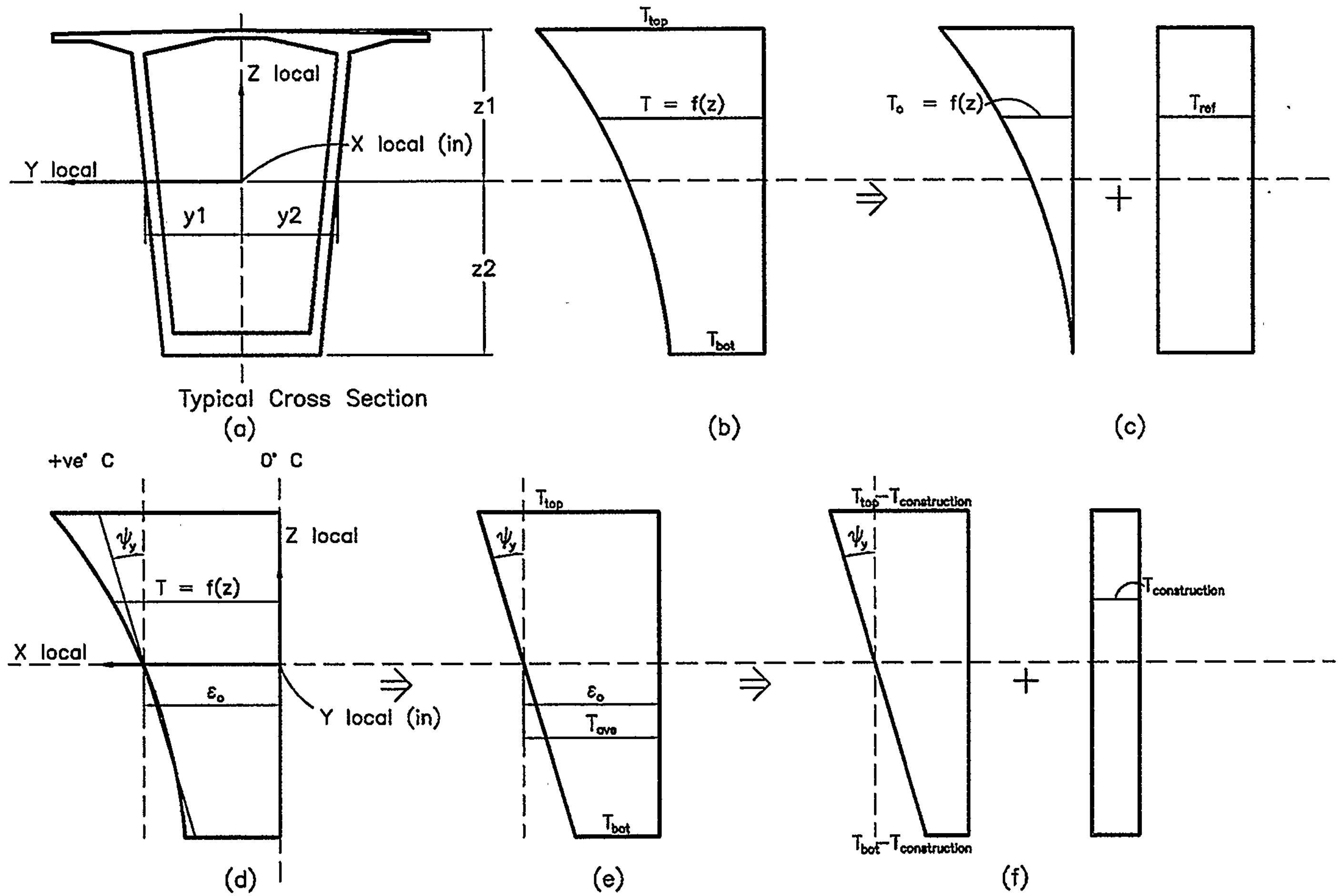

Figure 3.12 Manipulation of FETAB output
to obtain temperature load for SFRAME

$$T_{ave} = \frac{\varepsilon_o}{\alpha_T} \tag{3.10}$$

The temperature gradient about the y axis, through the depth of the cross section may be determined by,

$$T_{top} = T_{ave} + \frac{\psi_y z_1}{\alpha_T} \tag{3.11}$$

and,

$$T_{bot} = T_{ave} - \frac{\psi_y z_2}{\alpha_T} \tag{3.12}$$

Similarly, the temperature gradient about the z axis, across the width of the cross section may be determined by,

$$T_{side1} = +\frac{\psi_z y_1}{\alpha_T} \tag{3.13}$$

and,

$$T_{side2} = -\frac{\psi_z y_2}{\alpha_T} \tag{3.14}$$

The temperatures computed in equations 3.11 to 3.14 must be altered to account for the temperature at the time of construction, otherwise the rise in temperature would be overly severe. For a portal frame structure such as the Confederation Bridge the result would be very high bending moments at the base of the footings due to the expansion of the main girder.

However, there is some question as to what temperature to assume for the construction value. Also, it is doubtful that the temperature throughout the cross section was constant at the time of construction. This means that a slight temperature gradient, both through the depth and across the section may have been present at the time of construction. Therefore, it becomes increasingly difficult to compare a predicted absolute temperature displacement with a recorded value. One solution is to analyze different time steps and compare the difference between predicted displacements and recorded displacements.

It is important to note that the temperatures, determined by equations 3.11 to 3.14, are located at the nodes. The temperature model used in SFRAME is based on the assumption that the temperature gradient is constant along the length of the member. Hence, for each element, an equivalent temperature gradient must be computed. A small computer program was developed, FORCE, to manipulate the axial strain and curvatures computed by FETAB and calculate member temperature loads that may be input directly into SFRAME.

3.7 Cross Section Analysis with SFRAME - Transverse Direction

Thus far, this investigation has presented a computational method concerned with modeling the frame behaviour of the Confederation Bridge. The structure has been subjected to temperature gradients through the depth and across the section resulting in axial forces and bending moments along and about the global axis. It has been pointed out in the literature, Degenkolb (1977) and Precast Segmental Box Girder Bridge Manual (1978) that the rise in temperature of the top slab is often more than the rise in temperature of the bottom slab, resulting in bending moments being induced on the walls/webs of the box girder. Leonhardt (1965, 1970, 1979) has pointed out that significant stresses may develop when the thickness of the slabs differs from that of the walls/webs.

Therefore, the cross sections labeled here as S1 and S51 represent the largest and smallest cross sections in the bridge structure and will be modeled for use by SFRAME as an assemblage of beam elements. Curvatures, which computed from the recorded temperatures through the top and bottom slabs and the webs, will then be imposed on the cross section structure. Figures 3.13 and 3.14 contain the frames for the cross sections. Since recorded temperature data is readily available specifically for these two sections there is no need to perform a FETAB analysis on these two cross sections to obtain temperature distributions. Therefore the recorded temperature data is input directly into SFRAME.

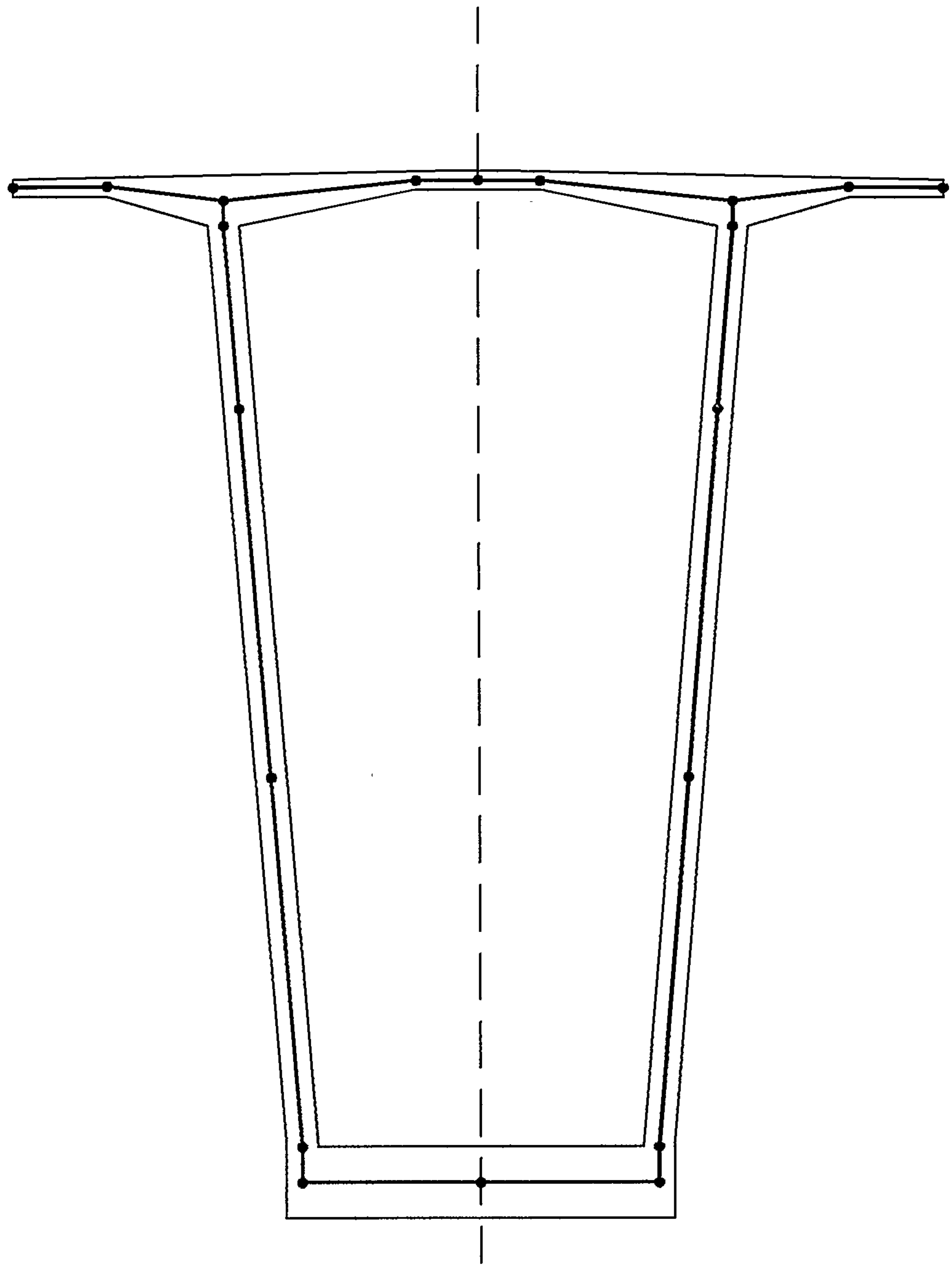

Figure 3.13 Section S1. Computer model for SFRAME analysis of cross section frame behaviour due to transverse temperature response

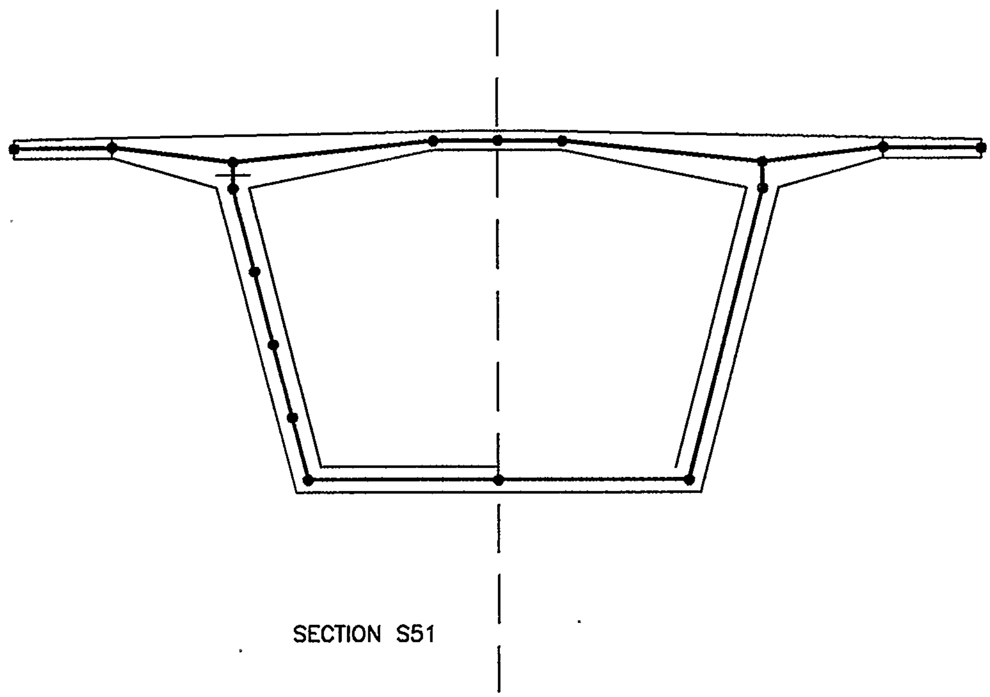

Figure 3.14 Section S51. Computer model for SFRAME analysis of cross section frame behaviour due to transverse temperature response

CHAPTER FOUR

IMPLEMENTATION OF ANALYTICAL METHOD

4.1 General Remarks

It can not be overstated that the results of any structural analysis are dependent on the assumptions made prior to the analysis. This is true whether the analysis is carried out by simple hand calculations or by a complex computer program. In the previous chapter, a summary of the computational methods was presented, while in this chapter there will be a summary of the values used for the various input variables in order to implement the analytical method.

4.2 Cross Section Analysis with FETAB - Input Parameters

In order to model the various cross sections using FETAB it was necessary to generate a finite element mesh. Following the example presented in the instruction manual to FETAB, the top slab was divided into a minimum of five elements through the thickness; the thickness of the girder webs were divided into four elements, and the bottom slab was divided into five elements. The simple examples presented in Chapter Three showed that sufficiently accurate outcomes may be obtained with fewer elements. However, in order to properly model the changes in temperature through the depth of a slab or webs four or five elements are necessary. Additional elements were required to represent the exact geometry of the cross section. The final finite element mesh was determined so that the number of nodes and elements remained constant for all cross sections. The element numbering remained the same for all cross sections, while the nodal dimensions of the top slab remained constant. The nodal dimensions of the girder webs and bottom slab varied. Each cross section finite element mesh contained 280 nodes and 322 elements. Of the 322 elements, 238 were normal four or three node elements. These "*conduction*" elements represented the geometry of the cross section. The remaining elements were boundary surface "*convection*" elements on the surface around the cross section.

4.2.1 Thermal Properties of the Conduction Element

The thermal properties of the conduction elements must accurately represent the concrete used in the girder construction. Gilliland (2001), while presenting research on the short term temperature response of the Confederation Bridge, compiled a summary of research values concerning High Performance Concrete. It was shown that the mechanical and thermal properties of concrete can be predicted with confidence using equations available in current research. The design data for the concrete used in the girder construction was specified on the contract drawings to have a 28 day compressive strength of 55 MPa. Therefore, values commonly reported for high strength/performance concrete were used in the analysis.

de Larrard, Acker and Leroy (Shah and Ahmad, 1994) note that the thermal properties of concrete are more complex than other materials used in engineering, since it is a composite material, made from other materials that each have different thermal properties. Then, to make matters more interesting, the thermal properties of each material depend on the moisture content and porosity. Neville (1981) notes that to a large extent the thermal properties of concrete are governed by the thermal properties of the aggregates. In particular, the mineralogy of the aggregate governs the thermal conductivity on the concrete - whether the aggregates come from igneous, metamorphic or sedimentary rocks. Neville notes that values of thermal conductivity - the ability of a material to conduct heat - vary from 1.38 W/m^2K to 3.68 W/m^2K depending on the type of aggregate. The more crystalline the rock, the higher the thermal conductivity.

Burg and Ost (1994) tested six high strength concrete mixes in a three year study and reported on various short and long term engineering properties. The 28 day compressive strengths of the mixes ranged from 73 MPa to 119 MPa, depending on the size of specimen and the curing conditions. The compressive strength at 1085 days (~3 years) ranged from 94 MPa to 136 MPa, again depending on the size of the test specimens and the curing conditions. All six design mixes contained the same type of aggregate (dolomite). The mix designs were varied for cement (Type 10), flyash, silica fume and fine aggregate content. The coarse aggregate content remained fairly constant at 1068 kg/m^3.

The thermal conductivity of the six design mixes varied from 1.64 W/m^{2}K to 2.29 W/m^{2}K. Burg and Ost reported that these values are of similar magnitude to normal strength concrete mixes that vary from 1.7 W/m^{2}K to 2.6 W/m^{2}K. For the present analysis with FETAB an initial thermal conductivity of 1.7 W/m^{2}K was used and then varied to observe the overall effect on the output. It was found that the curvatures and temperatures computed by FETAB varied only slightly when the value of the thermal conductivity was varied between 1.7 to 2.6 W/m^{2}K . Therefore, a value of 1.7 W/m^{2}K was used throughout the analysis. By comparison structural steel has a thermal conductivity of 45 W/m^{2}K.

The value of the coefficient thermal of expansion is another material property that varies with the composition of the mix design. Neville (1981) notes that the coefficient thermal of expansion of the cement paste can vary between 11.0 x 10^{-6} to 20.0 x 10^{-6} per °C, which is much higher than that of the aggregates. It follows that the coefficient thermal of expansion would vary with the cement content of the mix. Neville (1981) lists values for the coefficient thermal of expansion ranging from 8.5 x 10^{-6} to 13.1 x 10^{-6} per °C.

The values of the coefficient thermal of expansion reported by Burg and Ost (1994) ranged from 9.4 x 10^{-6} to 12.3 x 10^{-6} per °C.

Elbadry, Ghali and Megally (2001) reported a measured value for the coefficient thermal of expansion for the concrete used in the bridge of 8.3 x 10^{-6} per °C. This value will be used in this investigation.

Neville (1981) states the specific heat of concrete is not affected by the mineralogy of the aggregates , but varies with the moisture content of the concrete. In addition, Neville states that the specific heat of the concrete, determined by basic principles of physics, varies from 840 J/kg K to 1170 J/kg K.

Burg and Ost (1994) reported values for the specific heat ranging from 800-840 J/kg K for oven dried concrete, 960-1000 J/kg K for normally dry concrete, and 1000-

1050 J/kg K for SSD (saturated and surface dry). For the present investigation it was assumed that the concrete would be either normally dry or SSD, and values of 960 and 1000 J/kg K were used. The output results from FETAB varied very little if the specific heat was changed from 960 to 1000 J/kg K. Therefore as value of 1000 J/kg K was used throughout the analysis. Note that the value of specific heat for structural steel is 460 J/kg K.

The modulus of elasticity is another variable that is dependant on the properties of the various components of the concrete and is affected by both the cement paste strength and the type, size and strength of the aggregates. Concrete is not a true elastic material, so the modulus of elasticity is often taken as a tangent modulus between a pre-specified set of stresses and strains. It is also dependent on the loading rate.

Burg and Ost (1994) and Famy and Panaresse (1994) both recorded the modulus of elasticity in accordance with ASTM C 469, Standard Test Method for Static Modulus of Elasticity. There are a large number of equations that have been proposed for the modulus of elasticity, and the recorded values fell within the range predicted by ACI 318 and ACI 363. It should be noted that according to the above authors the value of the modulus of elasticity was also dependent on the size of the specimen and the curing conditions.

Neville (1981) summarized several of the equations that have been put forward by the British Code of Practice, CEB and ACI . All of these equations are slightly different, but the values predicted all fall within an acceptable tolerance - usually around +/- 2.5 GPa. This leads to the conclusion that there is no *absolute* correct equation. It is adequate to select an equation and be consistent throughout the analysis. Interestingly, the equation put forward by CSA A23.3-M94

$$E_c = 4500\sqrt{f_c'}MPa,$$

predicts values that are somewhat lower than those recorded by Burg and Ost (1994). The equation put forward by the previous edition of CSA A23.3,

$$E_c = 5000\sqrt{f_c'}MPa,$$

actually predicted values of the modulus of elasticity that are closer to those recorded by Burg and Ost (1994).

Elbadry, Ghali and Megally (2001) reported a measured value for the modulus of elasticity for the concrete used in the bridge of 38,700 MPa. This value will be used in this investigation.

4.2.2 Thermal Properties of the Convection Element

The thermal heat transfer properties utilized in FETAB: are the convection heat transfer coefficient, the emissive coefficient, and the solar radiation absorptive coefficient. Referring to equation 2.5, the total heat transfer is the sum of the heat transfer from convection, solar radiation and re-radiation.

The convection heat transfer coefficient is a measure of the heat loss per unit area per unit temperature difference, which is given by Newton's Law of cooling for heat due to temperature differences. Dilger and Ghali (1980) list relationships for the convection heat transfer coefficient for the various surfaces of the bridge which is dependent on the surrounding wind speed.

The absorptivity coefficient gives a measure of the amount of solar radiation that is absorbed by a surface. This coefficient varies between 0.0 and 1.0. As the sun emits radiation, only a portion of the total radiation reaches the surface of the earth. The total amount of radiation that is emitted by the sun is expressed by the solar constant. From this, the amount of radiation that reaches the surface of the earth, I, is expressed by multiplying the solar constant by a transmittance factor, K_t. The transmittance factor is dependent on the turbidity (defined later) and the air mass factor, which accounts for the variation of air pressure with altitude.

The total amount of solar radiation that is absorbed by the surface of a black body, R, is dependent on the angle of the surface to the surface of the earth and the radiation that reaches the earth, I. When the surface is not a black body the absorbed radiation is adjusted by the absorptivity coefficient, a. For exposed concrete surfaces the absorptivity is 0.5, for concrete surfaces not exposed to direct radiation 0.0 and for asphalt surfaces 0.9, (Elbadry and Ghali, 1983).

The emissivity coefficient is a measure of the heat transfer due to re-radiation and is dependent on the temperature of the surface and the surrounding air. The temperature difference is multiplied by a radiation heat transfer coefficient which is dependent on the two temperatures and the Stefan-Boltzmann constant. This yields the re-radiation heat transfer of an ideal black body. Therefore the emissivity coefficient, between 0.0 and 1.0, is applied. For concrete surfaces the emissivity coefficient is 0.9.

4.2.3 Meteorological Data

In order to perform a transient computer analysis a number of variables relating the position of the bridge relative to the sun must be determined. The day of the year, the maximum and minimum air temperature, the atmospheric turbidity, the altitude of the bridge above sea level, the latitude, and the orientation of the bridge relative to the north-south plane.

The day of the year governs the hours of sunlight during the day. This directly effects the amount of heat being input into the system being analyzed.

For maximum and minimum daily air temperatures, FETAB utilizes a sine relationship for the hourly variation of air temperature. The relationship assumes the daily minimum and maximum air temperature occur at 3:00 am and 3:00 pm, respectively.

The turbidity is a measure of the effect of cloud cover and pollution. Dilger and Ghali (1980) present a chart and equations reflecting values for summer and winter conditions for various surrounding landscapes - mountains, open country, metropolitan area, and industrial areas. For the Confederation Bridge the turbidity was based on the open country equations. As shown in Figure 3.5, the centreline deck elevation of the bridge span being considered is 40.8 m above mean sea level.

The latitude of the position of the Bridge is approximately 46 degrees.

The surface azimuth angle relates the alignment of the bridge deck centreline relative to due south (north). For the span considered here between piers 31 and 32 the bridge its at approximately 45° off of due north and south, see Figure 4.1.

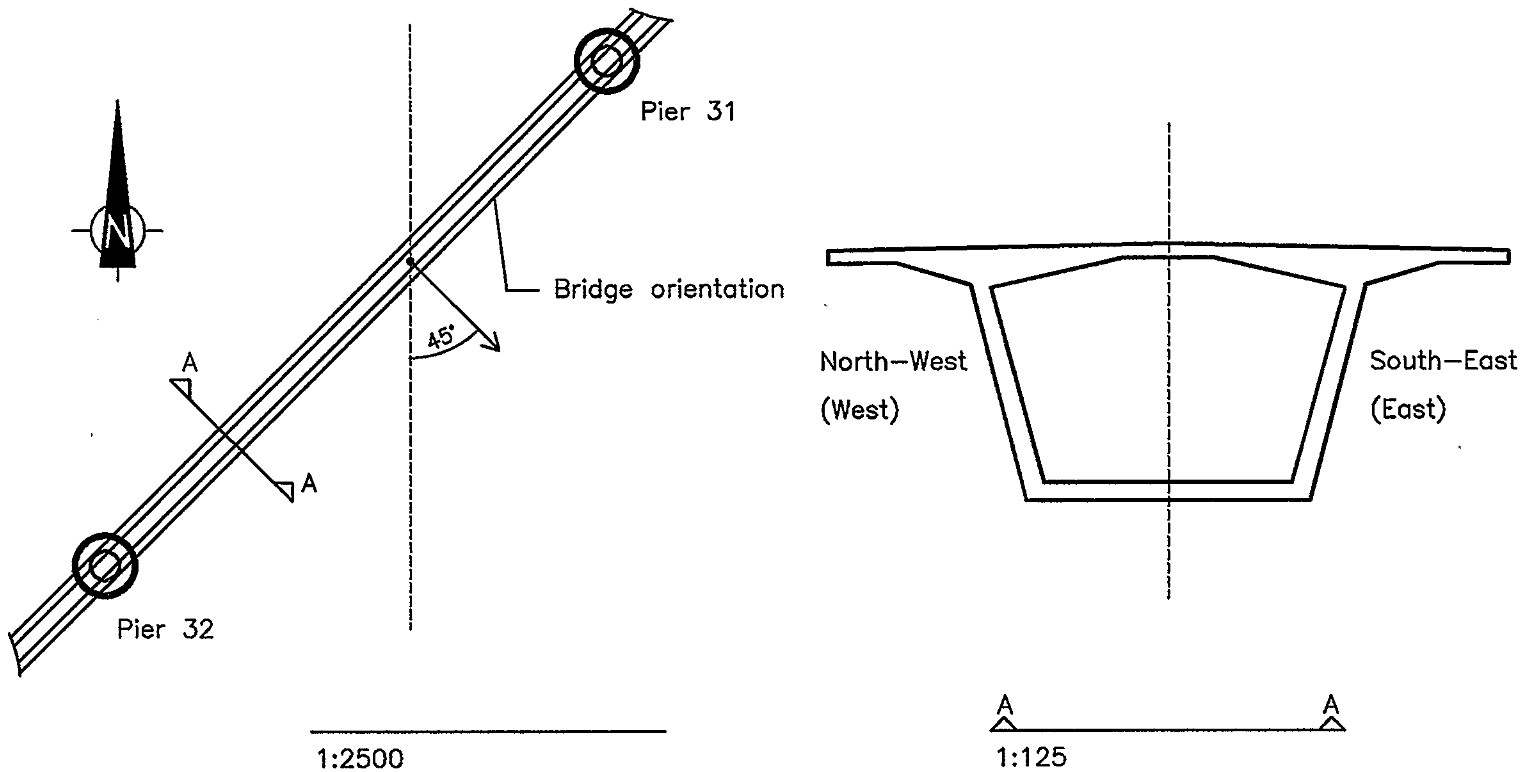

Figure 4.1 Pier Layout

4.2.4 Recorded Data

Once the required parameters were obtained and input to the computer program FETAB, the generated output was compared to the recorded data. For this investigation, recorded data was available for two cross sections in the main girder over an eighteen month period from early 1998 to mid 1999.

The two cross sections for which data was available are shown in Figure 4.2. During the construction of the Confederation Bridge thermocouples were embedded in the locations shown in Figure 4.2.

In order to obtain curvatures from the recorded temperatures the data needed to be manipulated. The locations of the embedded thermocouples for the recorded data matched the location of specific nodes in the Finite Element mesh. Therefore a subroutine was developed to interpolate the recorded data over each node of the computer mesh. Here a simple linear relationship was used to expand the data set for each node of the cross section.

As a test of the accuracy of this method, an arbitrary nodal temperature was set with an erroneous value. The difference in the resulting curvature was negligible. Therefore, the linear interpolation of the recorded temperatures was deemed to yield sufficiently accurate results for the calculation of the recorded curvatures.

4.3 Cross Section Analysis with FETAB - Output

One of the stated objectives of this investigation was to show the variation of temperature that can occur between the two webs of the box girder and determine the effect on the overall structure. In a related study Li (2003) compared the temperature distributions throughout the large section S1 . The present investigation is concerned with the structural response. Therefore the question of which day of the year to analyse must be answered. The actual time of year that experiences the maximum curvature is a matter that is best determined by a statistical analysis and is beyond the scope of this investigation. As a starting point, a subroutine was written in order to select the day of

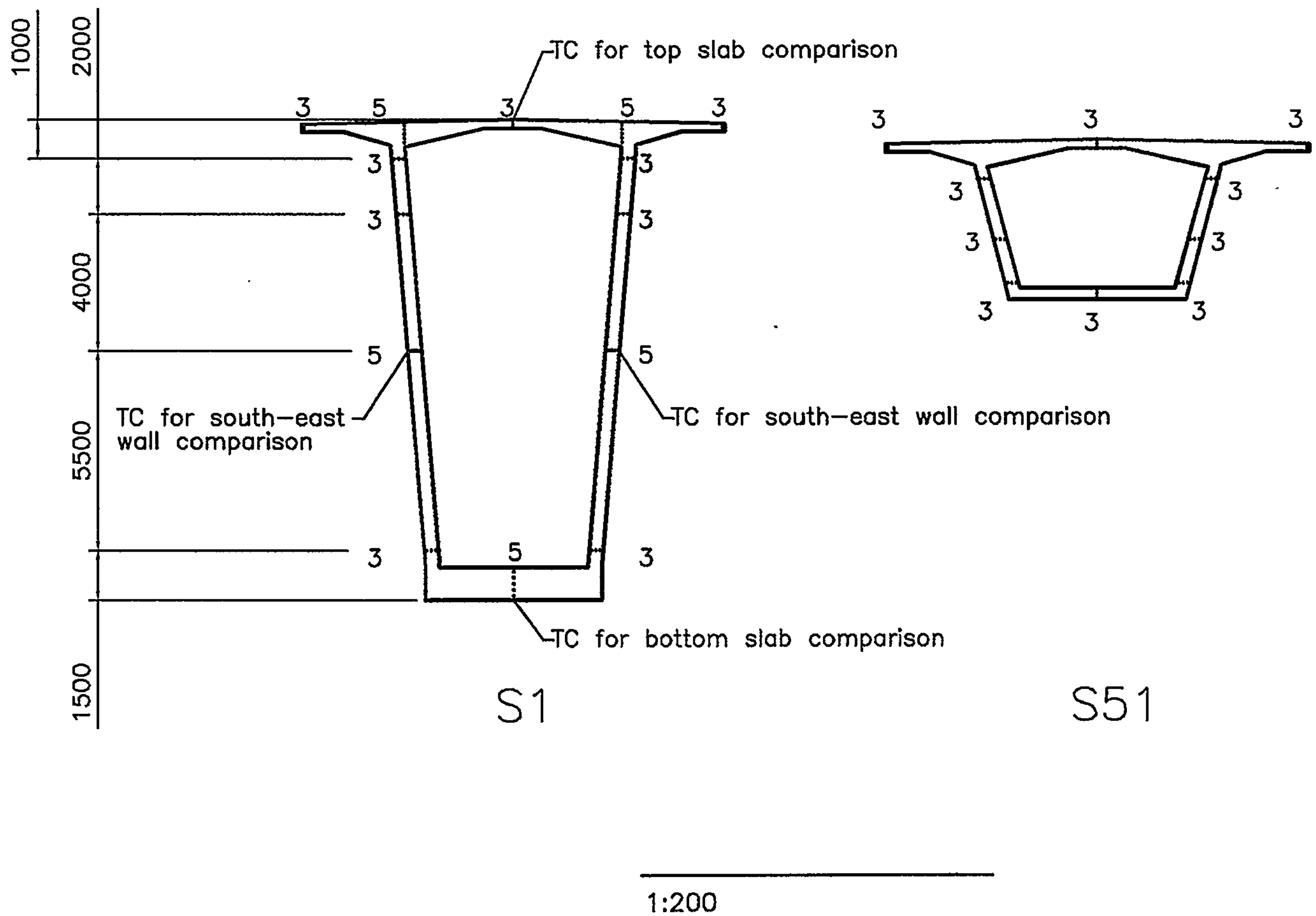

Figure 4.2 Thermocouple Locations for Cross Sections S1 and S51

the year which experienced the maximum daily air temperature. This day may not contain the maximum curvature, but it will contain one of the highest top slab temperatures, which will lead to a higher than average curvature.

For the available data, 1998, this occurred on day 221, which corresponds to August 9, 1998. The maximum and minimum daily air temperatures that occurred on this day were 26.8°C and 21.6°C, respectively. Figure 4.3 shows a comparison between the recorded daily air temperature and the values predicted with the sine relationship used in FETAB. It is obvious that the sine relationship is reasonably close on this day of the year. It should be noted that for Day 221, the average wind speed was 29.5 m/s.

Figure 4.4 presents a comparison between the predicted and recorded temperatures along the top slab and the bottom slab for section S1. The prediction of the temperatures is in very close agreement with the recorded values. It is very important to mention that the predicted top slab temperature was very close to the recorded values when the convection values over the top surface of the girder were based on a wind speed of 1 m/s. Note that when the convection values were based on the actual wind speed of 29.5 m/s the predicted temperatures were around 5°C lower than the recorded values. The reason for this is that the 1050mm high barriers on either side of the top slab act as wind breaks so that the wind speed acting on the top surface approaches zero. This observation has been corroborated by personal experiences of people working on the bridge during and shortly after construction. During construction, when the barriers were not yet in place, one observer noted that the wind speed was so high that two people had to walk along bridge during and shortly after construction. During construction, when the barriers were not yet in place, one observer noted that the wind speed was so high that two people had to walk along the centre of the top slab *"arm in arm"* in order to remain stable.

Another observer, while walking along the top surface of the bridge shortly after construction was completed, noted that while standing along the deck centreline there was no noticeable wind, yet when standing next to the barrier the wind speed was high enough to make people literally *"hold onto their hats"*.

The temperature predictions for the bottom slab were also computed with convection coefficients based on two speeds. For the bottom slab the predictions are closet to the recorded values when using the actual recorded wind speed of 29.5 m/s. Note that the predictions based on a wind speed of 1 m/s are 2 to 3°C lower than the recorded values.

This leads to the supposition that the air flow around the girder is such that barriers shelter the top surface of the bridge from the wind, thus nullifying the convection heat flow, while the convection from the bottom surface of the bridge is still governed by the actual recorded wind speed. This means that the air current splits and flows smoothly over the top of the barriers around the bottom of the girder.

Figure 4.5 contains a comparison between the predicted and recorded temperatures along the centreline of the outer surface of the girder walls, also for section S1. In both cases, the prediction of the walls outer surface temperature is in very good agreement with the recorded values. Another interesting observation is that the temperature predictions along the west (north-west) wall were computed using convection values based on the actual recorded wind speed of 29.5 m/s. However, the temperature predictions for the east (south-east) wall are computed using convection values based on a wind speed of 1 m/s. The recorded data for this day indicates that the wind came predominantly from the south so that the east (south-east) wall is on the wind exposed face and the west (north-west) wall is on the leeward side. This leads to another supposition that on the exposed face of the bridge, as the air current splits to flow around girder, there is a zone along the face that experiences very convection due to wind. On the leeward side of the bridge the air flow is likely turbulent; which would explain why the convection values based on the higher wind speed gave very good predictions.

Figure 4.6 contains a comparison between the predicted and recorded curvatures about the horizontal (x) and vertical (y) axis for section S1. The recorded curvatures are actually computed by using the recorded thermocouple temperature and interpolated across the nodes of the finite element mesh used in FETAB. The curvatures are in good

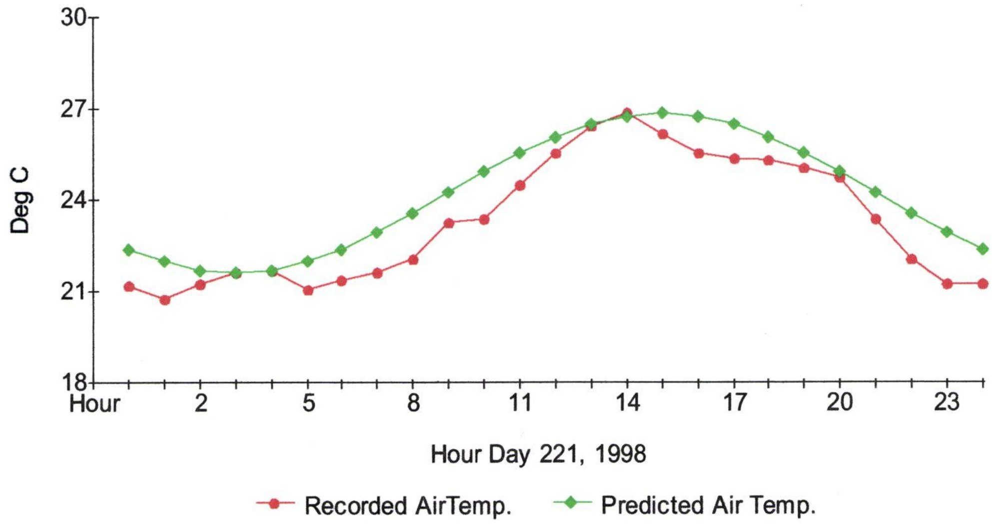

Figure 4.3 Recorded Air Temperature Compared with Sine Relationship Model.

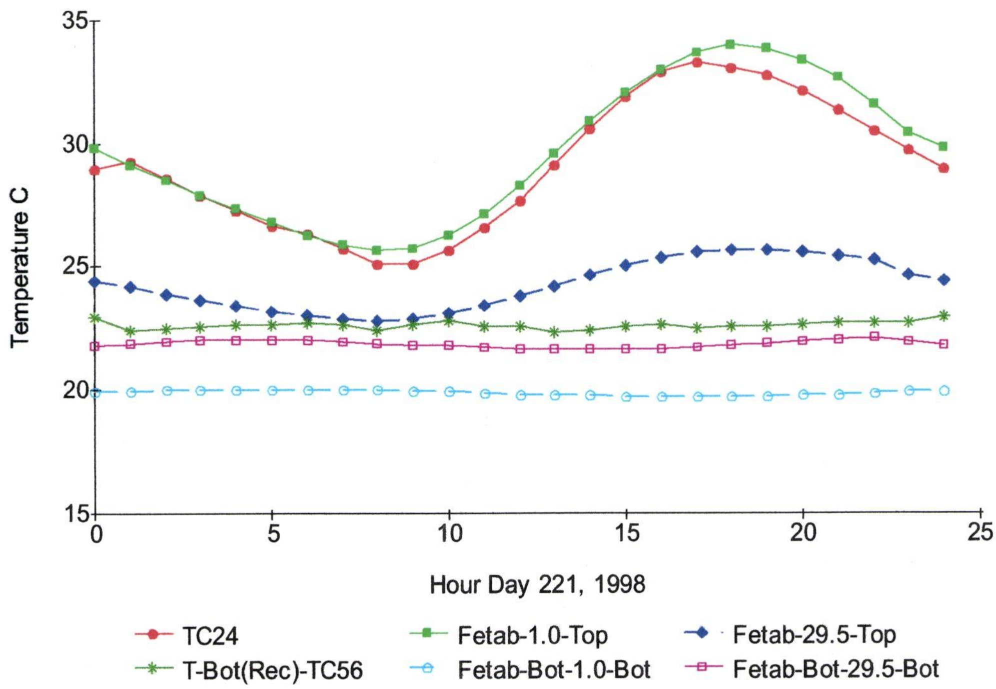

Figure 4.4 Top and Bot. Slab Temp. for Section S1, Day 221, Predicted and Recorded. Refer to Thermocouple (TC) locations in Figure 4.2.

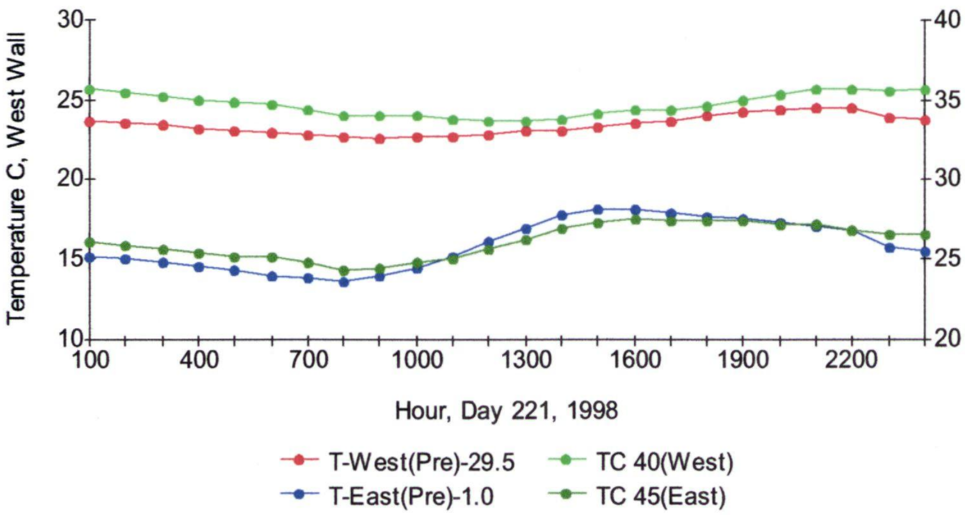

Figure 4.5 West and East Web Temp., Day 221, 1998, Section S1
Refer to Thermocouple locations in Figure 4.2

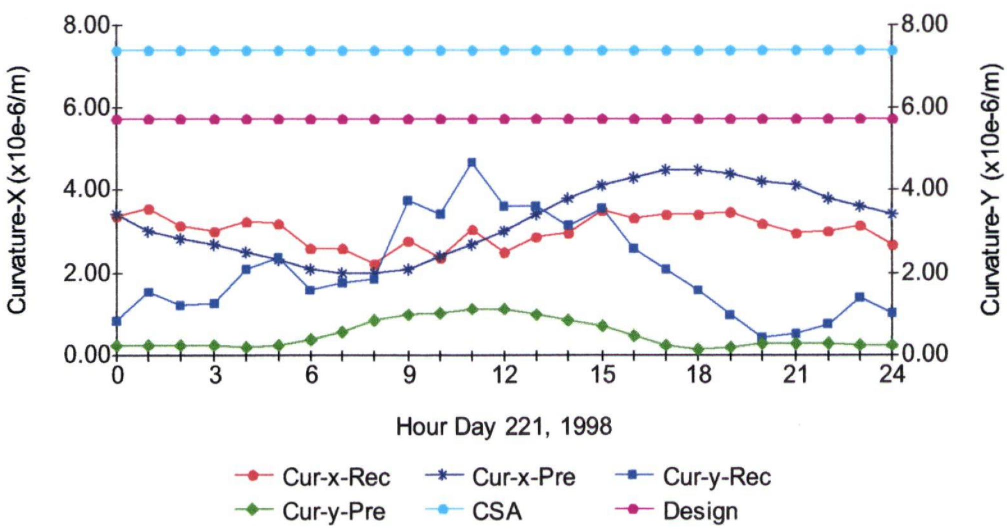

Figure 4.6 Predicted and Recorded Curvatures, Day 221, 1998, Section S1

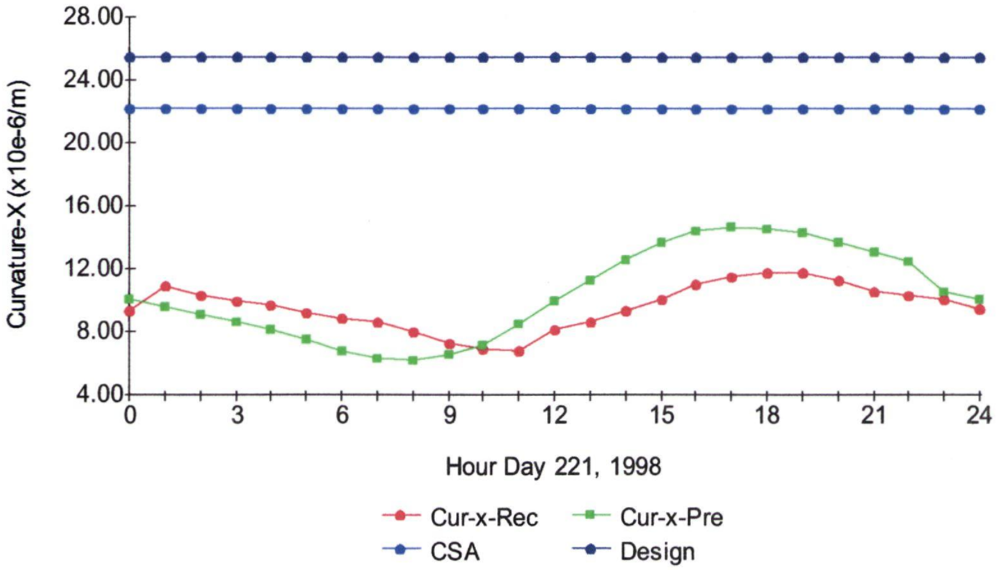

Figure 4.7 Predicted and Recorded Curvatures, Day 221, 1998, - S51

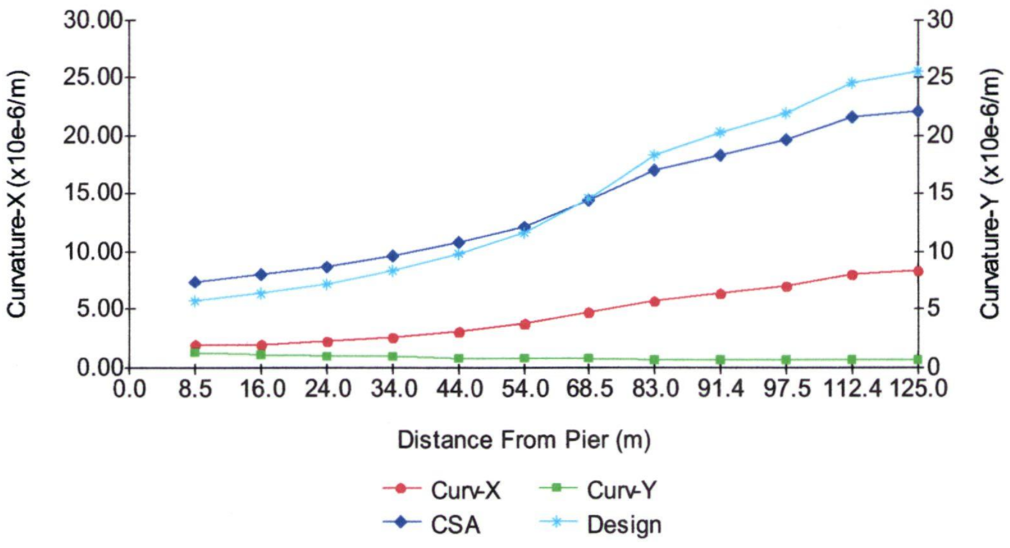

Figure 4.8 Curvature Along Bridge Centreline

agreement with those calculated from the recorded data. The design curvatures that are obtained from CSA-S6 and the contract drawings are also shown for completeness. Note that the recorded curvatures are much lower than those used in design. Even more noteworthy is the fact that the maximum value of the recorded curvature about the vertical axis is actually higher than that for the horizontal axis.

As a measure of the accuracy of the predicted curvatures, the average absolute difference between predicted and recorded curvatures may be computed. For the curvature about the horizontal axis the average difference between predicted and computed curvature is 0.63x10e-6/m and for the curvature about the vertical axis 1.58x10e-6/m. The discrepancy in the predictions of the curvature about the vertical axis are due to the variation between the recorded and predicted temperatures. One of the most important variables in calculating the curvature is the depth of the section. For the calculation of the curvature about the horizontal axis the predicted temperatures are used over a depth of 13.5m, while for the calculation of the curvature about the vertical axis depth of section is based on the distance between the two girder walls, which varies between 5m and 7.6m.

Figure 4.7 contains a comparison between the predicted and recorded curvatures about the horizontal (X) axis for section S51. The predicted curvatures are in good agreement with those calculated from the recorded data. Again, note how the predicted values follow the familiar sine relationship assumed for the daily air temperature. The design curvatures that are obtained from CSA-S6 and the contract drawings are also shown for completeness and are much higher than the recorded values. Given the accuracy of the temperature predictions for the deeper section S1, the differences between the predicted and recorded curvatures are more likely due to the calculation of the curvature from the recorded temperatures, which relies on interpolation.

Figure 4.8 shows the variation of curvature about the horizontal (X) axis along the length of the bridge. As expected, the curvature increases as the depth of the cross section decreases. Also, note that the value of the curvature about the vertical axis decreases as the depth of the cross section decreases, since the air volume in the closed girder section decreases.

Figure 4.9 shows a comparison of the predicted and recorded air temperature inside the concrete box girder cell for sections S1 and S51 with the recorded cell temperature. There were two recorded cell temperatures, one near the under side of the top slab and one near the bottom slab. The top temperature was approximately 0.75°C higher than the lower temperature. The computer program FETAB predicts a single cell air temperature, therefore an average recorded value was used for the comparison. Comparing the average recorded value and those predicted by FETAB showed that the predicted value of the air temperature inside the girder was in very good agreement with the recorded value.

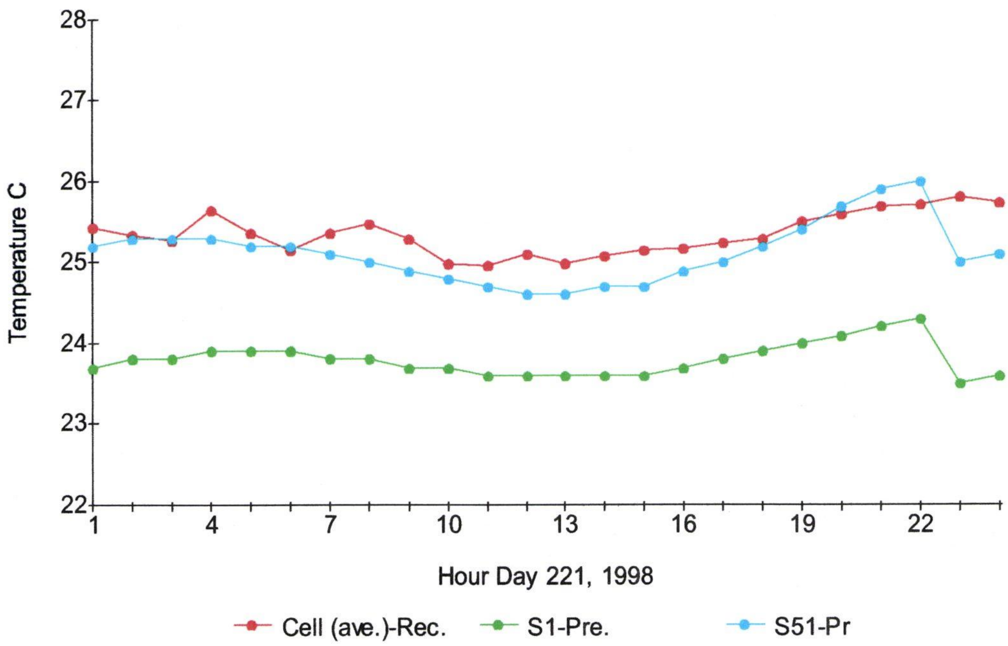

Figure 4.9 Cell Temperature Comparison

Figure 4.10 contains a comparison between the predicted and recorded temperatures through the depth of the top slab along the centre line of the deck, for two hours during Day 221, 1998: the day under consideration. Note that the predicted temperatures through the depth of the asphalt and concrete are in very good agreement

THERMOCOUPLE TEMPERATURES THROUGH SLAB AT CENTRELINE,
DAY 221, 1998 (August 9) — RECORDED

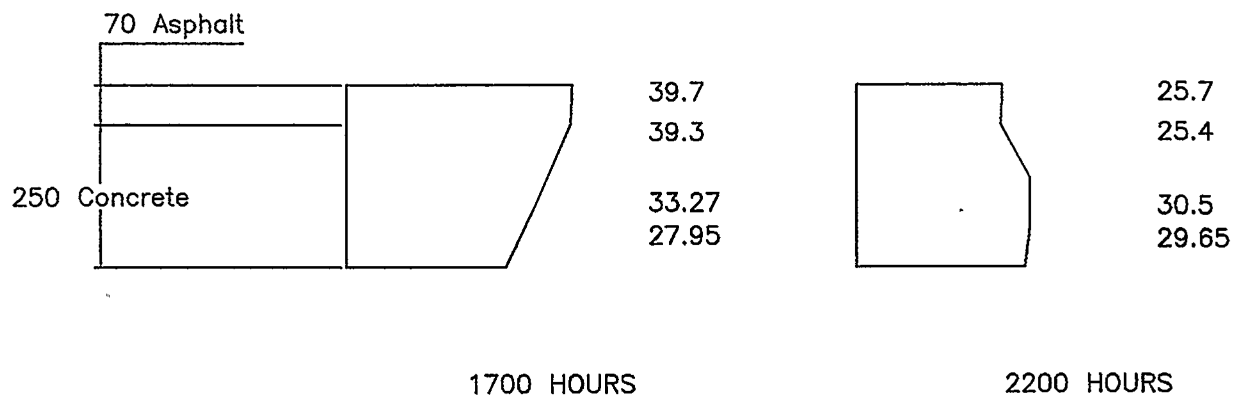

THERMOCOUPLE TEMPERATURES THROUGH SLAB AT CENTRELINE,
DAY 221, 1998 (August 9) — PREDICTED

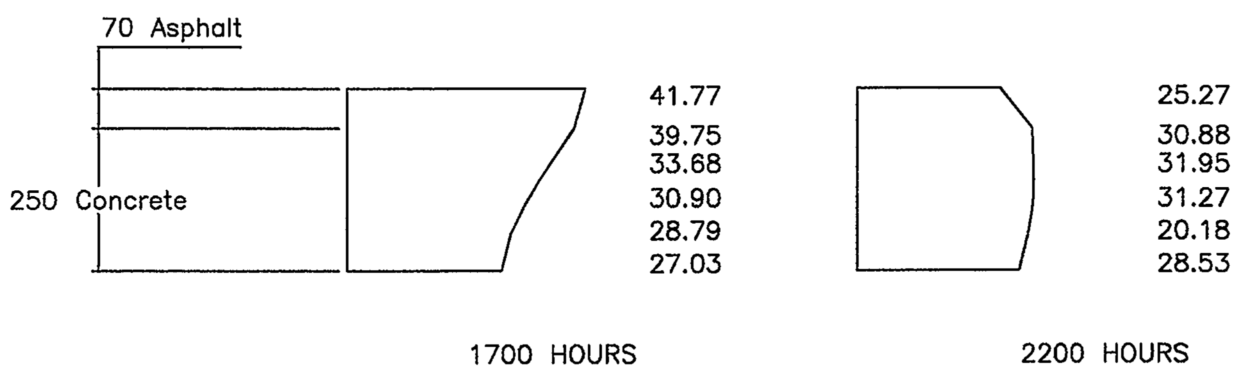

Figure 4.10 Temperature Comparison for Section S1, Day 221, 1998

with the recorded values.

Figure 4.11 contains a comparison between the predicted and recorded temperature through the depth of the girder webs for section S1 at 15:00 hrs on Day 221, 1998. This hour was chosen at random to display the accuracy that may be obtained through the use of the computer program FETAB, which incorporates heat transfer equations

Figures 4.12a and 4.12b display the predicted and recorded temperatures at the thermocouple locations for sections S1 and S51 at 15:00 hours on Day 221, 1998. The convection coefficients were based on the wind speeds already discussed. Note that the predicted and recorded temperatures are usually within a degree of each other. These Figures when combined with Figures 4.4 and 4.5 show that very accurate temperature predictions can be achieved when the proper convection coefficients are used. The convection coefficients used in this investigation are based on the actual recorded wind speed and the effects of that wind speed observed during and after construction.

4.4 Frame Analysis with SFRAME

The accuracy of the temperature and curvature predictions for the sections S1 and S51 obtained in section 4.3 indicate that the FETAB computer model is very reliable. Therefore the remaining cross sections, as listed in Figure 3.11 and Table 3.3, were analyzed using the computer program FETAB. The curvatures obtained from this analysis were then manipulated according to the method outlined in section 3.6.

The computer program SFRAME utilizes a linear temperature distribution through the depth or across the width of a member. However, for any given load case the temperature difference must be in only one local axis at a time. Therefore, in order to observe the effects of the combined temperature distributions through the depth and across the section two cases of loading must be combined.

One of the stated objectives of this investigation was to determine the structural response of the bridge and attempt to compare it to measured values. However, this is not as straight forward as it may first seem. One reason is that the construction

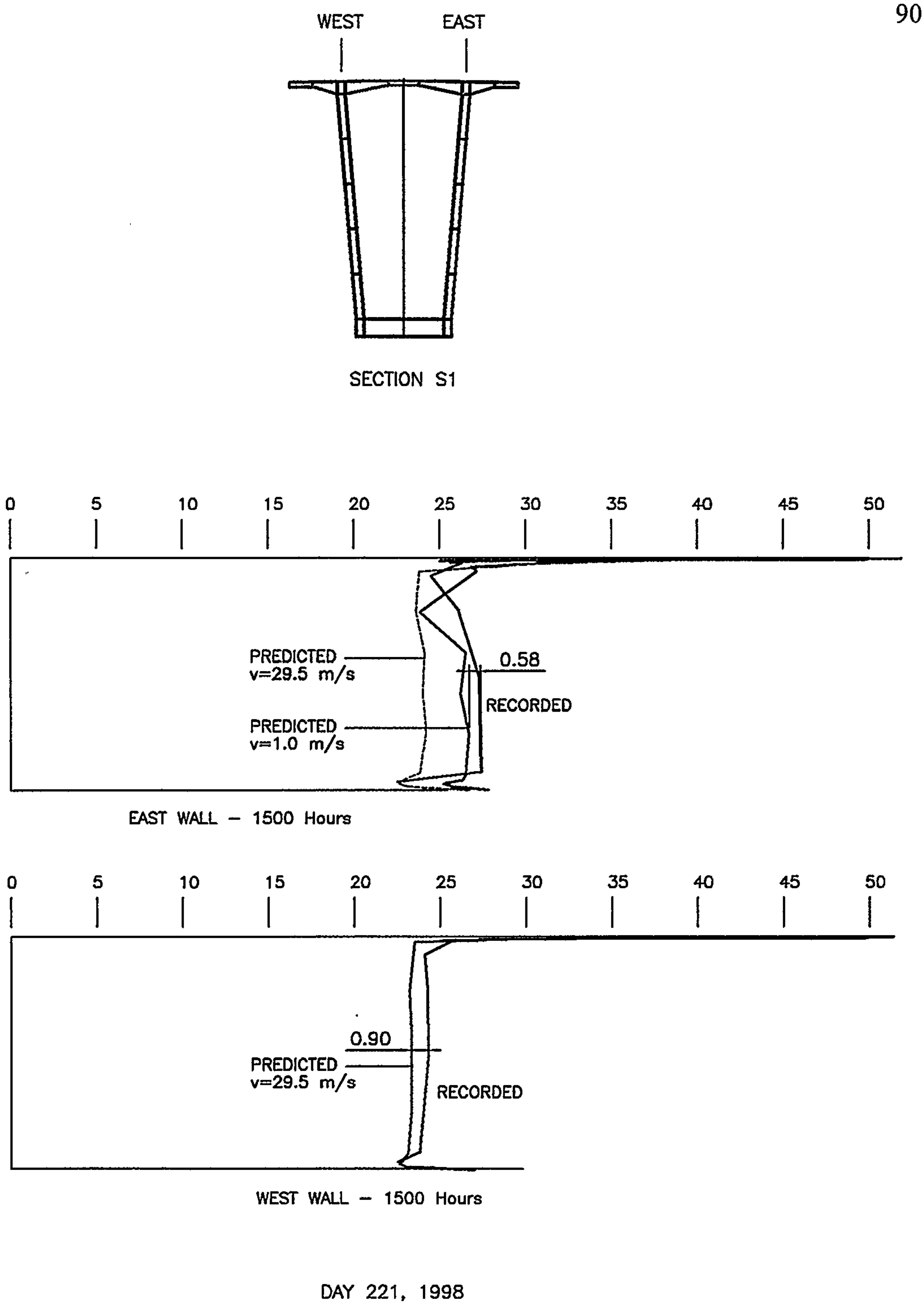

Figure 4.11 Predicted and recorded temperature comparisons for section S1 on day 221, 1998 at 15:00 hours.

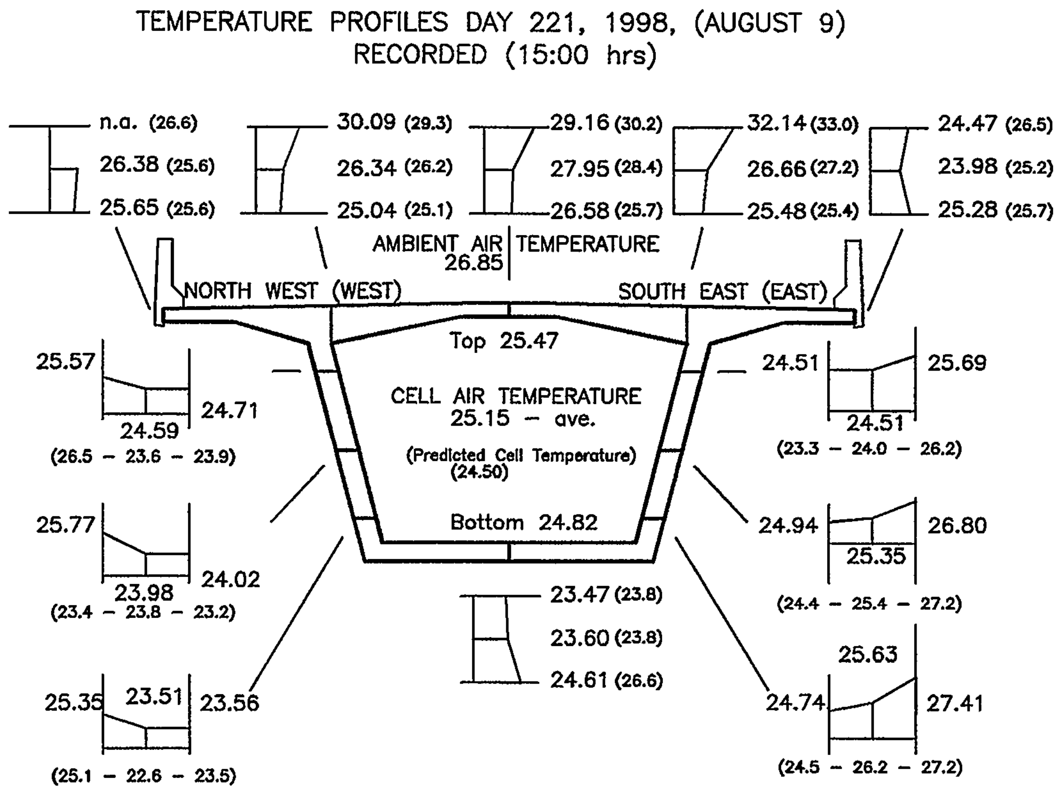

Predicted temperatures have been computed using the following wind speeds to compute the convection coefficients

Top surface	1 m/s
Bottom Surface	29.5 m/s
West wall (leeward side)	29.5 m/s
East Wall (windward side)	1 m/s
Underside of over hangs	29.5 m/s

Average daily wind speed: 29.5 m/s from South–West

Recorded Temperatures (Predicted Temperatures)

Figure 4.12a Recorded and Predicted Temperatures for Section S51 on day 221, 1998 at 15:00 hours.

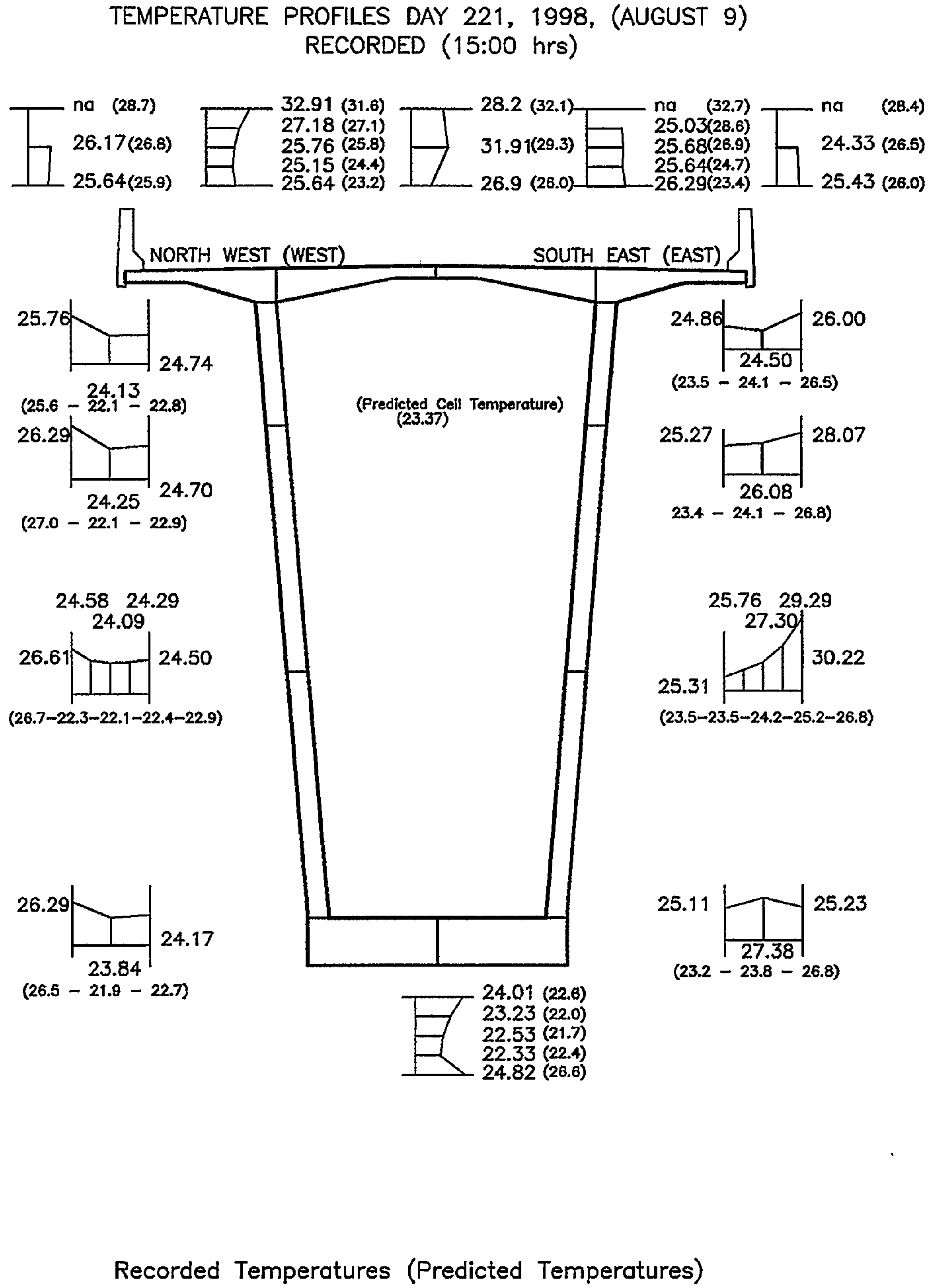

Figure 4.12b Recorded and Predicted Temperatures for Section S1 on day 221, 1998 at 15:00 hours.

temperature for each precast section of the bridge is unknown and may be different for each section. In order to negate the effects of the construction temperature a number of time steps were analyzed. Then, by reviewing the changes in deflection and internal forces a measure of the effects of temperature loading may be made.

Another reason is that the exact condition of live load (weight and position of vehicles) is unknown. Therefore, it is very difficult to obtain a set of internal forces on the computer that will correspond with the measured strains (stresses). The embedded thermocouples measure temperatures on an hourly basis. In addition six strain gauges are present in the cross section labelled S1 and four strain gauges in the cross section labelled S51. However, it will be here shown that the internal forces due to temperature loading are in the same order of magnitude as the internal forces due to vehicle (car and truck) loading and wind pressure.

There exists a vast amount of recorded data collected from strain gauges embedded in the cross sections of the Confederation Bridge. As a result, any number of days could be analyzed. However, the process of manipulating the curvatures obtained from the program FETAB into appropriate input for the program SFRAME is a laborious one. Therefore the number of load combinations will be limited to the following:

Ld Comb. No.	Description	
1	Day 221	02:00 Hrs
2	Day 221	09:00 Hrs
3	Day 221	15:00 Hrs
4	Day 221	22:00 Hrs
5	Day 274	04:00 Hrs
6	Day 274	12:00 Hrs
7	Day 274	19:00 Hrs
8	Day 274	22:00 Hrs
9	Day 1	08:00 Hrs
10	Day 1	13:00 Hrs

11	Day 1	22:00 Hrs
12	CS-600 Truck at end of cantilever	
13	CSA design gradients - summer conditions	
14	Design Gradient from Contract Drawings - summer conditions	
15	Self Weight	
16	Day 221	08:00 Hrs
17	Day 221	21:00 Hrs
18	Day 274	17:00 Hrs
19	Day 221	02:00 Hrs with Construction Temperature of 15°C
20	Day 221	15:00 Hrs with Construction Temperature of 15°C
21	Nominal vehicle loading on one lane, one side of girder	
22	Nominal truck loading at mid span	
23	Wind pressure due to 10 m/s wind speed	
24	Blue and Grey Truck	

For the analysis, Day 221 was chosen since it was first analyzed with FETAB. The other two days; Day 274, 1998 and Day 1, 1999, were chosen at random to negate the effects of the unknown construction temperature. The difference between computed values for the internal forces and the difference in the strain gauge readings may be compared.

The nominal vehicle loading, per lane, used in Load Combination 21 was taken from MacGregor (1997), which assumed the average vehicle to be 16 kN and 4.9 m in length. This corresponds to a uniform load of 3.2 kN/m. Note that this assumes the 16 kN vehicles are bumper to bumper along the entire length of the bridge span. CSA-S6 requires a design lane load of 9 kN/m - a healthy excess over "*average conditions*". The Nominal truck load used in Load Combination 22, again taken from MacGregor (1997), was found to be 525 kN. Note that only one truck was present in load combination 22, whereas the actual truck loading at any hour is unknown.

The wind speed analysed in load combination 23 is 10 m/s. This value was used as to depict a rough average of actual conditions. On Day 221, 1998, the average wind speed was 29.5 m/s. On other days the wind speed approaches 50 m/s, or is as low as 2 m/s. A wind speed of 50 m/s (176 km/h) is extreme. Using equations contained in the National Building Code of Canada, the 30 year design wind is approximately 120 km/h - to which gust factors are applied. For the structural behaviour due to the wind speed pressure coefficients tabulated in the commentary to the National Building Code of Canada were used to compute the lateral load. Note that by using a wind speed of 10 m/s for the elastic structural analysis it is easy to scale the results for other wind speeds. The wind pressure varies with the square of the wind speed.

The Blue and Grey trucks referred to in load combination 24 are two trucks that drove side by side along the Confederation Bridge, shortly before it opened to the public. Deflection measurements were taken and have been reported by Elbadry, Ghali and Megally (2001). These trucks were part of the monitoring program. However, the traffic monitoring program does not record vehicle weights and positions every hour on the hour, every day of the year.

The CSA design loading and the design loading taken from the contract drawings are gradient loadings from an unspecified reference temperature. The reference temperature being the construction temperature. In order that the results from these two load conditions may be compared to the results generated using the computer program FETAB the construction temperature of 15°C, as specified in CSA-S6, was added to the gradient loading. This is necessary because the structure that is analyzed is continuous and contains rigid piers. The reference temperature affects the longitudinal expansion of the bridge, which influences the bending moments in the piers and in the bridge girder, where it is connected to the piers.

The wind pressure was determined by incorporating the pressure, gust, and exposure coefficients found in the commentary to the National Building Code of Canada.

Tables 4.1 and 4.2 contain the predicted displacements for the 24 load combinations for node 1, at the end of the cantilever, and node 47, at mid span, respectively. Figure 4.13 presents the predicted internal forces for the specified locations. Note that for all load combinations, except number 15 which is for the self weight, the bending moments about the horizontal axis are in the same order of magnitude. In addition, note that the bending moment about the vertical axis due to wind pressure (load combination 23) is in the same order of magnitude as that due to the transverse temperature gradient (curvature about the vertical axis).

Note that the vertical displacements generated by SFRAME using curvatures computed from FETAB are of the same order of magnitude as the values obtained by the CSA code and the design gradient found in the drawings. Meaning that although the input curvatures may differ somewhat the over all effect on the structure is minimal.

Comparing the predicted values to the recorded values becomes difficult matter, since the exact circumstances of loading at any given hour is unknown.

The thermocouples and strain gauges were attached inside the formwork, prior to construction - typically to the face of reinforcing bars. During the placement of the concrete, care must be taken so that the number of thermocouples and gauges that get damaged is kept to a minimum, since vibration is applied to minimize the occurrence of honeycombing.

As the sections are poured and cured the thermocouples experience a wide range of temperatures resulting from heat of hydration and cooling. The sections were stored out doors. Therefore their internal temperature continually changed. Hence, the notion of a constant construction temperature for each section and within any one section is unrealistic. The strain gauges were subjected to shrinkage and creep strains, which could easily vary from one section to another and within any given section as well. At the time of construction they were also subjected to strains due to self weight and then compressive strains due to the post-tensioning process. It is commonly assumed that the equivalent pre-stressing force is constant for the cross section. For smaller cross sections this assumption is fairly reasonable. However, for large cross sections localized stresses

Load Comb. No.	X-Trans. m	Y-Trans. m	Z-Trans. m	X-Rot. Rad.	Y-Rot. Rad.	Z-Rot. Rad.
1	-0.0436	-0.0027	-0.0711	0	-0.0008	0
2	-0.0435	-0.0123	-0.0711	0	-0.0008	0.0002
3	-0.0475	-0.0127	-0.0895	0	-0.0012	0.0002
4	-0.0461	-0.0034	-0.0799	0	-0.001	0
5	-0.0306	-0.0228	-0.0454	0	-0.0005	0.0003
6	-0.0306	-0.0228	-0.0502	0	-0.0006	0.0003
7	-0.0302	-0.0144	-0.0507	0	-0.0006	0.0002
8	-0.0293	-0.0122	-0.0473	0	-0.0006	0.0002
9	0.0329	-0.007	0.0455	0	0.0005	0.0001
10	0.0307	-0.0183	0.0387	0	0.0004	0.0003
11	0.0308	-0.0117	0.0395	0	0.0004	0.0002
12	-0.0025	0	-0.0269	0	-0.0004	0
13	-0.0316	0	-0.08	0	-0.0012	0
14	-0.0386	0	-0.0855	0	-0.0012	0
15	-0.0226	0	-0.5696	0	-0.01	0
16	-0.045	-0.011	-0.0719	0	-0.0009	0.0002
17	-0.0487	-0.0032	-0.0812	0	-0.001	0
18	-0.038	-0.0055	-0.0636	0	-0.0008	0.0001
19	-0.025	-0.0027	-0.0458	0	-0.0006	0
20	-0.0326	-0.0127	-0.0696	0	-0.001	0.0002
21	-0.0003	-0.0002	-0.0071	0	-0.0001	0
22	-0.0002	0	0.0025	0	0	0
23	0	0.0129	0	-0.0001	0	-0.0001
24	-0.0003	0	0.0035	0	0	0

Table 4.1 Node 1 Displacements

Load Comb. No.	X-Trans. m	Y-Trans. m	Z-Trans. m	X-Rot. Rad.	Y-Rot. Rad.	Z-Rot. Rad.
1	0	-0.0007	0.0638	0	0	0
2	0	-0.0014	0.0636	0	0	0
3	0	-0.0018	0.0649	0	0	0
4	0	-0.0008	0.0653	0	0	0
5	0	-0.0024	0.0473	0	0	0
6	0	-0.0024	0.0454	0	0	0
7	0	-0.0018	0.0442	0	0	0
8	0	-0.0015	0.0437	0	0	0
9	0	-0.0006	-0.0509	0	0	0
10	0	-0.0014	-0.0494	0	0	0
11	0	-0.001	-0.0494	0	0	0
12	-0.0022	0	0.0026	0	0.0001	0
13	0	0	0.0315	0	0	0
14	0	0	0.0491	0	0	0
15	0	0	-0.4472	0	0	0
16	0	-0.0007	0.0662	0	0	0
17	0	-0.0001	0.0698	0	0	0
18	0	-0.0003	0.0553	0	0	0
19	0	-0.0007	0.0362	0	0	0
20	0	-0.0018	0.0432	0	0	0
21	0	-0.0003	-0.0057	0	0	0
22	0	0	-0.0121	0	0	0
23	0	0.0076	0	-0.0001	0	0
24	0	0	-0.0168	0	0	0

Table 4.2 Node 47 Displacements

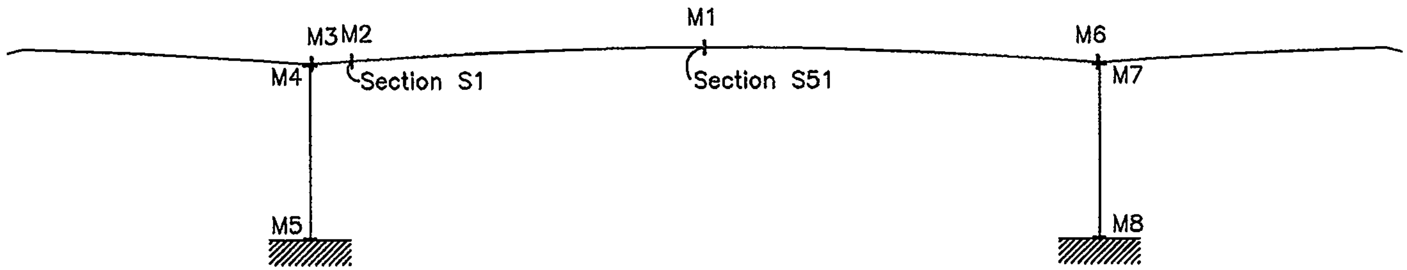

Load Combination	M1	M2	M3	M4	M5	M6	M7	M8
	(MNm)	(MNm)	(MNm)	(MNm)	(MNm)	(MNm)	(MNm)	(MNm)
1	−7.12	11.75	15.30	−15.30	−237.92	15.30	−15.30	−237.92
2	−6.99	11.81	15.35	−15.35	−237.22	15.35	−15.35	−237.22
3	0.68	20.24	23.92	−23.92	−254.70	23.92	−23.92	−254.70
4	−4.47	15.10	18.79	−18.79	−249.80	18.79	−18.79	−249.80
5	−7.05	6.37	8.89	−8.89	−167.28	8.89	−8.89	−167.28
6	−3.87	9.19	11.65	−11.65	−265.80	11.65	−11.65	−165.80
7	−3.17	9.66	12.07	−12.07	−163.49	12.07	−12.07	−163.49
8	−4.32	8.28	10.65	−10.65	−159.32	10.65	−10.65	−159.32
9	11.42	−3.54	−6.36	6.36	182.91	−6.36	6.36	182.91
10	12.76	−1.45	−4.12	4.12	171.73	−4.12	4.12	171.73
11	12.41	−1.81	−4.48	4.48	172.23	−4.48	4.48	172.23
12	−0.25	−14.16	−15.91	−35.69	−0.13	8.24	−8.24	27.31
13	12.58	24.01	26.16	−26.16	−161.01	26.16	−26.16	−161.01
14	10.83	25.46	28.22	−28.22	−200.91	28.22	−28.22	−200.91
15	210.12	−1493.58	−1961.11	−130.35	−112.72	−1961.11	−130.35	−112.72
16	−8.23	11.28	14.95	−14.95	−245.26	14.95	−14.95	−245.26
17	−7.26	13.70	17.65	−17.65	−265.05	17.65	−17.65	−265.05
18	−4.76	11.51	14.57	−14.57	−206.54	14.57	−14.57	−206.54
19	−1.32	9.47	11.50	−11.50	−138.84	11.50	−11.50	−138.84
20	5.24	18.45	20.93	−20.93	−176.84	20.93	−20.93	−176.84
21	2.81	−17.94	−22.69	−1.58	−1.46	−22.69	−1.58	−1.46
22	7.48	−17.61	−20.24	20.24	−16.11	−20.24	−20.24	−16.11
23	0	0	0	0	0	0	0	0
24	10.53	−24.343	−27.98	27.98	−22.27	−27.98	−27.98	−22.27

Figure 4.13 Bending Moments for the various load combinations

concentrations result in a pre-stressing force that is not constant throughout the section. Typically one cable is stressed at a time. Based on the construction drawings, the equivalent pre-stressing force, after losses, at mid span is in the order of 37 MN. This force is localized with approximately 12 MN along the top slab and 25 MN along the bottom slab. The resulting pre-stressing stress is approximately 4 MPa. It should be remembered that tension is applied to the steel reinforcement in a post-tensioned system (cables, bars, cable groups, etc..) through the use of hydraulic jacks. The level of tension applied to any one cable is determined by the elongation. However, the elongation is governed by the modulus of Elasticity of the steel. Note that a 5% variance in the value of the modulus of elasticity of the prestressing steel could easily vary the stress at a particular location in the concrete section by as much a 0.2 MPa.

The effects of creep, shrinkage and pre-stressing force should remain fairly constant for short term loading conditions. Therefore, the comparisons between recorded and predicted values may be made simpler by considering the change between loading conditions. This will also negate the effect of the construction temperature. In must be remembered that since the effects of the recorded/predicted temperature loading are in the same order of magnitude as those resulting from traffic and wind it will still be very difficult to obtain an exact match to the recorded strain gauge measurements. Figure 4.14 contains the location of the four strain gauges embedded in section S51. The available data sets of recorded information contain hourly readings.

Here, the mid span section (S51) will be reviewed for comparison. The construction temperature will be taken as 0°C. This simplifies the analysis and by reviewing the difference between loading cases cancels out of the equation. Consider load combination three, Day 221 at 15:00 hours. The predicted axial force is -4.114 MN, the predicted bending moment about the horizontal axis is 0.6828 MNm, and the predicted bending moment about the vertical axis is 3.4872 MNm. The stresses that result from these forces are then added to the self-equilibrating and are tabulated in Figure 4.14.

Next, consider a different time step, load combination six, Day 274 at 12:00

hours. For this time step the predicted axial force is -2.75 MN, the predicted bending moment about the horizontal axis is -3.87 MNm, and the predicted bending moment about the vertical axis is 6.44 MNm. Again, the stresses that result from these forces are then added to the self-equilibrating and are tabulated in Figure 4.14.

Taking the difference in stresses between load combination six and three results in stress differentials, tabulated in Figure 4.14.

Measured strains were computed from the recorded voltages and the corresponding difference between the two time steps, tabulated in Figure 4.14. Since the exact case of loading for each time step is unknown, all that can be stated for certain is that the computed stresses are in the correct order of magnitude and may be considered to be reasonable. As noted earlier, the bending moments due to nominal vehicle loading and wind pressure are in the same order of magnitude as these values from temperature loading. It must be remembered that the number of load combinations resulting from temperature, vehicle and or wind pressure is almost infinite.

Another explanation for the variance is the computed self-equilibrating stresses. The self-equilibrating stresses in the walls are very sensitive to slight temperature variations. Therefore, the self-equilibrating stresses computed by FETAB will be slightly different from the actual values. Given the relatively low stress level, a slight change in self-equilibrating stresses will change the summation of stresses.

The deep section S1, located in the continuous side precast section C1, also contains strain gauges, as does the hinged side precast section H1. The difference in the strain gauge measurements will give a measure of the bending moment due to continuity. Table 4.3 contains values of the difference between the strain gauge measurements for precast sections C1 and H1 for the various days picked, at random for the longitudinal frame analysis with SFRAME. Note the very small magnitude of strain. More important is the fact that there is light change in the differential strain gauge measurements. It is evident that the magnitude of the bending moments due to continuity resulting from live loading is very small. Therefore it would appear that although the day selected for the primary FETAB analysis, Day 221, 1998, may not

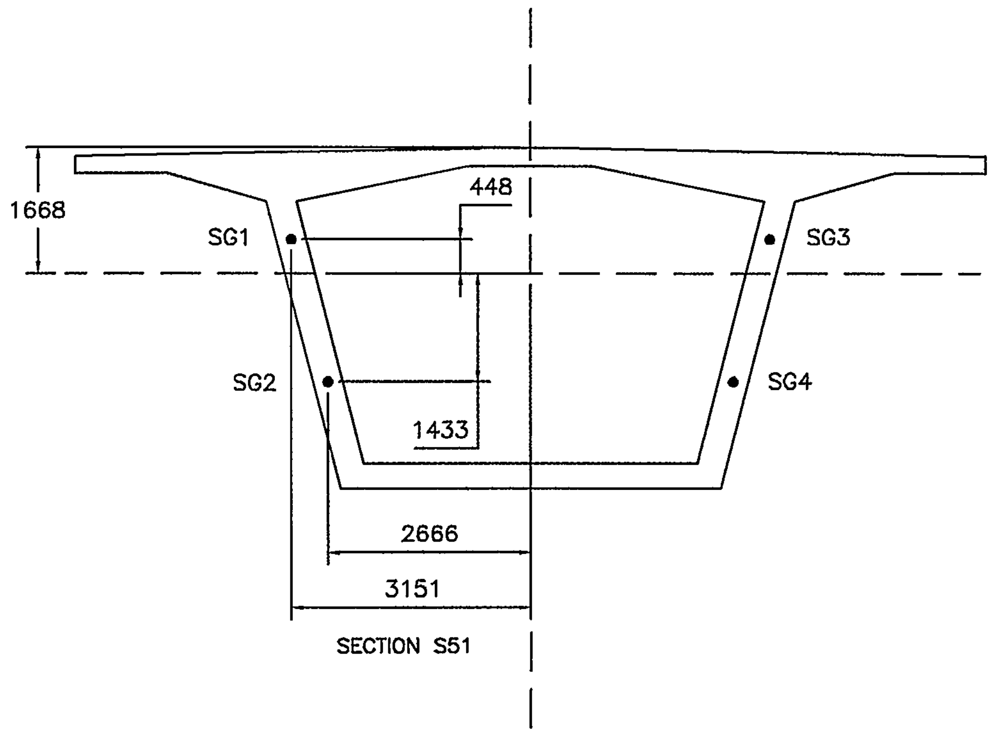

Tiime Step One Day 221 – 15:00 hrs

Location	SG1	SG2	SG3	SG4
Continuity Stress	−0.61 MPa	−0.53 MPa	−0.32 MPa	−0.29 MPa
Self–equilibrating STress	1.01 MPa	0.12 MPa	1.13 MPa	−0.38 MPa
Combined Stress	0.40 MPa	−0.41 MPa	0.80 MPa	−0.67 MPa

Time Step Two Day 274 – 12:00 hrs

Location	SG1	SG2	SG3	SG4
Continuity Stress	−0.64 MPa	−0.31 MPa	−0.11 MPa	−0.14 MPa
Self–equilibrating STress	0.53 MPa	−0.08 MPa	0.66 MPa	−0.87 MPa
Combined Stress	−0.11 MPa	−0.38 MPa	0.55 MPa	−0.73 MPa

Difference Between Time Steps

Location	SG1	SG2	SG3	SG4
Change in Stress	−0.51 MPa	0.02 MPa	−0.25 MPa	−0.05 MPa

Stress from Difference in Recorded Strain

Location	SG1	SG2	SG3	SG4
Change in Stress	−0.73 MPa	0.0 MPa	0.0 MPa	0.18 MPa

Figure 4.14 Position of Strain Gauges in Section S51
and Strain Gauge Comparisons

Year	Day	Hour	Strain Gauge 1 (micro-strain)	Strain Gauge 2 (micro-strain)	Strain Gauge 3 (micro-strain)	Strain Gauge 4 (micro-strain)	Strain Gauge 5 (micro-strain)	Strain Gauge 6 (micro-strain)
1998	221	100	-8.244E+00	-6.517E+00	-4.375E+00	3.519E+00	-3.532E+00	-6.772E+00
1998	221	200	-8.409E+00	-6.646E+00	-4.203E+00	3.791E+00	-3.714E+00	-6.646E+00
1998	221	300	-8.409E+00	-6.646E+00	-4.028E+00	3.519E+00	-3.714E+00	-6.251E+00
1998	221	400	-8.488E+00	-6.517E+00	-4.028E+00	3.519E+00	-3.714E+00	-6.251E+00
1998	221	500	-8.409E+00	-6.646E+00	-4.203E+00	3.519E+00	-3.532E+00	-6.517E+00
1998	221	600	-8.409E+00	-6.646E+00	-4.028E+00	3.519E+00	-3.714E+00	-6.251E+00
1998	221	700	-8.409E+00	-6.646E+00	-4.028E+00	3.249E+00	-3.532E+00	-6.385E+00
1998	221	800	-8.409E+00	-6.646E+00	-4.203E+00	3.249E+00	-3.532E+00	-6.646E+00
1998	221	900	-8.328E+00	-6.646E+00	-4.203E+00	3.519E+00	-3.714E+00	-6.646E+00
1998	221	1000	-8.328E+00	-6.646E+00	-4.203E+00	3.519E+00	-3.346E+00	-6.517E+00
1998	221	1100	-8.488E+00	-6.646E+00	-4.028E+00	3.519E+00	-3.158E+00	-6.517E+00
1998	221	1200	-8.488E+00	-6.772E+00	-3.487E+00	3.791E+00	-3.346E+00	-6.646E+00
1998	221	1300	-8.488E+00	-6.646E+00	-4.028E+00	3.519E+00	-3.158E+00	-6.517E+00
1998	221	1400	-8.488E+00	-6.646E+00	-3.851E+00	3.791E+00	-3.158E+00	-6.646E+00
1998	221	1500	-8.488E+00	-6.896E+00	-4.028E+00	3.519E+00	-3.158E+00	-6.517E+00
1998	221	1600	-8.328E+00	-6.896E+00	-4.203E+00	3.519E+00	-3.158E+00	-6.517E+00
1998	221	1700	-8.328E+00	-6.772E+00	-4.203E+00	3.791E+00	-3.346E+00	-6.646E+00
1998	221	1800	-8.328E+00	-6.896E+00	-4.375E+00	3.519E+00	-3.346E+00	-6.517E+00
1998	221	1900	-8.328E+00	-6.772E+00	-4.544E+00	3.791E+00	-3.532E+00	-6.517E+00
1998	221	2000	-8.244E+00	-6.646E+00	-4.710E+00	3.519E+00	-3.532E+00	-6.517E+00
1998	221	2100	-8.244E+00	-6.646E+00	-4.544E+00	3.791E+00	-3.714E+00	-6.385E+00
1998	221	2200	-8.328E+00	-6.646E+00	-4.203E+00	3.791E+00	-3.894E+00	-6.646E+00
1998	221	2300	-8.328E+00	-6.517E+00	-4.375E+00	3.791E+00	-3.714E+00	-6.646E+00
1998	221	2400	-8.409E+00	-6.772E+00	-4.375E+00	3.519E+00	-3.714E+00	-6.385E+00
1998	274	100	-8.563E+00	-6.896E+00	-4.203E+00	2.718E+00	-3.894E+00	-6.517E+00
1998	274	200	-8.488E+00	-6.772E+00	-4.028E+00	2.718E+00	-3.894E+00	-6.385E+00
1998	274	300	-8.488E+00	-6.772E+00	-4.203E+00	2.718E+00	-3.894E+00	-6.385E+00
1998	274	400	-8.488E+00	-6.896E+00	-3.851E+00	2.982E+00	-3.894E+00	-6.517E+00
1998	274	500	-8.488E+00	-6.772E+00	-4.203E+00	2.718E+00	-3.714E+00	-6.385E+00
1998	274	600	-8.409E+00	-6.772E+00	-4.028E+00	2.718E+00	-3.714E+00	-6.517E+00
1998	274	700	-8.563E+00	-6.772E+00	-4.203E+00	2.718E+00	-3.714E+00	-6.251E+00
1998	274	800	-8.488E+00	-6.772E+00	-4.028E+00	2.718E+00	-3.894E+00	-6.517E+00
1998	274	900	-8.409E+00	-6.772E+00	-3.670E+00	3.249E+00	-3.894E+00	-6.772E+00

Table 4.3 Comparison of Change in Strain Between Hinged and Continuous Side of Pier

1998	274	1000	-8.488E+00	-6.772E+00	-4.203E+00	2.982E+00	-3.714E+00	-6.385E+00
1998	274	1100	-8.488E+00	-6.772E+00	-4.375E+00	2.718E+00	-3.532E+00	-6.517E+00
1998	274	1200	-8.488E+00	-6.896E+00	-4.375E+00	2.982E+00	-3.532E+00	-6.385E+00
1998	274	1300	-8.563E+00	-6.896E+00	-4.203E+00	2.982E+00	-3.714E+00	-6.251E+00
1998	274	1400	-8.636E+00	-6.772E+00	-4.375E+00	2.718E+00	-3.714E+00	-6.251E+00
1998	274	1500	-8.563E+00	-6.896E+00	-4.544E+00	2.982E+00	-3.532E+00	-6.517E+00
1998	274	1600	-8.563E+00	-6.896E+00	-4.375E+00	2.718E+00	-3.346E+00	-6.251E+00
1998	274	1700	-8.636E+00	-7.016E+00	-4.544E+00	2.718E+00	-3.346E+00	-6.385E+00
1998	274	1800	-8.563E+00	-6.896E+00	-4.710E+00	2.982E+00	-3.714E+00	-6.385E+00
1998	274	1900	-8.563E+00	-7.016E+00	-4.544E+00	2.982E+00	-3.346E+00	-6.517E+00
1998	274	2000	-8.563E+00	-7.016E+00	-4.375E+00	3.249E+00	-3.714E+00	-6.517E+00
1998	274	2100	-8.563E+00	-6.896E+00	-4.375E+00	2.982E+00	-3.532E+00	-6.385E+00
1998	274	2200	-8.488E+00	-6.772E+00	-4.375E+00	2.718E+00	-3.714E+00	-6.517E+00
1998	274	2300	-8.409E+00	-6.772E+00	-4.544E+00	2.718E+00	-3.532E+00	-6.385E+00
1998	274	2400	-8.636E+00	-6.772E+00	-4.544E+00	2.457E+00	-3.714E+00	-6.251E+00
1999	1	100	-8.488E+00	-7.249E+00	-3.851E+00	3.519E+00	-3.532E+00	-6.385E+00
1999	1	200	-8.409E+00	-7.249E+00	-4.028E+00	3.519E+00	-3.714E+00	-6.517E+00
1999	1	300	-8.409E+00	-7.471E+00	-3.851E+00	3.249E+00	-3.532E+00	-6.251E+00
1999	1	400	-8.409E+00	-7.471E+00	-4.028E+00	3.519E+00	-3.346E+00	-6.251E+00
1999	1	500	-8.409E+00	-7.471E+00	-4.203E+00	3.519E+00	-3.532E+00	-6.385E+00
1999	1	600	-8.409E+00	-7.471E+00	-4.710E+00	3.519E+00	-3.346E+00	-6.113E+00
1999	1	700	-8.409E+00	-7.577E+00	-4.028E+00	3.791E+00	-3.714E+00	-6.385E+00
1999	1	800	-8.488E+00	-7.577E+00	-4.203E+00	3.519E+00	-3.714E+00	-6.385E+00
1999	1	900	-8.488E+00	-7.577E+00	-4.375E+00	3.249E+00	-3.714E+00	-6.517E+00
1999	1	1000	-8.563E+00	-7.681E+00	-4.375E+00	3.519E+00	-3.532E+00	-6.772E+00
1999	1	1100	-8.563E+00	-7.681E+00	-4.203E+00	3.519E+00	-3.346E+00	-6.251E+00
1999	1	1200	-8.488E+00	-7.681E+00	-4.375E+00	3.519E+00	-3.346E+00	-6.113E+00
1999	1	1300	-8.488E+00	-7.782E+00	-4.544E+00	3.519E+00	-3.532E+00	-6.251E+00
1999	1	1400	-8.636E+00	-7.782E+00	-4.375E+00	3.519E+00	-3.532E+00	-6.385E+00
1999	1	1500	-8.636E+00	-7.681E+00	-4.375E+00	3.519E+00	-3.346E+00	-6.385E+00
1999	1	1600	-8.563E+00	-7.681E+00	-4.544E+00	3.519E+00	-3.532E+00	-6.517E+00
1999	1	1700	-8.563E+00	-7.681E+00	-4.375E+00	3.519E+00	-3.532E+00	-6.646E+00
1999	1	1800	-8.636E+00	-7.681E+00	-4.710E+00	3.249E+00	-3.532E+00	-6.517E+00
1999	1	1900	-8.563E+00	-7.577E+00	-4.710E+00	3.519E+00	-3.532E+00	-6.251E+00
1999	1	2000	-8.636E+00	-7.577E+00	-4.873E+00	3.249E+00	-3.532E+00	-6.517E+00

Table 4.3 Comparison of Change in Strain Between Hinged and Continuous Side of Pier

1999	1	2100	-8.488E+00	-7.361E+00	-4.873E+00	3.249E+00	-3.532E+00	-6.517E+00
1999	1	2200	-8.328E+00	-7.471E+00	-4.028E+00	4.344E+00	-3.714E+00	-6.896E+00
1999	1	2300	-8.563E+00	-7.577E+00	-4.873E+00	3.519E+00	-3.532E+00	-6.385E+00
1999	1	2400	-8.488E+00	-7.577E+00	-4.873E+00	3.249E+00	-3.714E+00	-6.385E+00

Table 4.3 Comparison of Change in Strain Between Hinged and Continuous Side of Pier

contain the absolute maximum curvature about the horizontal axis, it is representative of the structural behaviour of the bridge. Therefore, it may be suggested that although the curvatures about the horizontal axis may change throughout the year for each cross section, the structural response of the Confederation Bridge, due to the curvatures, remains fairly constant and the magnitude of the forces due to continuity of the structure is also relatively small.

The maximum predicted deflection at mid span due to load combination 24 was 16.8 mm. This value is very close to the measured value 17 mm reported by Elbadry, Ghali and Megally (2001), and is slightly closer to the measured value than the predicted value of 14 mm reported by Elbadry et al (2001). Of interest is the relatively small magnitude of the displacements, both vertically and horizontally.

Elbadry et al (2001) reported temperature predicted deflections for June 12, 1998 (Day 163) of 75 mm (downward) at the end of the cantilever, and 60 mm (upward) at mid span. The reported data for this day included a top slab temperature of 27.3 °C. In addition, the temperature through the depth of the section was reported to be 18.3 °C at the underside of the top slab and 17.3 °C at the underside of the bottom slab. These temperatures are also close to those measured on Day 221, which was analyzed in load combinations one through four. For day 221, the predicted downward deflection at the end of the cantilever varied between 71 mm in the morning to 89.5 mm at mid afternoon and the predicted upward deflection at mid span varied between 63.8 mm and 65.3 mm. These deflections are, again, in very good agreement with those reported by Elbadry et al (2001).

Note that the transverse displacements due to temperature (y-Translation) are very small. Although the transverse gradient in the larger section is of a larger magnitude than the horizontal gradient, the effect is minimal on the overall structure for several reasons. First, the larger section occurs at the pier supports. Out in the span of the bridge where the smaller sections occur, the transverse curvature is much smaller. Hence smaller displacements. In addition, the moment of inertia of the cross sections about the vertical axis is larger than that about the horizontal axis for sections in the middle 160 m of the 250 m span. As a result, the structure has very high stiffness in the transverse direction, which also leads to small displacements.

From this it may be seen that the overall structural effect of the temperature differences through the depth and across the section on this structure is minimal.

4.5 Cross Section Analysis with SFRAME

The effect of the transverse temperature differences through the top and bottom slabs and the webs will now be reviewed for a cross section. As noted in section 3.7, it has been pointed out in the literature, Degenkolb (1977) and Precast Segmental Box Girder Bridge Manual (1978) that the temperature difference through the depth of the section results in bending moments being induced on the webs of the box girder.

Since recorded temperature data is readily available specifically for the two sections that will be analyzed, namely S1 and S51 representing the deepest and shallowest sections, there is no need to perform a FETAB analysis on these two cross sections to obtain temperature distributions. Therefore the curvatures computed from the recorded temperature data are input directly into SFRAME.

Once again, the computer program SFRAME was utilized to model the cross sections as an assemblage of beam elements. Figures 4.15 and 4.16 display the nodal layout used to model sections S1 and S51.

For this analysis day 221 was selected as a result of the work already presented. The selection of 01:00 hours may seem a curious choice to produce a maximum effect, but it was at this time of the day that a single temperature difference between points on the outer surface of the two walls was at a maximum. It should be noted that although the difference in temperature between two points on the two wall surfaces was a maximum, this did not yield the maximum transverse gradient. The maximum transverse gradient occurred later in the morning at 11:00 hours. A possible explanation for this could be the dimensional size of the top slab. Since the top slab cantilevers out from the walls of the box section, the temperatures in the top slab will have a noticeable effect on the transverse gradient.

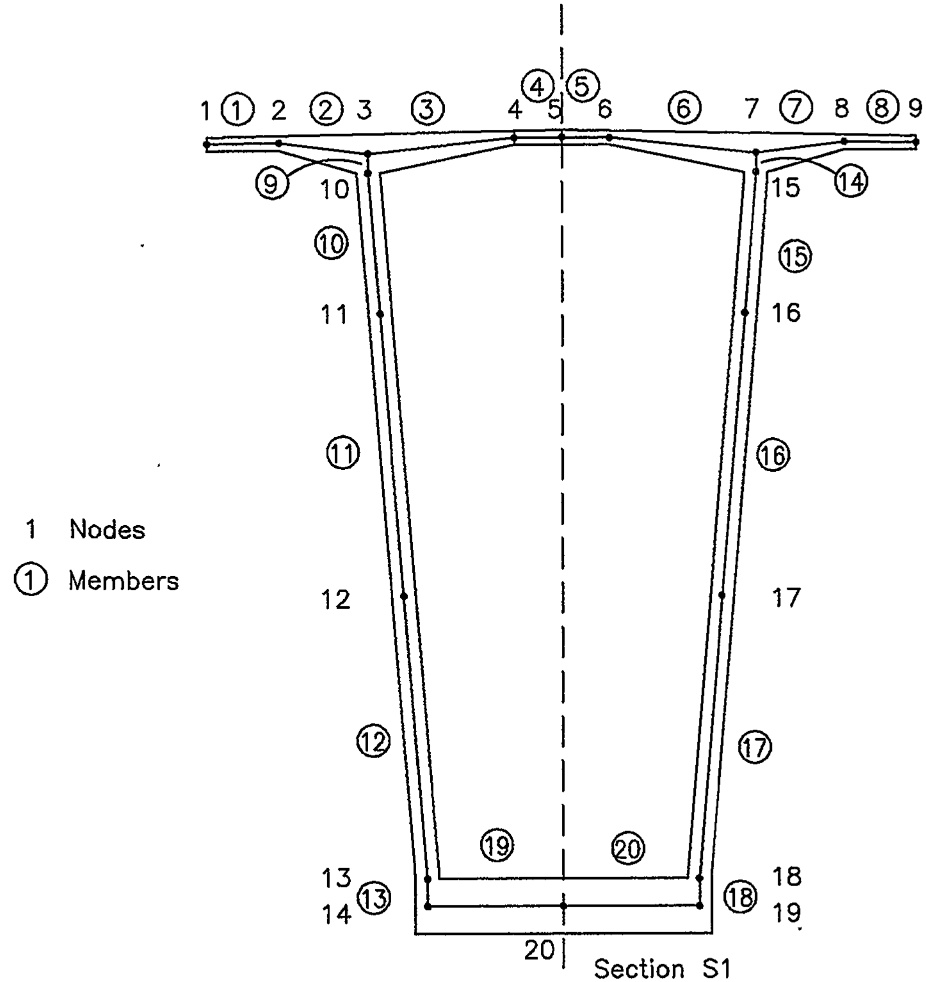

Figure 4.15 SFRAME computer model for transverse effects, section S1

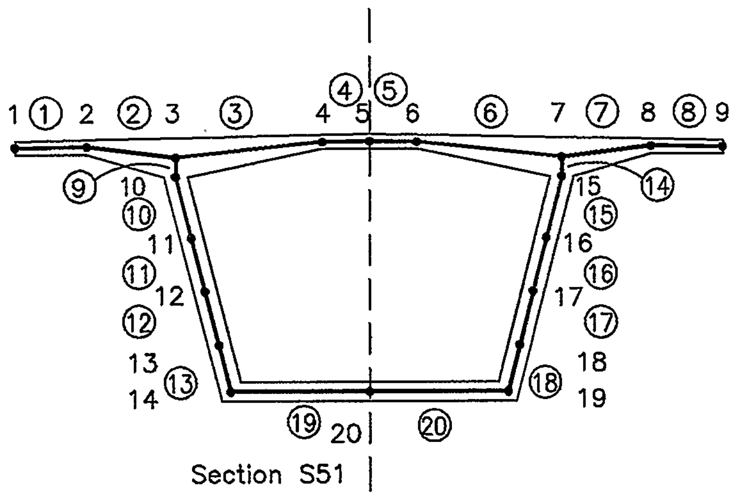

1 Nodes

1 Members

Figure 4.16 SFRAME computer model for transverse effects, section S51

Figures 4.17 and 4.18 contain the bending moment diagrams for sections S1 and S51, respectively. Note that the maximum moment that produced a tensile stress on the outside face of one of the walls of section S1 is only 7.6 kNm, which results in a tensile stress of 0.28 MPa. For section S51, the maximum bending moment that produced a tensile stress on an outside face is 6.9 kNm, resulting in a tensile stress of 0.46 MPa.

Hence, for this day the effects of the transverse temperature gradient are not critical for frame behaviour of the cross sections for the Confederation Bridge. Note that the bending moments present in the cross section S1 are actually higher than those in the cross section S51. This is opposite to what would be expected. At first glance, the deeper section, S1, would appear to be more flexible, giving rise to the assumption that this section would yield lower bending moments. However, the deeper section has thicker walls and the moment of inertia of the walls in the deeper section is approximately 2.4 times that in the smaller section, S51. However, in neither section were stresses found to be above the cracking limit.

A subroutine was then written to compare the recorded temperatures on the exterior and interior faces of the girder walls, determine the maximum difference and when it occurred .

First, consider section S51. For the data set available, the maximum difference between the exterior and interior faces on the south-east wall of the girder section occurred on Day 35, 1999 at 12:00 hrs.

Day 35, 1999, 12:00 hrs Section S51

$T_{exterior} = 15.49\ ^{\circ}C$ $\quad$ $T_{interior} = 0.14\ ^{\circ}C$ $\quad$ $\Delta T = +15.35\ ^{\circ}C$

Again, for the data set available, the maximum difference between the exterior and interior faces on the north-west wall of the girder section occurred on Day 161, 1998 at 20:00 hrs.

Day 161, 1998, 20:00 hrs Section S51

$T_{exterior} = 24.87\ ^{\circ}C$ $\quad$ $T_{interior} = 13.26\ ^{\circ}C$ $\quad$ $\Delta T = +11.61\ ^{\circ}C$

The corresponding data for cross section S1 was reviewed for the same days.

Day 35, 1999, 12:00 hrs Section S1

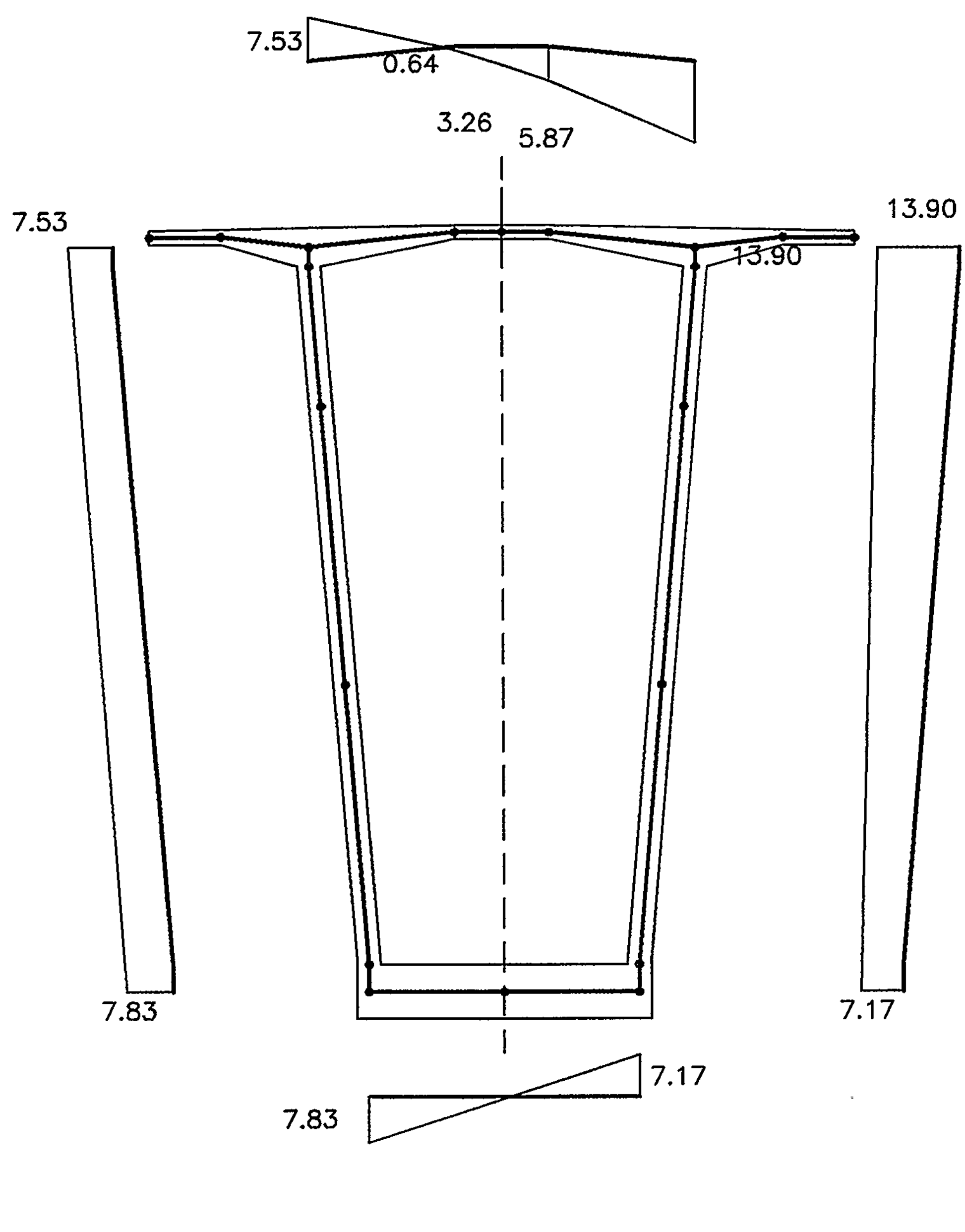

Figure 4.17 Day 221, 1998 – 01:00 hrs
Transverse Bending Moments kNm/m

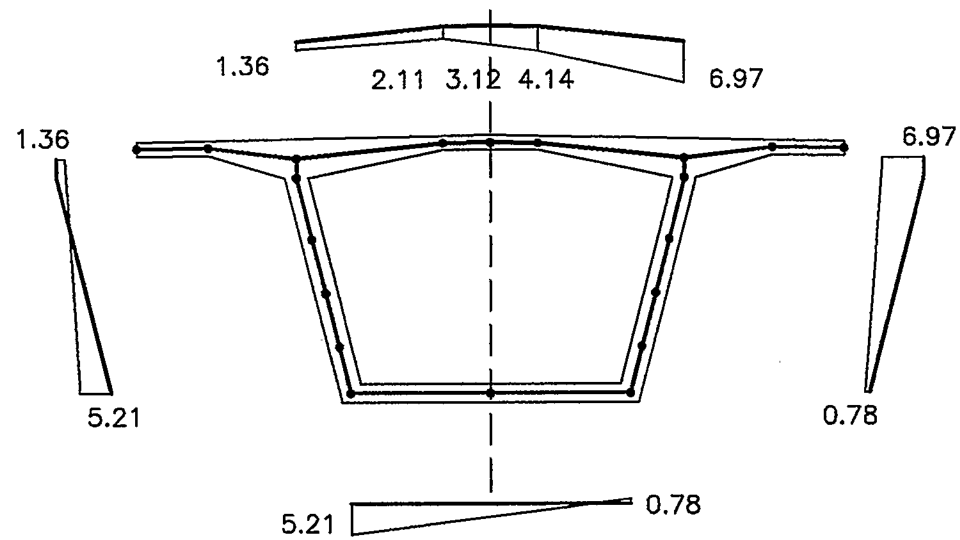

Figure 4.18 Day 221, 1998 – 01:00 hrs – Transverse Bending Moments kNm/m

$T_{exterior} = 19.5\ ^{o}C$ $T_{interior} = -1.13\ ^{o}C$ $\Delta T = +20.63\ ^{o}C$

These temperature distributions are shown in Figures 4.19 and 4.20. Note that for Day 35 (Feb 4, 1999) the temperatures along the eastern web of the girder are very high, while the ambient temperature is approximately 0°C. One plausible explanation for these recordings is the lack of convection along the windward face of the girder, as discussed in section 4.3. On this day, at the hour shown, the angle of the sun is low so that the barriers, no doubt, shade the top surface of the bridge and the south-east face web of the girder gets direct solar radiation. If the air current splits, as supposed in section 4.3, there will be a zone along the face of the web where the heat loss due to convection will be very small, resulting in higher temperatures.

The recorded temperatures were used to generate input curvatures for a frame analysis in the transverse direction. In order to compare the severity of the recorded temperatures the two cross sections were analyzed using temperature differences set out in the Canadian Bridge Code (2000). There are no recommendations in the code for temperature differences through the various members of a concrete box girder cross section. The temperature difference meant to be applied through the depth of a cross section were applied through the thickness of each web and slab of the concrete box girder section. Considering the box girder to be an assemblage of four thin slabs, clause 3.9.4.4.1 of the Canadian Highway Bridge Design Code specifies a temperature difference of 15°C.

Figure 4.21 contains a bending moment diagram for a temperature load case on section S1 where the top slab, bottom slab and west web were subjected to no temperature gradient, and the east wall subjected to a 15°C temperature gradient through the thickness of the wall. The higher temperature being on the outer surface. A maximum tensile bending stress of 2.3 MPa occurs on the outside face of the east wall. It is interesting to note that when the recorded temperatures on Day 35, 1999 at 12:00 hrs were analyzed, Figure 4.22, the maximum bending stresses and magnitudes are of the same order and in the same location as in Figure 4.21. The theoretical tensile strength of concrete in bending, for the girders, according to CSA-S6 is 2.96 MPa.

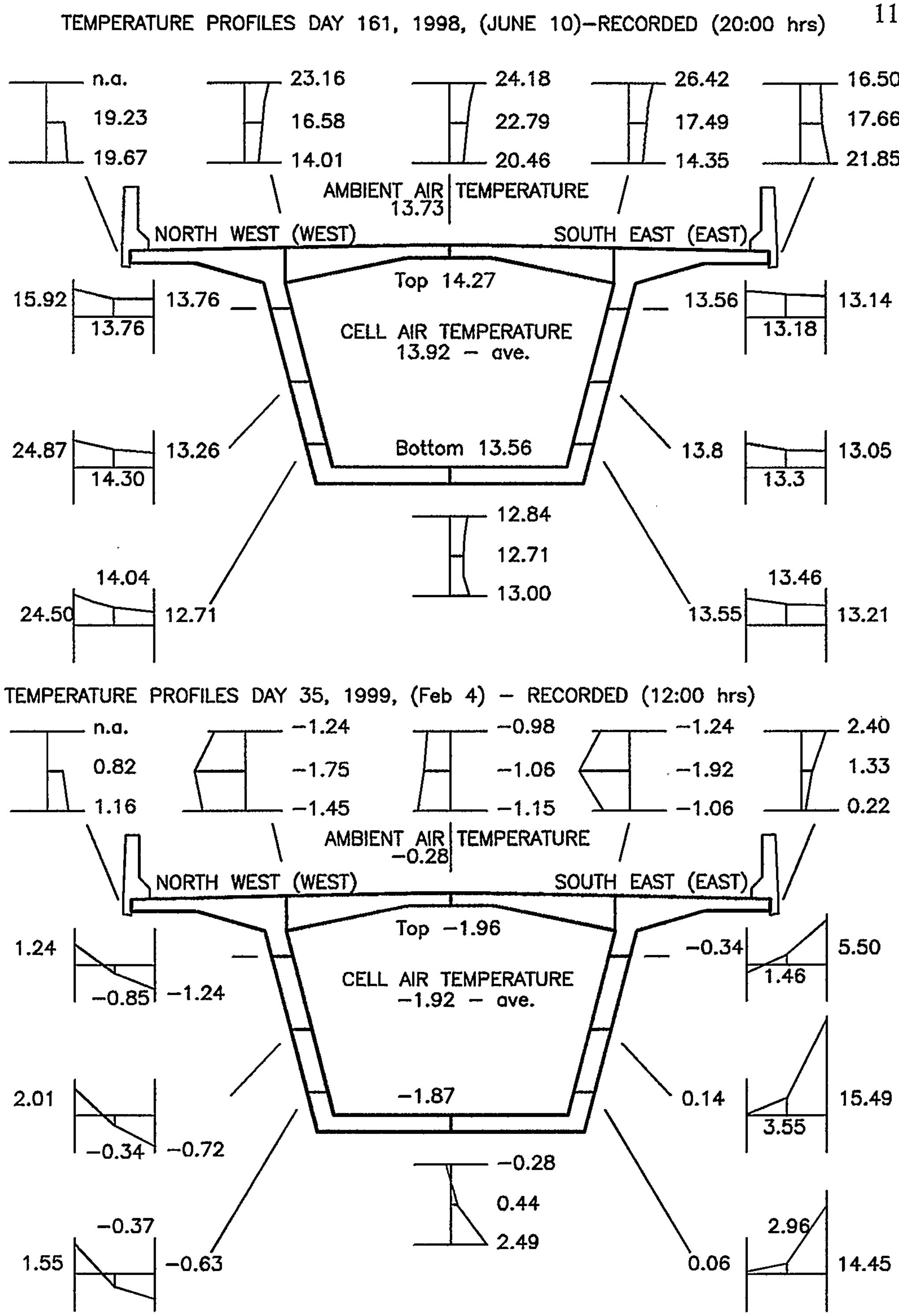

Figure 4.19 Recorded Temperatures for Section S51 used for The Analysis of Transverse Frame Behaviour

TEMPERATURE PROFILES DAY 35, 1999, (Feb 4) – RECORDED (12:00 hrs)

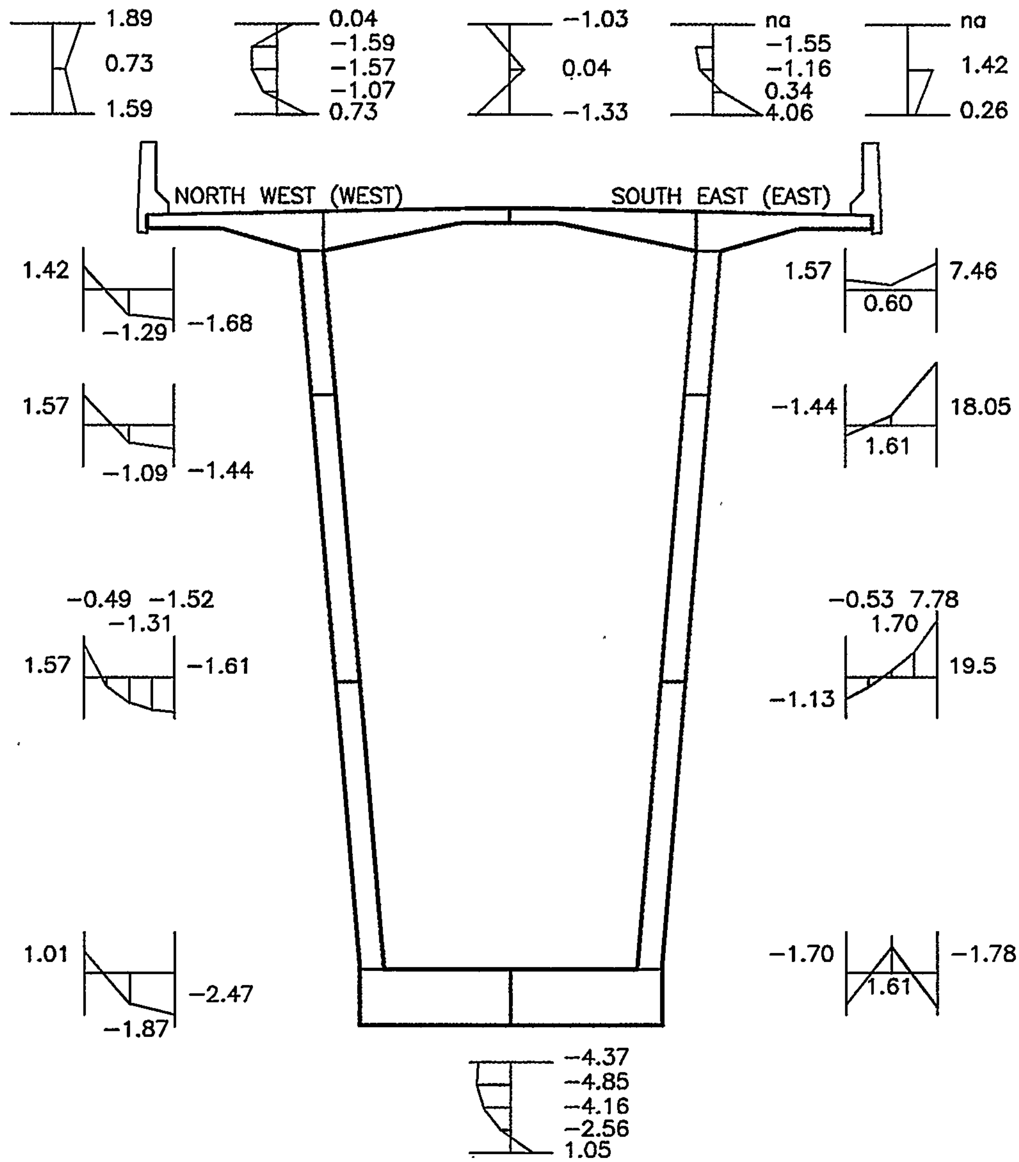

Figure 4.20 Recorded Temperatures for Section S1 used for The Analysis of Transverse Frame Behaviour

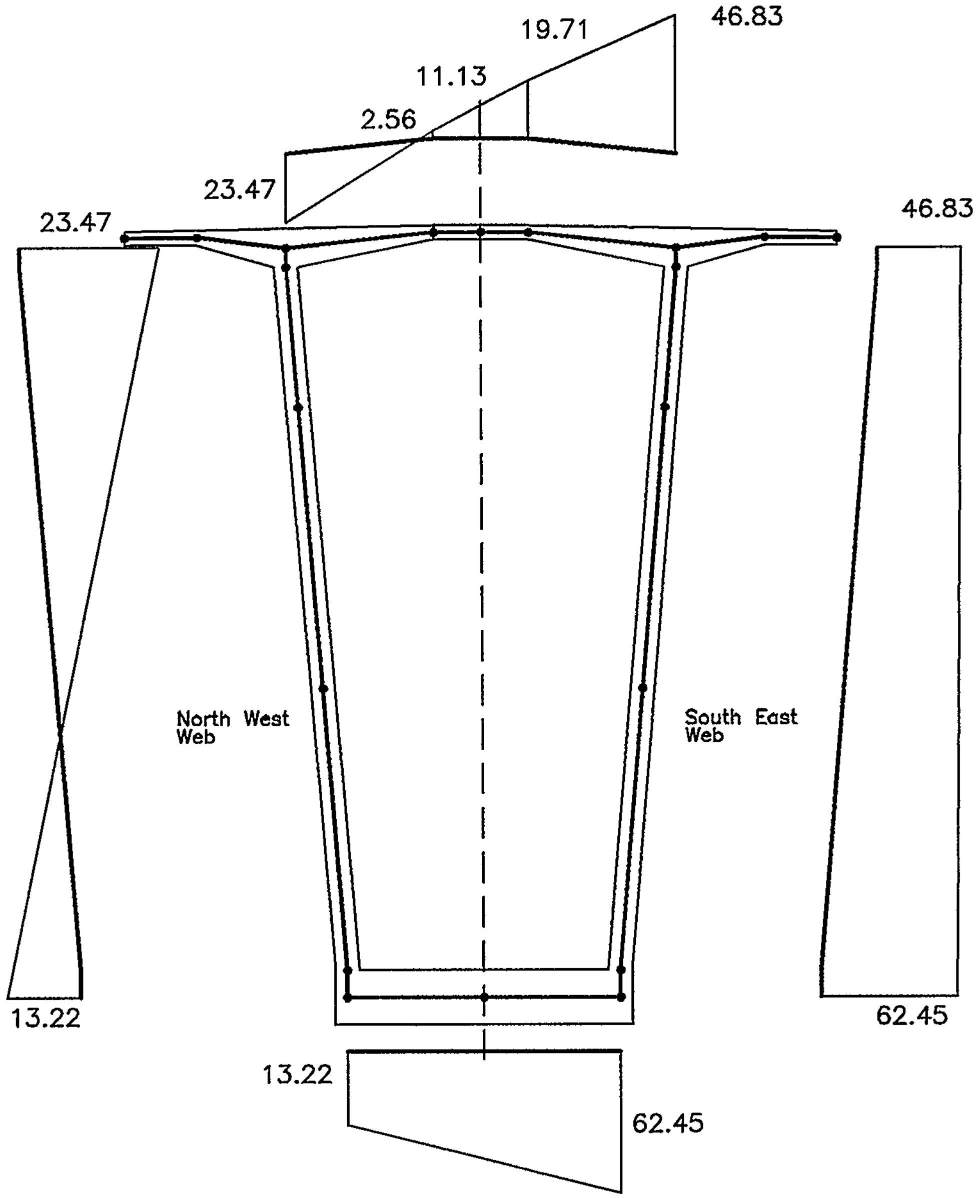

Figure 4.21 Code Temperature – 15°C Gradient in the East Web. Transverse Bending Moments (kNm/m)

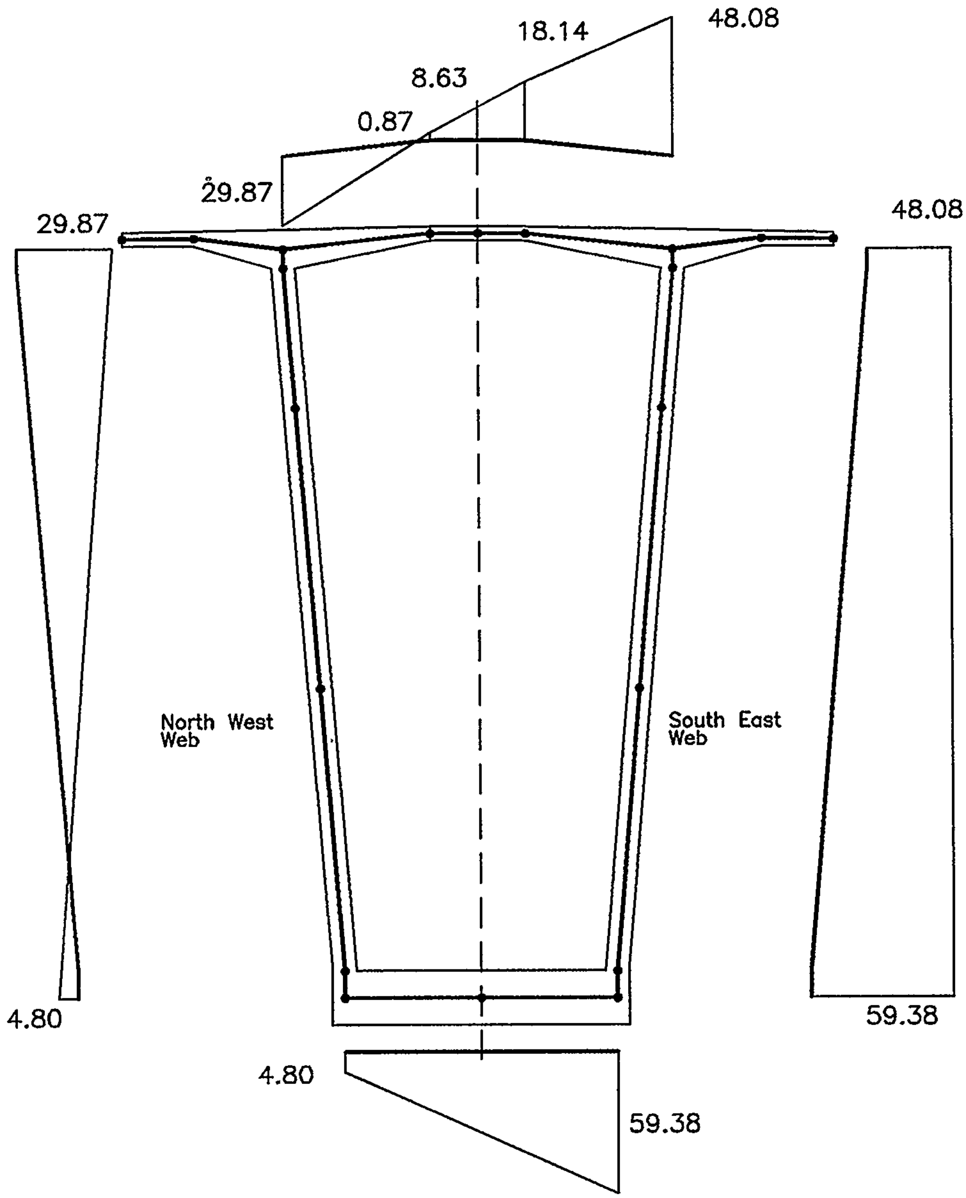

Figure 4.22 Day 35, 1999 — Transverse Bending Moments (kNm/m)

However, when the effects of shrinkage are incorporated the actual tensile strength becomes markedly reduced. If the section cracks, the bending stiffness is significantly reduced, leading to a redistribution of bending stresses. Hence, the cracked section will have a reduction is bending stress and other sections will have an increase in bending stress, leading to further cracking.

Figure 4.23 contains a bending moment diagram for a temperature load case on section S51 where the top slab, bottom slab and west wall were subjected to no temperature gradient, and the east wall subjected to a 15°C temperature gradient through the thickness of the wall. The higher temperature being on the outer surface. A maximum tensile bending stress of 1.5 MPa occurs on the outside face of the east wall. It is interesting, again, to note that when the recorded temperatures on Day 35, 1999 at 12:00 hrs were analyzed, Figure 4.24, the maximum bending stresses and magnitudes are of the same order and in the same location as in Figure 4.23. Further, it is interesting that when the recorded temperatures on Day 161, 1998 were analyzed, Figure 4.25, the magnitudes of the resulting bending stresses are very close to those from Day 35, 1999. The difference being the location of the tensile stress.

In terms of design, it is important to analyze the frame for a temperature that will yield a maximum tensile bending stress. Comparing Figure 4.21 to Figure 4.22 and Figure 4.23 to Figures 4.24 and 4.25 reveals that the 15°C temperature difference across the thickness of the web underestimates the actual conditions by a small margin. Therefore, Figures 4.26 and 4.27 contain the bending moment diagrams for sections S1 and S51, respectively, when they are subjected to a 20°C difference. The bending moments contained in these two Figures are more suitable for design purposes.

Although it is critical to determine the maximum bending moments in the frame structure, it is also important to know the relative magnitude of the temperature induced bending moments to the bending moments due to self weight and wheel loads due to vehicles. The Canadian Highway Bridge Design Code specifies the CL-625 truck loading, with a maximum wheel point load of 87.5 kN. A typical lane width is 3.0m and the truck centred in this lane with the wheel spaced 1.8m centre to centre. Figure 4.28a

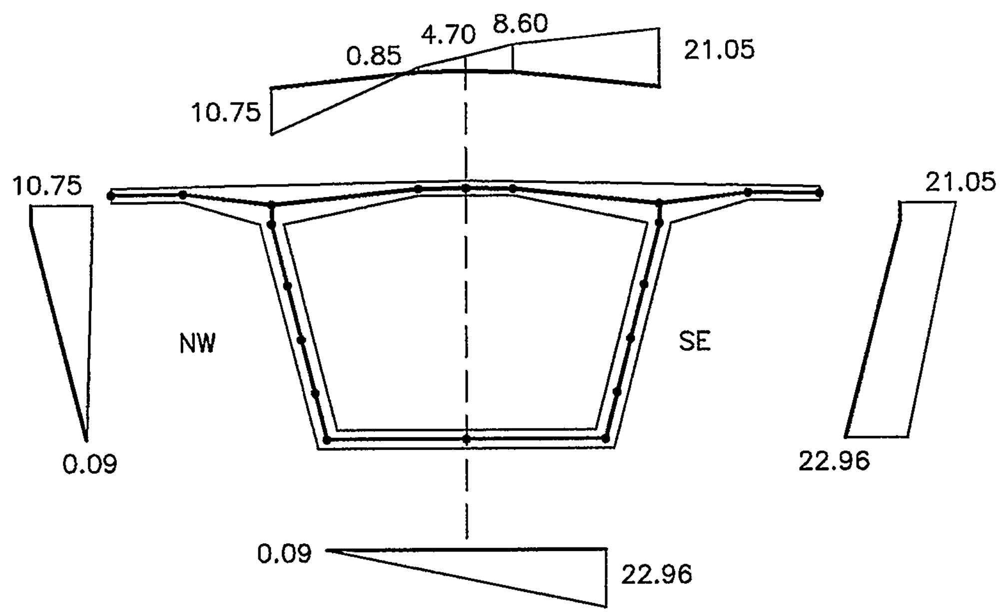

Figure 4.23 Bending Moment Diagram (kNm/m) due to a 15°C Temperature Gradient in the SE Web

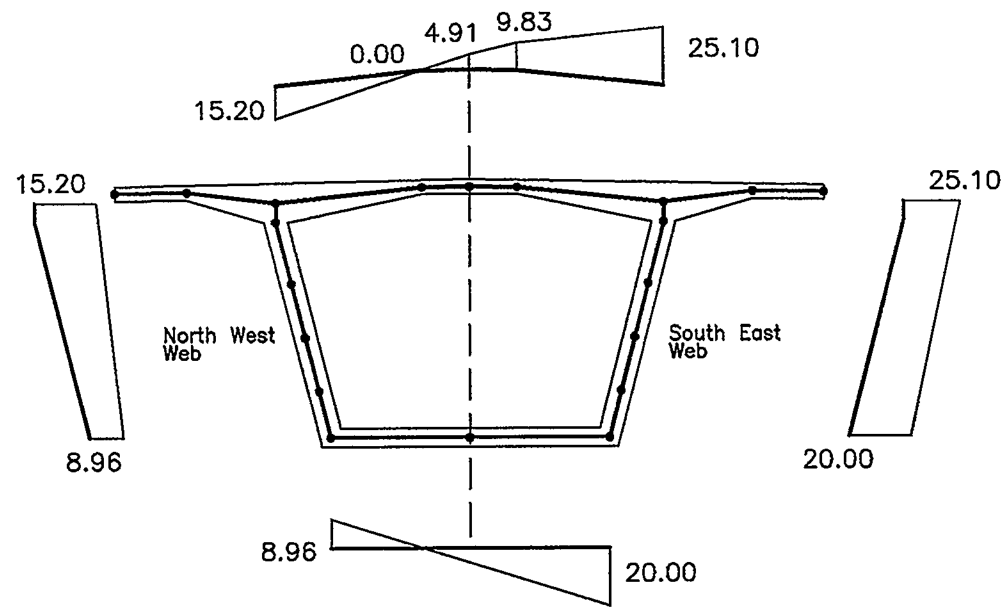

Figure 4.24 Day 35, 1999 Transverse Bending Moment Diagram (kNm/m)

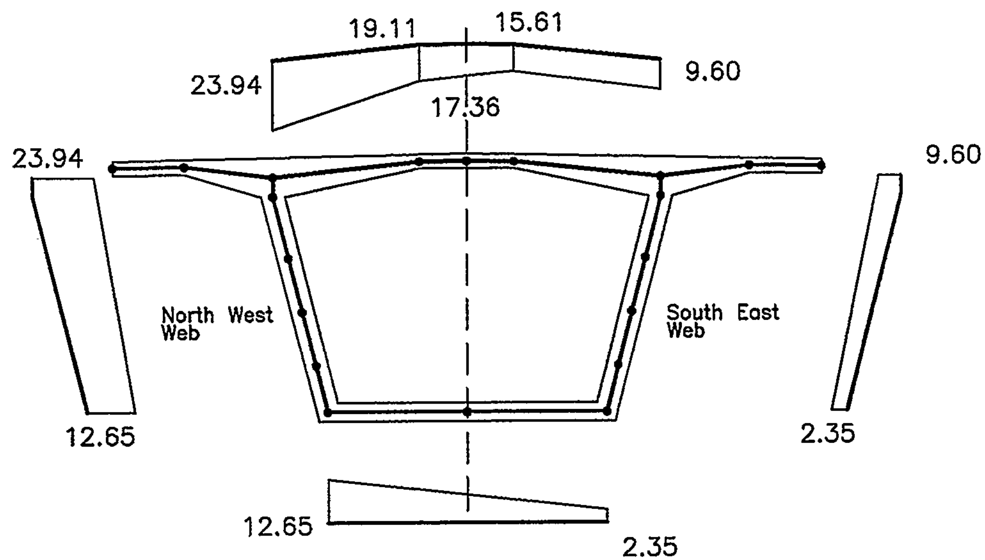

Figure 4.25 Day 161, 1998 Transverse Bending Moment Diagram (kNm/m)

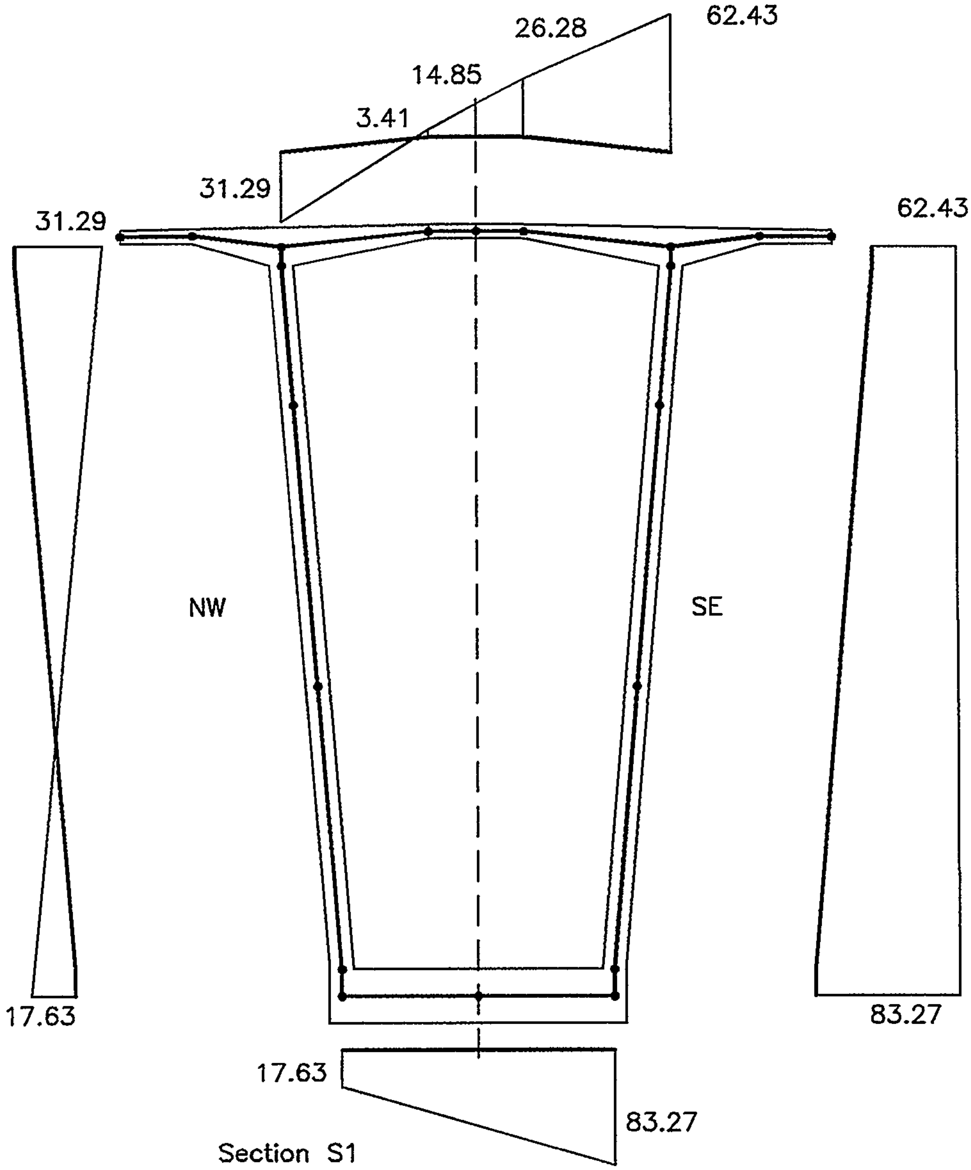

Figure 4.26 Bending Moment Diagram (kNm/m) due to a 20°C Temperature Gradient in the SE Web

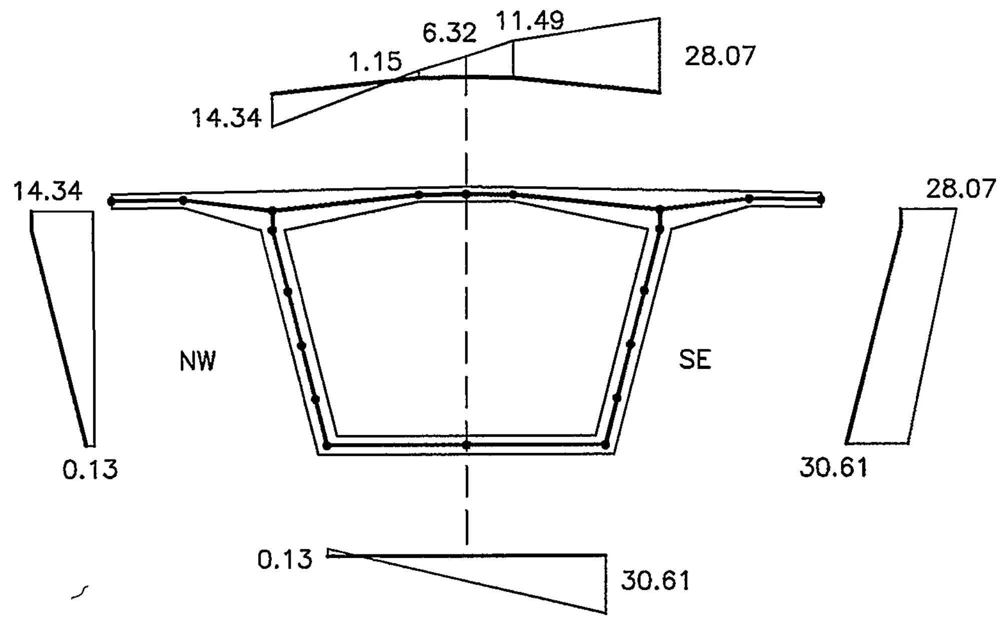

Section S51

Figure 4.27 Bending Moment Diagram (kNm/m) due to a 20°C Temperature Gradient in the SE Web

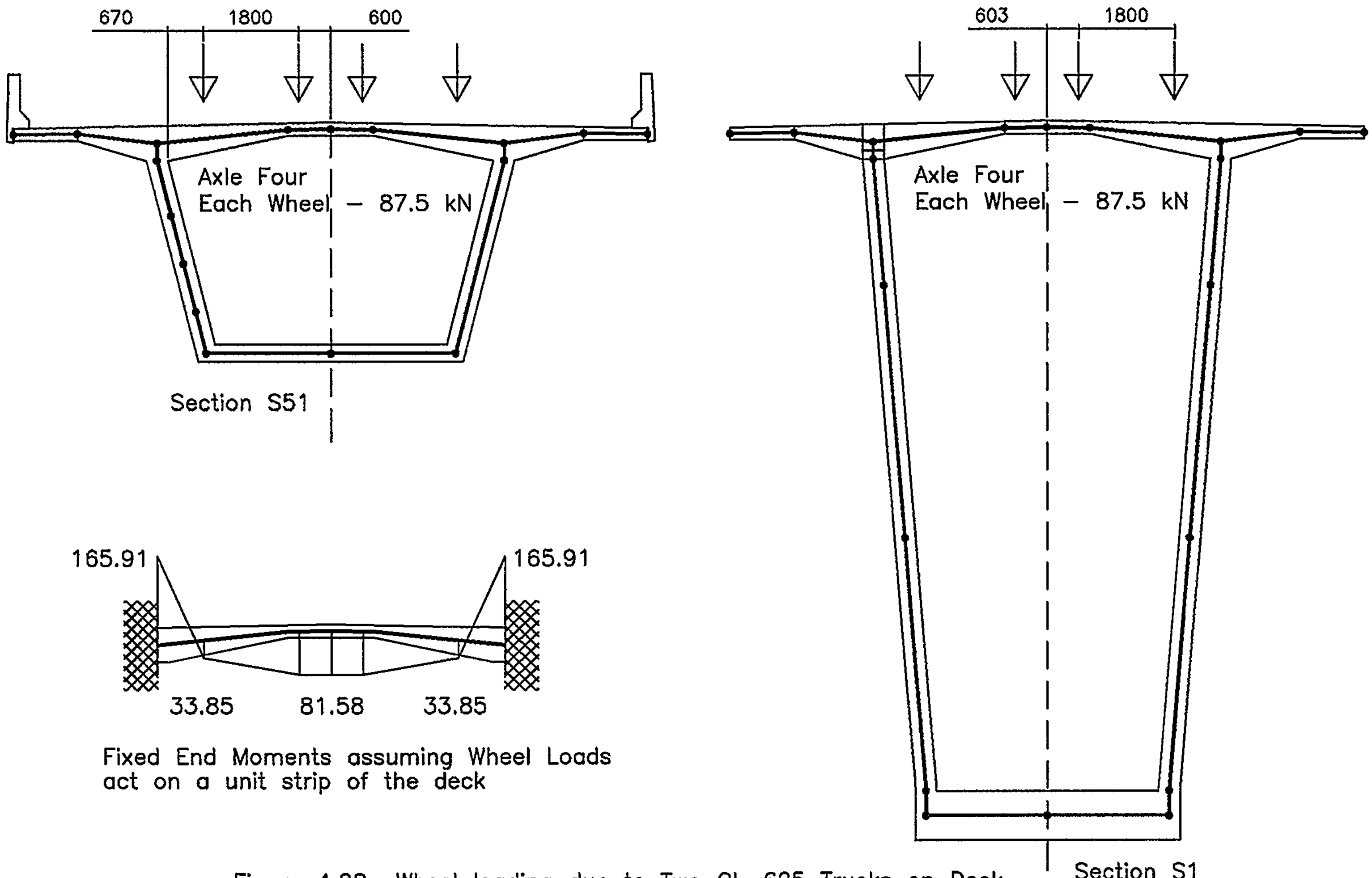

Figure 4.28a Wheel loading due to Two CL–625 Trucks on Deck

contains the two cross sections, S1 and S51, with the wheel loads positioned such that they will produce a maximum tensile stress on the exterior face of the walls of the box girder. For this analysis the bending moments resulting from self weight and temperature will be combined with those from wheel loads. Therefore, an equivalent wheel loading that may be applied to a unit strip of a cross section must be computed. Note that Figure 4.28a also shows the fixed end moments that result when the point loads are assumed to be applied on the unit strip. This leads to an over estimation of the actual bending moment. The fixed end bending moment, shown in Figure 4.28a, is actually distributed over a finite length of the deck depending on the geometry of the cross section.

In order to analyze the distribution of the fixed end bending moments in the deck slab, it is necessary to use plate bending finite elements. Bakht (1981) presented a simplified analysis in order to compute the bending moments in a cantilevered span. However, the bending moments in the deck span depend on the relative stiffness of the webs and must be determined through a three dimensional analysis. Figure 4.28b shows an schematic drawing of the finite element mesh generated in order to analyze the 60 m drop in span of the Confederation bridge. Note that for this analysis, the cantilevers are left off the finite element mesh since the truck wheel loads are confined to the deck slab. Two trucks, traveling in opposite directions were positioned at the middle of the drop in span, as shown in Figure 4.28c.

The maximum bending moment at the face of the web occurred where the fourth axles of the two trucks aligned and was found to be 92.43 kNm, see Figure 4.28c, and is significantly lower than the bending moment of 165.91 kNm, see Figure 4.28a where the wheel loads were assumed to be distributed on a 1m width of the cross section. Here, the peak bending moment is distributed over a distance of 1.8 m. This is still fairly concentrated, but it must be remembered that the ends of the deck slab are very stiff. The thickness of the slab next to the webs is approximately 650 mm.

The wheel loads that must be used in the 1m strip for the cross section analysis must be reduced accordingly. Figure 4.28c contains the reduced wheel loads that result

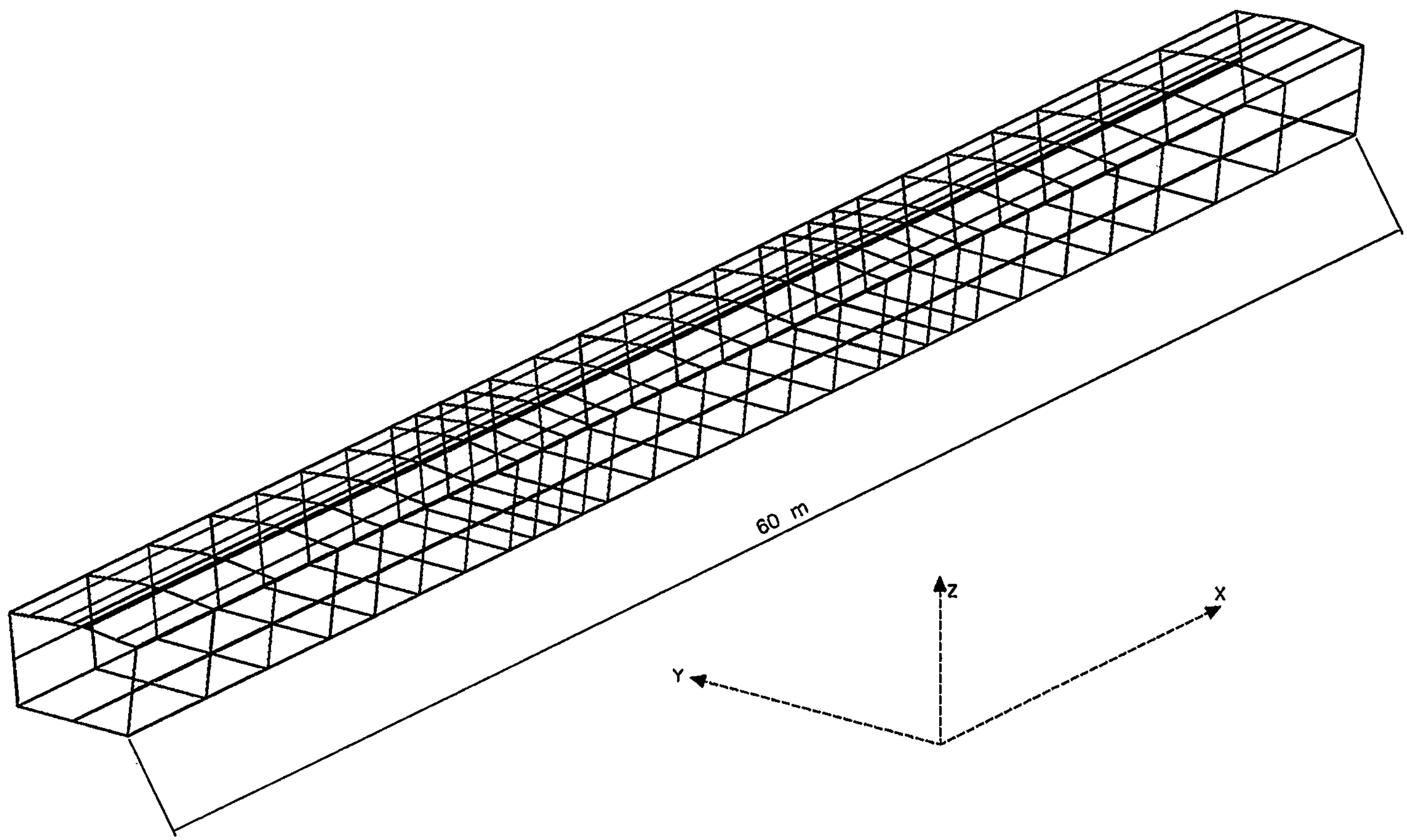

Figure 4.28b Finite Element mesh with plate bending elements of 60m drop–in span, schematic only. Not to scale

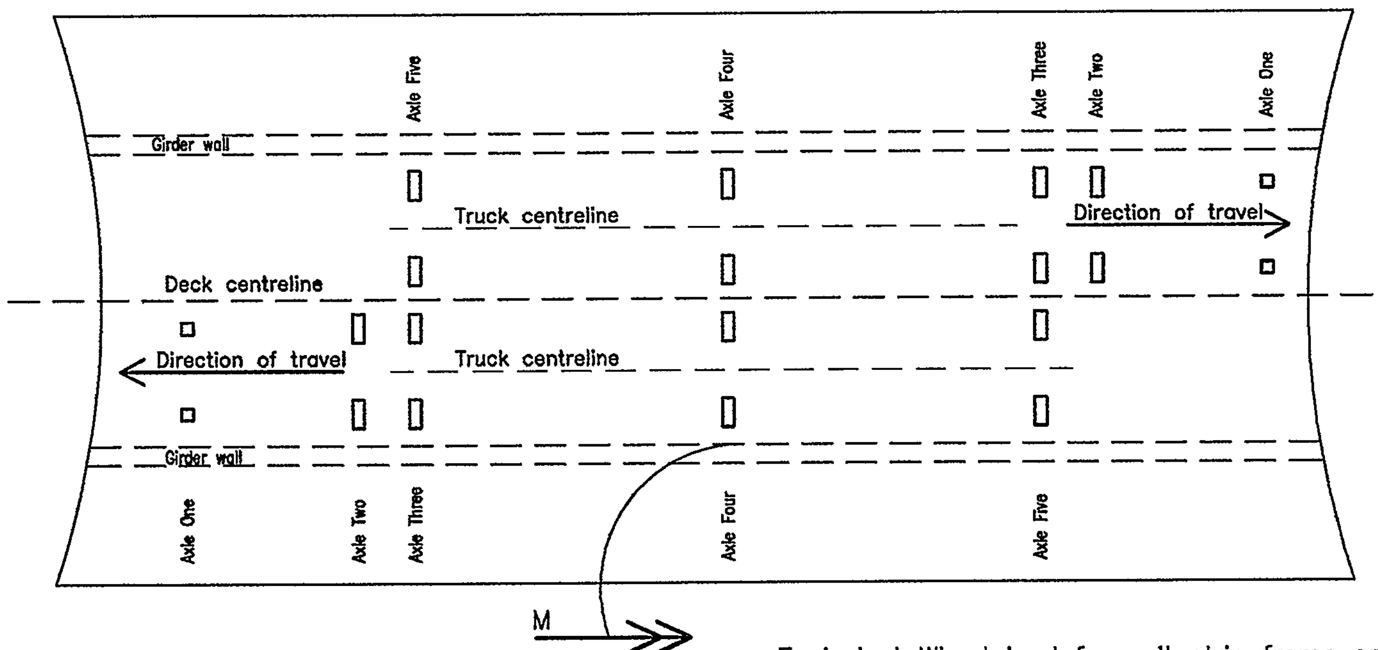

Maximum Bending Moment along inside of web
M = 92.43 kNm at axle four

Equivalent Wheel load for unit strip frame analysis

$$87.5 \text{ kN} \times \frac{92.43 \text{ kNm}}{165.91 \text{ kNm}}$$
$$\times 1.4 \text{ DLA}$$
$$\times 0.9 \text{ Multilane factor}$$
$$= 61.4 \text{ kN}$$

Figure 4.28c Wheel loading distribution on deck from the longitudinal distribution of bending moments. Here, the wheel loads are adjusted for the dynamic effects and multilane loading. The effective wheel load on a unit strip of the cross section becomes 62.4 kN/m. Again, this analysis is simply to compare the relative magnitudes of each of the three load cases and is not meant to be a rigorous design check.

It should be noted that the maximum value of the bending moment due to wheel loading on the cantilevered slab of the Confederation Bridge was considered. However, this case of loading produces a bending moment resulting in tension on the inside face of the girder wall. For this investigation the temperature loading was determined such that it would produce a maximum tension along the outside face of the girder wall.

Figure 4.28d and Figure 4.28e contain the cracking moment envelopes for section S1 and section S51, respectively. These diagrams will aid in comparing the relative magnitude of transverse bending moments due to self weight, wheel loading and transverse temperature distributions. The cracking moments have been calculated based on the section modulus for each slab and wall and the modulus of rupture specified in CSA-S6 (2000), clause 8.1.4.8.

Figure 4.29 presents the bending moment diagram due to self weight of section S1, Figure 4.30 contains the bending moment diagram for section S1 due to self weight combined with those due to the wheel loading, and Figure 4.31 contains the bending moment diagram due to the combination of self weight, wheel loading and the temperatures from Figure 4.26. Note that the increase in bending moments that produce a tensile stress on the exterior face of the wall is 50% (165.63 kNm/m from 110.26 kNm/m, while the cracking moment is only 79.1 kNm/m)

Figures 4.32, 4.33 and 4.34 contains the bending moment diagrams for section S51 due self weight, self weight plus wheel loading, and self weight plus wheel loading combined with those from temperature in Figure 4.27. The relative increase in bending moments that produce a tensile stress on the exterior face of the wall is 23% (143.01 kNm/m from 116.63 kNm/m, while the cracking moment is only 44.5 kNm/m).

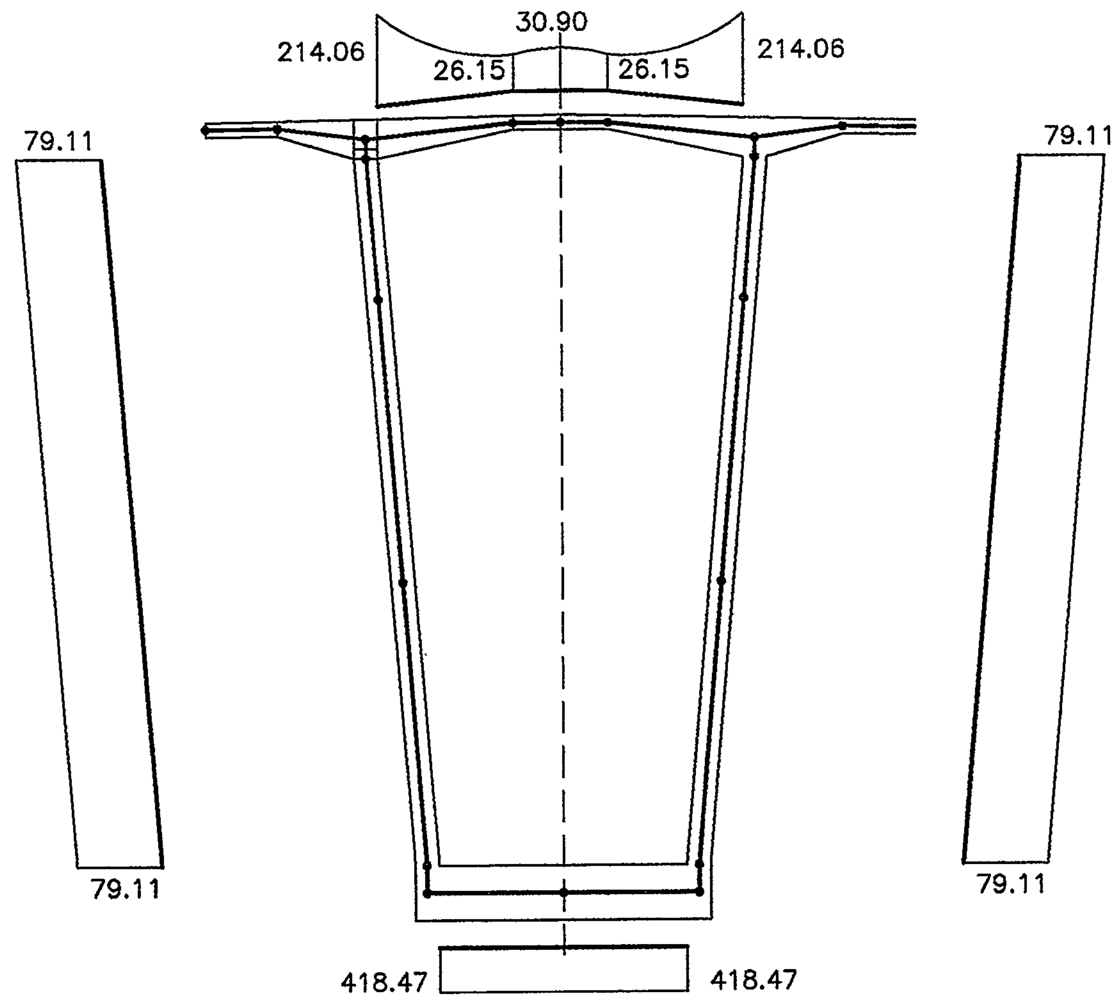

Figure 4.28d Transverse Bending Moments – Section S1 Cracking Moment kNm/m

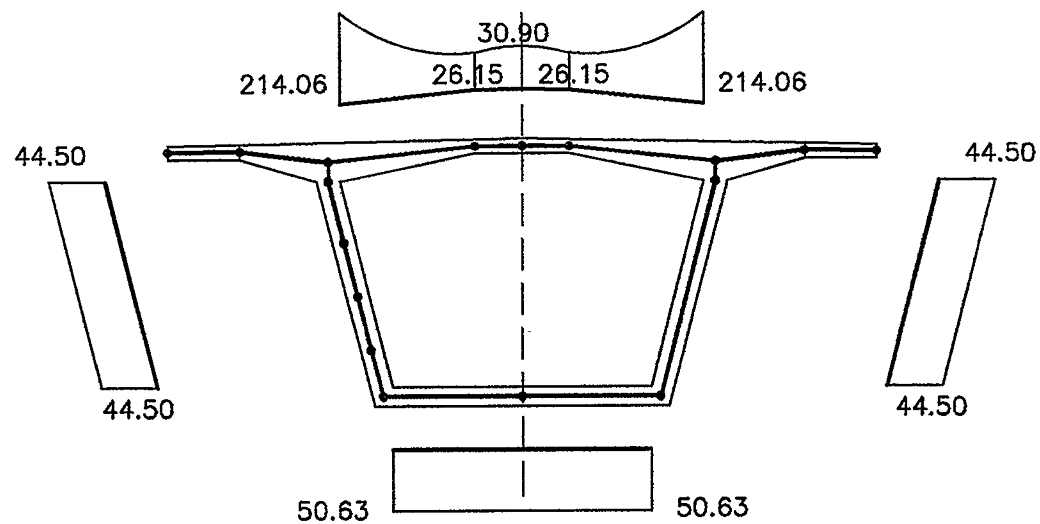

Figure 4.28e Transverse Bending Moments — Section S51 Cracking Moment kNm/m

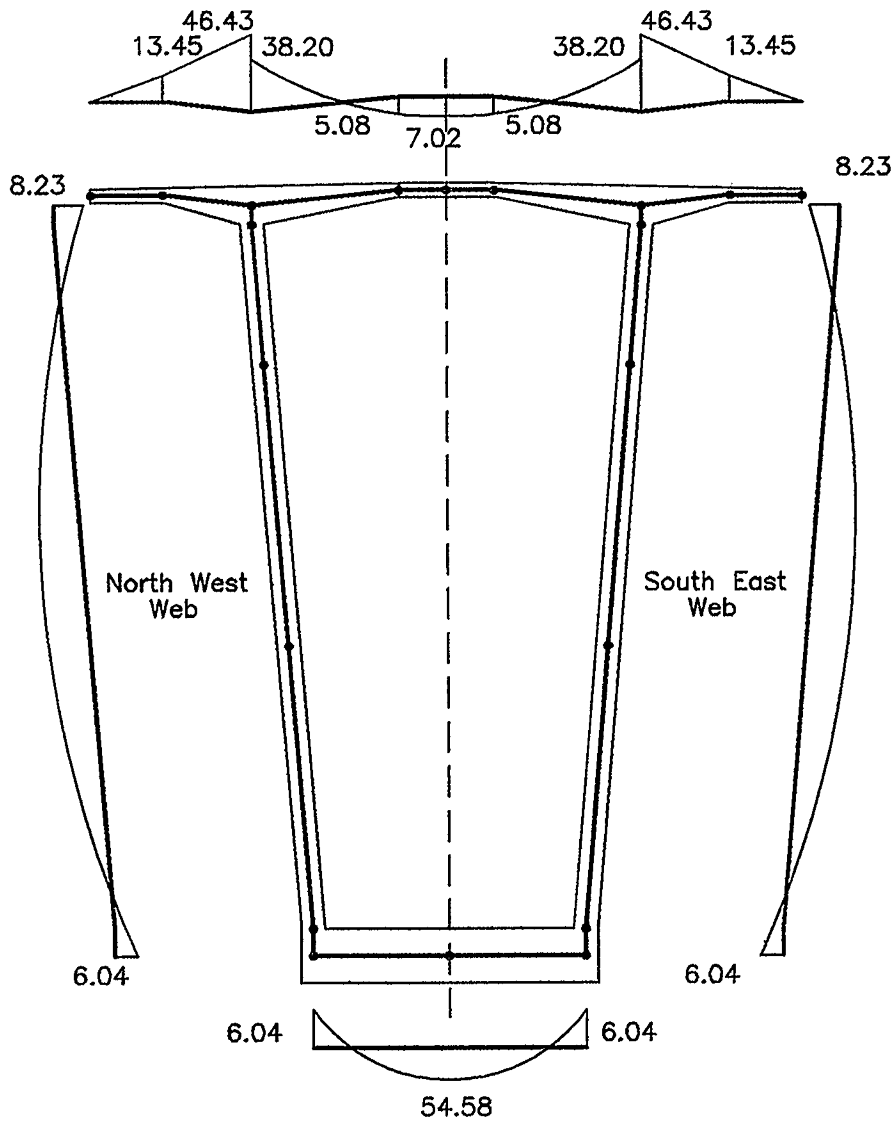

Figure 4.29 Self Weight Transverse Bending Moment Diagram (kNm/m) for section S1

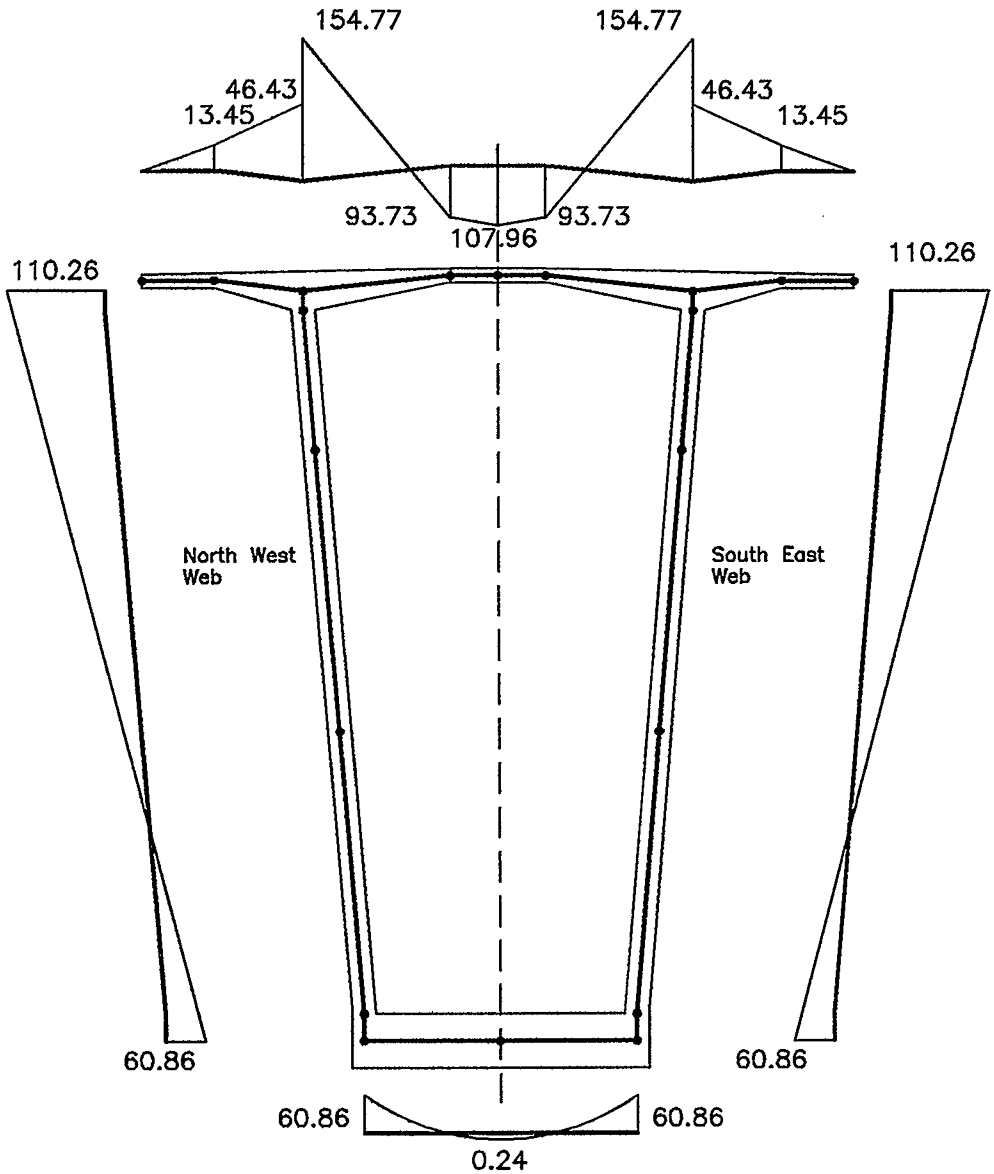

Figure 4.30 Self Wt. and Wheel Load Transverse Bending Moment Diagram (kNm/m), for section S1

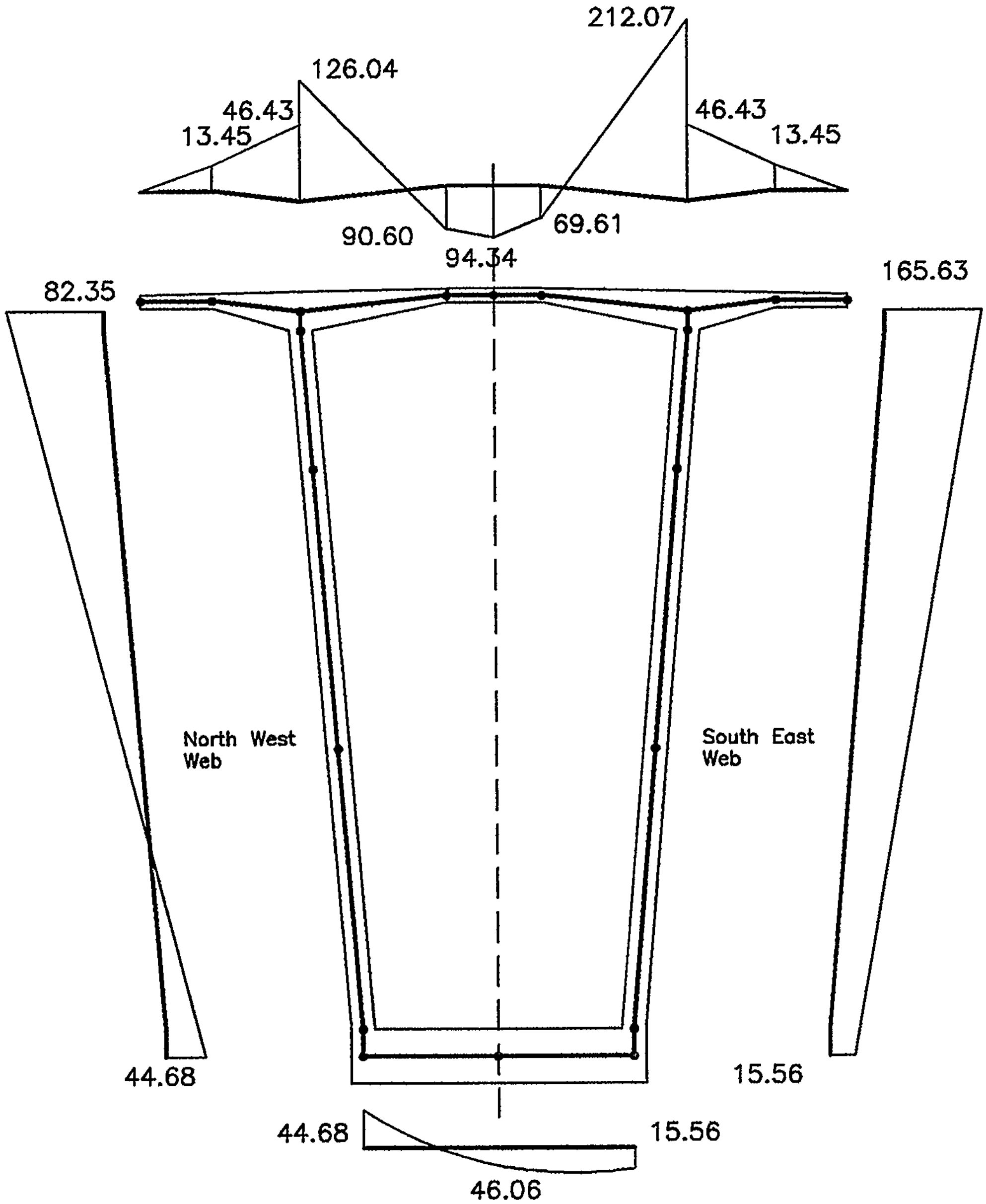

Figure 4.31 Bending Moment Diagram due to Self Wt., Wheel Load and a 20°C Temperature Gradient in the SE Web of section S1 (kNm/m)

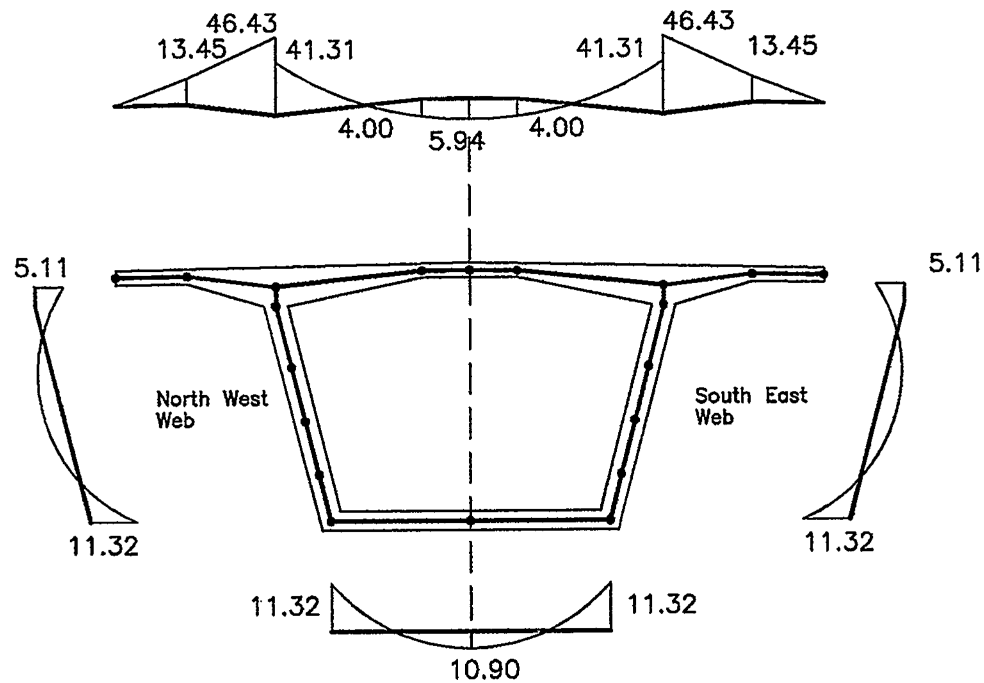

Figure 4.32 Self Weight Transverse Bending Moment Diagram (kNm/m), for section S51

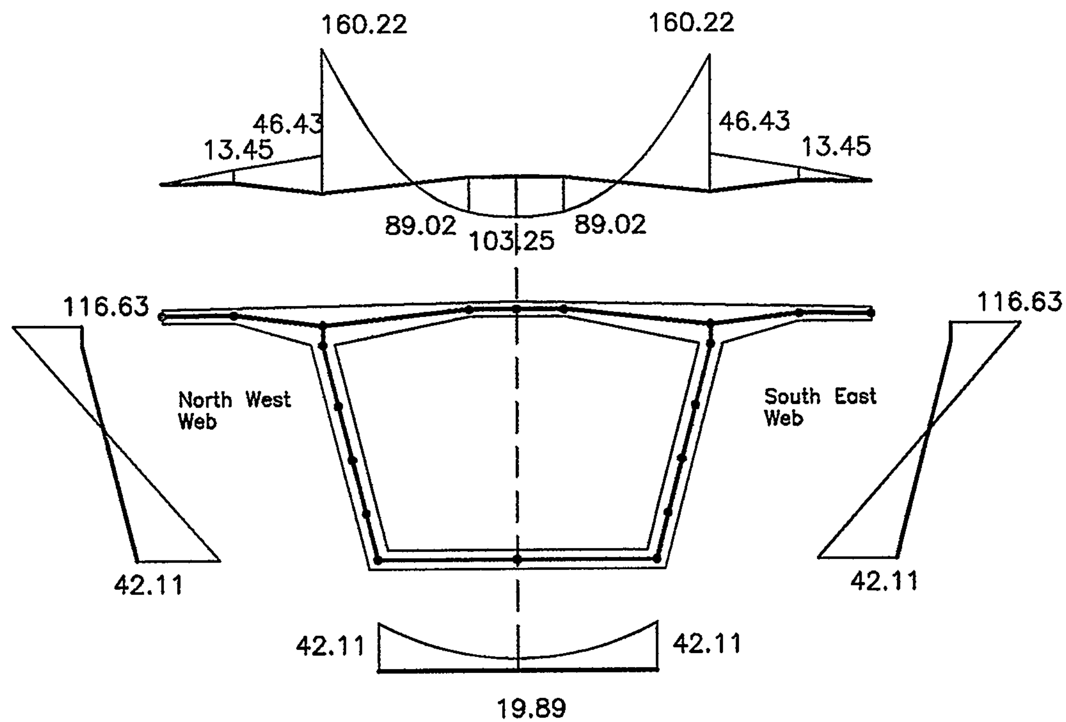

Figure 4.33 Self Weight and Wheel Load Transverse Bending Moment Diagram (kNm/m) for section S51

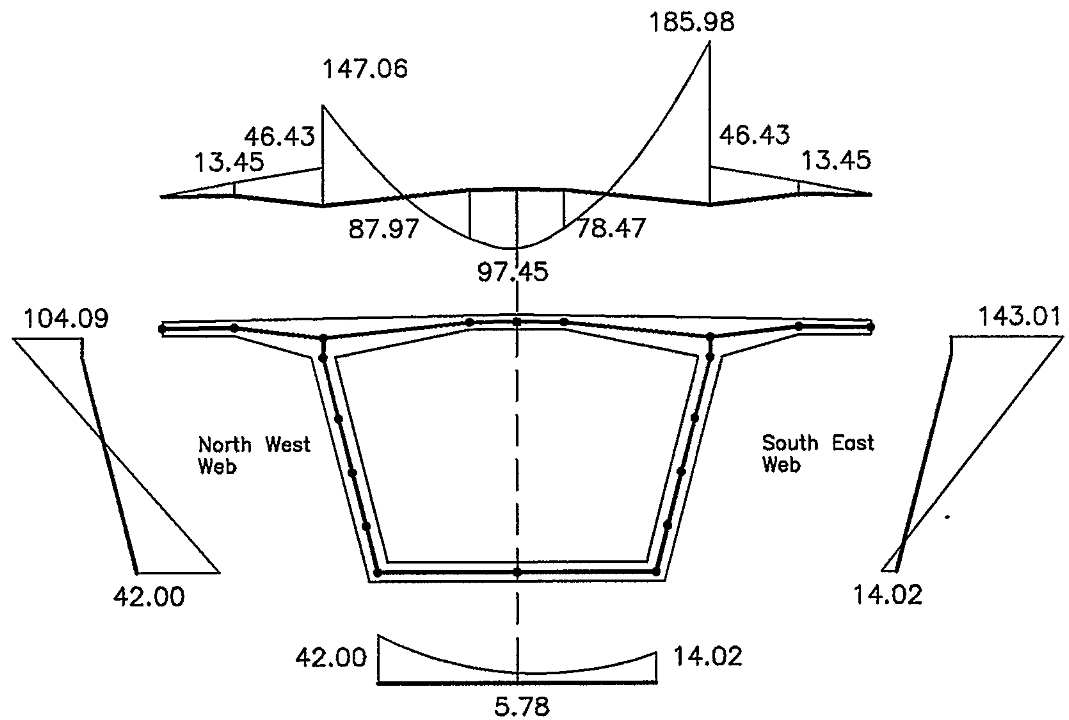

Figure 4.34 Bending Moment Diagram due to Self Wt., Wheel Load and a 20°C Temperature Gradient in the SE Web for section S51

CHAPTER FIVE
DISCUSSION

The major thrust of this thesis has been to establish the existence of the transverse temperature differentials that may occur in a concrete box girder bridge and then determine the structural response of the bridge due to these temperature differentials. A review of the literature established the history of the need to incorporate the effects of temperature into a successful design of a bridge structure. In the literature, several analytical models have been put forward for the prediction of temperature gradients throughout a bridge cross section. Priestley (1978) proposed a thermal distribution to be used for the structural behaviour along the longitudinal axis of the bridge. Churchward and Sokol (1981) monitored three bridges in Australia and after a statistical analysis concluded that the proposal by Priestley (1978) gave the best estimate for curvature - for these three bridges. In addition, they developed a model to predict the temperatures throughout the cross section of the bridge and although the temperatures predictions were accurate the curvatures were underestimated. They concluded that it may be difficult to accurately predict the temperature distribution and the curvature at the same time.

Dilger and Ghali (1980), as well as many other researchers, proposed a numerical method using finite elements to predict the temperature distribution and curvatures in bridge cross sections. The results from Dilger and Ghali (1980) were compared to data recorded on the Muskwa Bridge in Northern British Columbia, Canada. Excellent agreement was found between predicted and measured data for the concrete slab and steel box girder bridge. Note that the literature reveals that excellent or very good agreement between theoretical and measured values is often obtained for composite sections since the steel girder(s) will have a fairly uniform temperature. The literature also reveals that it is often difficult to achieve complete uniformity between predicted and recorded temperatures for concrete sections since there are at least four concrete slabs (two horizontal and two vertical) present instead of one. In a steel box girder the temperature of the steel throughout the webs and bottom flange is essentially constant. In a concrete box girder this is not the case. A temperature difference occurs through the thickness of each web and slab, as well as through the depth of the section.

The present investigation showed that excellent agreement between predicted and recorded temperatures can be achieved provided that appropriate convection coefficients are incorporated, based on the recorded wind speed. On-site observations of the actual wind flow around the bridge structure are helpful in determining the appropriate convection heat loss coefficients.

The current Canadian Bridge Code (S6-00), as well as the previous edition (S6-88) and previous editions of the Ontario Highway Bridge Design Code (1992), neglect the effect of any transverse temperature differences. However, many design manuals emphasize the effect of the transverse temperature gradient that can occur in a box girder cross section, Degenkolb (1977) and PCI-PTI (1978). These design manuals also point out that the frame behaviour of the cross sections needs to be taken into account. Leonhardt (1965, 1970, 1979) has reported many case studies where the frame behaviour of the cross section resulted in structural damage. The current Canadian Code (S6-00), like it's predecessors, of course stipulate that transverse bending moments due to live loads must be taken into account for box girder sections. No guidance is given as to whether the box section must be analyzed with the top slab having a greater temperature rise than the bottom slab, if this should be taken into account with a gradient as well, or, if the webs of the box should be analyzed with one web having a different curvature than the other and a slightly higher temperature than the other.

MacGregor et al (1997) summarized the temperature design criteria for the Confederation Bridge. However, there is no mention of a transverse temperature gradient. Also, a review of the structural drawings for the Confederation Bridge reveals that the effect of a transverse differences was not incorporated in the design.

In the present investigation a numerical method was developed to first predict the curvatures, both transverse and through the depth of the section, and then to determine the structural response due to those curvatures, along the longitudinal axis of the bridge. The method consisted of combining two existing computer programs: FETAB and SFRAME for Windows. The curvatures computed by FETAB for various cross sections along the bridge were manipulated and input into SFRAME. Material properties were determined for the concrete used in the construction of the Confederation Bridge based on the 28 day compressive strength specified on the contract drawings. These assumptions were based on material properties reported in recent research on high strength/performance concrete.

The numerical method was tested by comparing predicted deflections to those reported by Elbadry et al (2001). The predicted deflections resulting from two test trucks at mid span of the bridge and then temperature data were found to be in very close agreement with those reported in this work. However, although the predicted deflections were found to be in very close agreement - an indication that the bending moments were correct - with measured values, it was very difficult to compute a set of strains from bending moments due to temperature that matched the recorded strain gauge measurements. The main reason is that the exact conditions of loading at any given hour are unknown. The temperature distribution throughout two cross sections is available via the thermocouple readings taken on an hourly basis. However, as the analysis revealed, the bending moments due to temperature are of the same magnitude as, or slightly smaller than, those resulting from a single truck traveling across the bridge or regular car traffic throughout one lane of the bridge. By performing load combinations for varying numbers of trucks and cars in a single span, bending moments in excess of those resulting from temperature may be obtained. Then, as shown through load combination 23, wind pressure due to a fairly low level of wind speed results in similar transverse bending moments as those resulting from the transverse temperature gradient. Therefore, it can not be stated with certainty what load condition the strain gauges are actually measuring. Simply knowing the wind speed is indeed helpful, but it would be more helpful to know if the pressure coefficients, as set out in the National Building Coded of Canada, include a sizeable safety margin or are fairly accurate, even at low wind speeds.

However, having revealed the very small magnitude of continuity bending moments due to temperature and/or vehicle loading, this is not necessary. The bending moments due to truck traffic and temperature are in the order of one percent of the self weight bending moments. It was also shown that the bending moments due to continuity varied very little throughout the year. Hence they are far from critical for this structure.

The transverse bending moments for frame behaviour of the cross section due to temperature loading were found to be very significant. In particular, section S1 experienced an increase of 50% in bending moments when those from temperature were added to those from self weight and wheel loading. Typically engineers design to within 5% of their design forces, thus a 50% increase in the design force is critical. The total combined bending moment, at service load, from this analysis was 165.63 kNm/m, at the top of the exterior face of the east wall of section S1, while the thickness of the wall is only 400 mm. Based on CSA-S6 clause 8.1.4.8 the cracking moment is only 79.1 kNm/m. Hence the cross section will become cracked.

The same situation was found for cross section S51. The section S51 experienced an increase of 23% in bending moments when those from temperature were added to those from self weight and wheel loading. The total combined bending moment, at service load, from this analysis was 143.01 kNm/m, at the top of the exterior face of the east wall of section S51, while the thickness of the wall is only 300 mm. Based on CSA-S6 clause 8.1.4.8 the cracking moment is only 44.5 kNm/m. Hence the cross section will also become severely cracked.

CHAPTER SIX

CONCLUSIONS AND RECOMENDATIONS

6.1 Conclusions

Based on the information presented in this investigation, the following conclusions and recommendations may be reached and put forward:

1) The temperature distributions predicted with FETAB were very accurate. The program FETAB does not take into account the effect of shade on the top slab due to the 1.1m high concrete barriers. The effect of this is not known. The amount of solar radiation that is absorbed by the top slab can vary due to such factors as shade, humidity or the amount of surface water on the deck. It was also determined that the barriers also act to shelter the top surface of the bridge from the wind. As a result, the heat loss due to convection is much lower than that due to the recorded wind speed. In addition, the convection coefficients along the windward face of the girder appear to be lower due to the nature of the wind current around the cross section. An interesting research study would be to measure the wind speed around the cross section to record the differences and confirm the convection coefficients supposed in this investigation.

2) It is important to have an accurate prediction of temperature as well as curvature. If the proper curvature is achieved and the axial strain under estimated, the resulting longitudinal expansion will be under estimated. In continuous structures this will result in smaller bending moments at the supports and larger bending moments in the span.

3) The predicted curvatures about both the horizontal and vertical axis were in good agreement with those calculated from the recorded temperatures. Note that for the particular days and sections analyzed, the predicted maximum curvatures were in good agreement with the recorded values.

With the inclusion of the convection coefficient due to the hourly wind speed the accuracy of the predictions were noticeably increased.

4) The computer analysis developed to model frame behaviour of the Confederation Bridge was found to be very accurate. Predicted deflections (Load Combination 24) were found to be in very close agreement with recorded values for the two test truck driving across the bridge prior to being opened to the public Elbadry et al (2001).

5) The bending moments due to frame behaviour resulting from temperature gradients were found to be of the same order of magnitude as those resulting from traffic loads. This made it very difficult to compute strains that matched the recorded values. However, the deflections due to temperature were in fact within the same order of magnitude as those reported by Elbadry et al (2001). As a result they may be deemed to be correct.

6) It may be very difficult to incorporate the self equilibrating "eigen" stresses in a design situation. The total stress at a specific location is dependent on the stress due to loading (continuity) and the self equilibrating stress (temperature distribution). The exact temperature distribution can be very difficult to reproduce and it follows that the same can be said for the eigen stresses, which follow the temperature distribution. Silveira et al (2000) note that it is impossible to produce the maximum eigen stresses with one temperature distribution. Therefore a statistical analysis is required for every cross section so that maximum and minimum eigen stresses can be determined. This is not a simple matter, especially considering the difficulties involved in computing temperatures which correspond to recorded values.

7) The presence of the transverse gradient was confirmed, through the recorded data and the FETAB analysis, and found to be more significant for the deeper section, here labelled S1, than for the shallower section, S51. However, due to the size and stiffness of the bridge the transverse deflections were found to be minimal.

8) The cross section frame analysis performed with SFRAME revealed that the transverse temperature gradient is a significant case of loading for this structure. It was not the transverse temperature gradient of the gross cross section about the vertical axis, as originally thought, but the transverse temperature gradient though the individual walls. The analysis of this case of loading was significant in that the bending stresses in the walls reached approximately half of the theoretical concrete tensile strength. When combined with other load cases these stresses increase dramatically; 45% for section S1 and 19% for section S51. As mentioned earlier, the literature contains several references to the detrimental effects of the transverse temperature gradient. However, this is due to the different rise of temperature between the top slab and bottom slab. There is no mention of a temperature gradient through the thickness of the girder walls. Therefore, it is recommended that the current design code specify a transverse temperature difference to be incorporated into the analysis, in both the longitudinal and transverse direction. In addition, the code commentary should include some guidance for analyzing a cross section frame behaviour due to transverse temperature effects.

The matter of proposing a transverse gradient for frame behaviour of a cross section also requires more work. A concrete box girder section is formed by a minimum of four thin *"plates"*, two horizontal and two vertical. Some box sections will have two or three cells.

The 2000 edition of CSA-S6 contains a graph relating curvature (temperature differential) to the depth of the section, clause 3.9.4.4.1. Thinner sections are attributed higher temperature differences: ie curvatures. It is reasonable to take this approach, with the top slab having a slightly higher temperature than bottom slab. However, the two walls should also have slightly different temperatures. Additional work should be carried out to determine what this temperature difference should be.

As an example, refer again to Figure 2.5.2.which contains temperature differentials for various depths of structure (CSA-S6-00). If the concrete box girder cross section is considered to be an assemblage of four thin plates, each plate will be subjected to a temperature differential of 15 °C. This will produce a gradient in all four slabs. Now consider sections S1 and S51. This type of loading condition is shown in Figure 6.1 and was used to produce the bending moment diagrams found in Figures 4.21 And 4.23. In these two diagrams, dT for the east wall was assumed to be 15 °C, while dT for the west wall and the two slabs was assumed to be 0 °C. When comparing these bending moment diagrams to those resulting from recorded temperatures it was found that dT should be in the order 20 °C to produce a maximum bending moment diagram. More work should be done in this area to make recommendations concerning what gradients should be used in the design of a concrete box girder for transverse frame behaviour, depending on whether there is one, two or three air cells present., hence the temperature distributions will be different from this investigation. Hence a more detailed statistical analysis may be required to confirm the exact value for the transverse temperature difference in the girder webs, and whether this temperature difference should act with or without a temperature difference through the thickness of the top slab. It is reasonable to assume that a statistical analysis would reveal that two conditions of loading should be considered. One for summer conditions and another for winter conditions.

6.2 Recommendations

Based on the conclusions put forward in the above sections the following

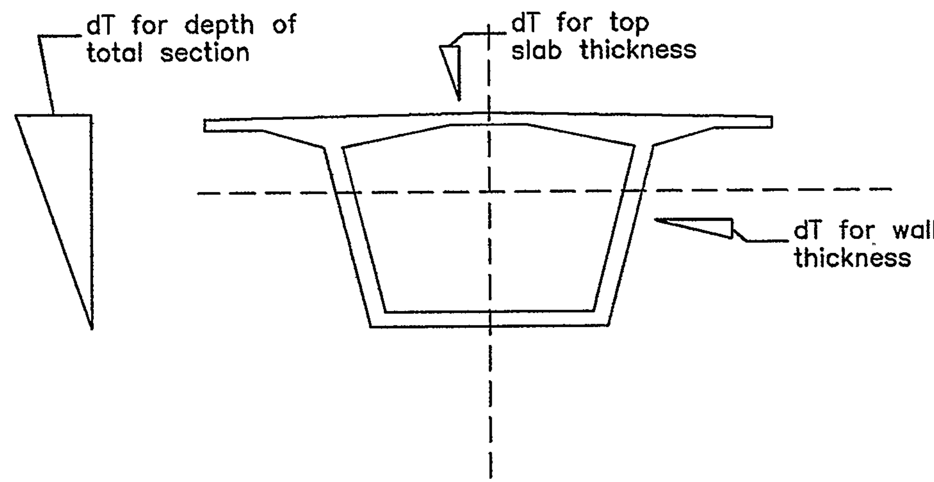

Figure 6.1 Proposed Temperature Loading for Transverse Effects

revision to CSA-S6-00 are proposed.

Code Clause 3.9.3 should read:

(Note the proposed changes are underlined)

"3.9.3 Structure Types

Temperature effects shall be considered for the following types of superstructures:

(a) Type A - steel beam, box or truss systems with steel decks, and truss systems that are above the deck;

(b) Type B - steel beam, box or deck truss systems with concrete decks;

(c) Type C - concrete slab and beam systems with concrete decks;

(d) Type D - concrete box systems with concrete decks."

Code Table 3.9.4.1 should be altered to read:

"Table 3.9.4.1 Maximum and Minimum Effective Temperatures

Superstructure Type	*Maximum Effective Temperature*	*Minimum Effective Temperature*
A	*25 °C above maximum daily mean*	*15 °C below maximum daily mean*
B	*20 °C above maximum daily mean*	*5 °C below maximum daily mean*
C	*10 °C above maximum daily mean*	*5 °C below maximum daily mean*
D	*20 °C above maximum daily mean*	*20 °C below maximum daily mean*

Code clause 3.9.4.4 should be altered to read:

"3.9.4.4 Thermal Gradient Effects

The effect of thermal gradients through the depth shall be considered in the design of Type A, B, C and D structures.

A thermal gradient is positive when the top surface of the superstructure *is warmer than the bottom surface.*

Values of temperature differentials are given for Type A and Type C structures in Figure 3.9.4.4. For winter conditions, positive and negative differentials shall be considered. For summer conditions, only positive differentials shall be considered.

For composite and no-composite Type B structures, a positive temperature differential decreasing linearly by 30 °C from the top to the bottom of the deck slab shall be considered. The temperature shall be assumed to remain constant throughout the beam or truss below the slab. <u>*Negative differentials need to be considered.*</u>

<u>*Values of temperature differentials are given for concrete box girder Type D structures in Figure 3.9.4.4. Positive and negative differentials shall be considered. A temperature differential through the depth of the cross sections shall be computed from Figure 3.9.4.4. The walls of the box sections and the top slab shall be considered with a 20 °C differential, positive and negative, each acting separately or in conjunction in order to produce the most severe result"*</u>

Alberta Transportation and Utilities, (1993), "Bridge Maintenance Standards for Local Road Authorities.", 1993.

Alberta Transportation and Utilities, (1994), "Bridge Inspection and Maintenance System Inspection Manual", 1994

American Concrete Institute, (1984), State of the Art Report on High-Strength Concrete, ACI 363R-84, American Concrete Institute, Detroit, 1984.

American Concrete Institute, (1988), "Analysis and Design of Reinforced Concrete Bridge Structures.", ACI343R-88, Detroit, Michigan, 1988.

American Concrete Institute, (1989), ACI Committee 318, Building Code Requirements for Reinforced Concrete and Commentary, ACI 318R-89, American Concrete Institute, Detroit, 1989.

American Concrete Institute, (1991), "Guide for Concrete Highway Bridge Deck Construction", Detroit, Michigan, 1991.

American Concrete Institute, (1992), "Routine Maintenance of Concrete Bridges", Detroit, Michigan, 1992.

American Concrete Institute, (1994), "Concrete Bridges in Aggressive Environments", Philip D. Cady International Symposium, 1994.

Bakht, B., "Simplified Analysis of Edge-Stiffened Cantilevered Slabs", ASCE Structural Journal, Vol. 107, March 1981.

Branco, F., and Mendes, P.,(1993), “Thermal Actions for Concrete Bridge Design”, Journal of Structural Engineering, ASCE, Vol. 119, No. 8, August 1993, pp. 2313 - 2331.

British Code of Practise for the Structural Use of Concrete CP 110: 1972.

Burg, R. G., and Ost, B. W. (1994), "Engineering Properties of Commercially Available High-Strength Concrete (Including Three-Year Data)." Portland Cement Association, Research and Development Bulletin RD 104T.

CAN/CSA-S6-00-Canadian Highway Bridge Design Code., Canadian Standards Association International, Toronto, Ontario, 2000.

CSA/CAN3-A23.3-M94, Design of Concrete Structures for Buildings, Canadian Standards Association, Toronto, 1994.

CEB-FIP, Model Code for Concrete Structures, pp.348 (Comite Euro-International du Beton, 1990).

Carslaw, H.S., and Jaeger, J.C., “Conduction of Heat in Solids”, 2nd. Ed., Clarendon Press, Oxford, England, 1959.

Channon, J. R., and Ramsay, R- J. (1986), "Bridge Structures Design Criteria." Alberta Transportation and Utilities, Revised 6 April, 1992.

Cheung, M.S., Tadros, G.S., Brown, T., Dilger, W.H., Ghali, A., and Lau, D.T., (1997), “ Field Monitoring and Research on Performance of the Confederation Bridge”, Canadian Journal of Civil Engineering, Vol. 24, No. 6, December 1997, p.p. 951-962.

Churchward, A., and Sokal Y. J., (1981), "Prediction of Temperatures in Concrete Bridges." Journal of the Structural Division, Proceedings of the American Society of

Civil Engineers, Vol. 107, No. STI 1, August 1981, pp. 2163 - 2176.

"CSA-S6-88-Design of Highway Bridges", (1988), Canadian Standards Association, Toronto, Ontario, 1988.

"CSA-S6-88-Design of Highway Bridges-Commentary", (1990), Canadian Standards Association, Toronto, Ontario, 1990.

Degenkolb, O. H. (1977). "Concrete Box Girder Bridges." American Concrete Institute.

Dilger, W. H., Beauchamp, J. C., Cheung, M. S., and Ghali, A., (1981), "Field Measurements of Muskwa River Bridge," Journal of the Structural Division, ASCE, Vol. 107, No. ST 11, Nov. 1981, pp. 2147-2161.

Dilger, W. H. and Ghali, A., (1980), "Temperature Induced Stresses in Composite Box Girder Bridges.", Research report by Dilger-Ghali Civil Engineering Consulting Ltd., submitted to the Department of Supplies and Services, Canada, October 1980, 179pp.

Dilger, W. H., Ghali, A., Chan, M., Cheung, M. S., and Maes, M.A., (1983), "Temperature Stresses in Composite Box Girder Bridges.", Journal of Structural Engineering, ASCE, Vol. 109, No. 6, June, 1983, pp. 1460 - 1478.

Dunker, K. F., and Rabbat, B. G. (1990), "Highway Bridge Type and Performance Patterns." Journal of performance of Constructed Facilities, Vol. 4, No. 3, pp. 161 - 173.

Dunker, K, F., and Rabbat, B. G. (1990), "Performance of Highway Bridges." Concrete International, Vol. 12, No. 8, pp. 40 - 43.

Dunker, K F., and Rabbat, B. G. (1992), "Performance of Prestressed Concrete Highway Bridges in the United States - The First 40 years." Precast Prestressed Concrete Institute, Vol. 37, No. 3, pp. 48 - 64.

Dunker, K, F., and Rabbat, B. G. (1993), "Why America's Bridges are Crumbling." Scientific American, March 1993, pp. 66 - 72.

Elbadry, M. M., (1982), "Thermal Response of Concrete Box-Girder Bridges", Thesis presented to the University of Calgary, at Calgary, Alberta, Canada, 1982, in partial fulfilment of the requirements for the degree of Master of Science in Engineering.

Elbadry, M. M., and Ghali, A., (1982), "User's Manual and Computer Program FETAB: Finite Element Thermal Analysis of Bridges", Department of Civil Engineering Research Report No. CE82-10, University of Calgary, October 1982, Revised July 1984.

Elbadry, M. M., and Ghali, A., (1983), "Nonlinear Temperature Distribution and its Effects on Bridges." ETH-Honggerberg, Zurich, Switzerland. IABSE Peridica 3/1983 (August), pp. 169 - 191.

Elbadry, M. M., and Ghali, A., (1983), "Temperature Variations in Concrete Bridges," Journal of Structural Engineering, ASCE, Vol. 109, No. 10, October 1983, pp. 2355 - 2374.

Elbadry, M.M., Ghali, A., and Megally, S., (2001), "Deflection prediction for Concrete Bridges: Analysis and Field Measurements on a Long-Span Bridge", Structural Concrete, Journal of the CEB-FIP, Vol. 2., No. 1, March 2001, pp. 1-14.

Famy. J.A., and Panarese, W.C., "High Strength Concrete", Portland Cement Association, Skokie, Illinois, 1994.

Froli, M., Hariga, N., Orlandini, M., and Nati, G., (1996), "Research on the Longitudinal Thermal Behaviour of a Prestressed Concrete Box Girder Bridge in Italy", Structural

Engineering International, International Association of Bridge and Structural Engineers, Vol. 6, No. 4, 1996, pp. 237-242.

Ghali, A., Favre, R., and Elbadry, M. M., "Concrete Structures: Stresses and Deformations." E&F Spon, London, England, 2002.

Gilliland, J.A., "Thermal and Shrinkage Effects in High Performance Concrete Structures During Construction", Ph.D. Thesis, University of Calgary, 2000, 259pp.

Hambly, E.C., (1978), "Temperature Distributions and Stresses in Concrete Bridges", The Structural Engineer, Vol. 56A, No. 5, May 1978, pp. 143 - 148.

Hirst, M. J. S., and Dilger, W. H., (1989), "Prediction of Bridge Temperatures." ETH-Honggerberg, Zurich, Switzerland, IABSE Peridica 3/1989 (August), pp. 109 - 120.

Kay, J. M., and Nedderman, R. M., (1957), "An Introduction to Fluid Mechanics and Heat Transfer", 3rd Edition, Cambridge University Press, Cambridge, UK.

Leonhardt, F., Kolbe, G., and Peter, J., (1965), "Termperturunterschiede geared Spannbetonbrucke", Beton-und Stahlbetonbau 60 (1965) Vol. 7, pp.157-163.

Leonhardt, F., and Lippoth, W., (1970), "Folgerungen aus Schaden an Spannbetonbrucken", Beton-und Stahlbetonbau 65 (1970) Vol. 10, pp.231-244.

Leonhardt, F., (1979), "Risschaden an Betonbrucken-Ursachen und Abhilef", Beton-und Stahlbetonbau 74 (1979) Vol. 2, pp.36-44.

Li, D., Maes, M.A., Dilger, W.H., (2003), "Thermal Design Criteria for Deep Prestressed Concrete Girders Based on Data from Confederation Bridge", Accepted for publication Canadian Journal of Civil Engineering, 2004.

Maes, M.A., Dilger, W.H., and Ballyk, P.D., (1992), "Extreme values of Thermal Loading Parameters in Concrete Bridges", Canadian Journal of Civil Engineering, Vol. 19, No. 6, December 1992, p.p. 935-946.

MacGregor, J.A., Kennedy, D.J., Bartlett, F.M., Chernenko, D., Maes, M.A., and Dunaszegi,.L., (1997), "Design Criteria and Load and Resistance Factors for the Confederation Bridge", Canadian Journal of Civil Engineering, Vol. 24, No. 6, December 1997, p.p. 882-897.

Massicotte, B., and El-Alam, P., (1996), "Critical Thermal Gradients in a Prestressed Concrete Box Girder Bridge", Canadian Society for Civil Engineering Annual Conference Proceedings, May 29 to June 1, 1996, pp. 407-418.

Molesini, P., and Massicotte, B., (1993), "Thermal Behaviour Modeling of a Deep Concrete Box Girder Bridge", Canadian Society for Civil Engineering Annual Conference Proceedings, June 8-11, 1993, pp. 67-76.

Moorty, S., and Roeder, C., (1992), "Temperature-Dependent Bridge Movements", Journal of Structural Engineering, ASCE, Vol. 118, No. 4, April 1992, pp. 1090 - 1105.

Neville, A. M., "Properties of Concrete", 3rd Edition, Longman Scientific and Technical, New York, 1981.

"Ontario Highway Bridge Design Code", 3rd Edition, Ontario Ministry of Transportation, Quality and Standards Division, Toronto, Ont., 1992.

"Ontario Highway Bridge Design Code-Commentary", 3rd Edition, Ontario Ministry of Transportation, Quality and Standards Division, Toronto, Ont., 1992.

Portland Cement Association, (1995), "Durability of Concrete Bridge Decks, A Cooperative Study", 1995.

Precast Prestressed Concrete Institute, (1978), "Precast Segmental Box Girder Bridge Manual", Chicago, Illinois, 1978.

Priestley, M. J. N., (1972), "Thermal gradients in bridges - some design consideration", New Zealand Engineering, 15 July 1972, pp. 228 - 233.

Priestley, M. J. N., (1978), "Design of Concrete Bridges for Temperature Gradients," American Concrete Institute Journal, Title No. 75-23, May 1978, pp. 209-217.

Saetta, A., Scotta, R., and Vitalianni, R., (1995), "Stress Analysis of Concrete Structures Subjected to Variable Thermal Loads", Journal of Structural Engineering, ASCE, Vol. 121, No. 3, March 1995, pp. 446 - 457.

Shaw, S. P., and Ahmad, S. H., "High Performance Concrete: Properties and Applications", McGraw-Hill, Inc., 1994.

Silveria, A.P., Branco, F.A., and Castanheta, M., (2000), "Statistical Analysis of Thermal Actions for Concrete Bridge Design", Structural Engineering International, January 2000, pp. 33 - 38.

Sivakumaran, K. S., and Dilger, W. H., (1984), "Analysis of Concrete Structures Subjected to Sustained Temperature Gradients", Canadian Journal of Civil Engineering, Vol.11, No.3, 1984, pp.404-410.

Skeet, J., and Kriviak, G., (1994), "Service Life Prediction of Protective Systems for Concrete Bridge Decks in Alberta." Alberta Transportation and Utilities, report no. ABTR/RD/RR-94/01, 1994.

"Steel Bridges, Design - Fabrication – Construction, 1994". 2-day course, February 17 and 18, 1994, Edmonton, Alberta.

"Steel Bridges, Design - Fabrication – Construction, 2001". 2-day course, September 25 and 26, 2001, Edmonton, Alberta.

Suprenant, B. A., and Murray, M. A., (1993), "How to place durable partial-depth patches." Concrete Repair Digest, November 1993, pp. 251 - 255.

Tadros, G.S., (1997), "The Confederation Bridge: An Overview", Canadian Journal of Civil Engineering, Vol. 24, No. 6, December 1997, p.p. 850-866.

The element conduction matrix becomes:

$$[S_c^e]=\left(\frac{Ak_x}{L}\right)\begin{bmatrix}1 & -1\\ -1 & 1\end{bmatrix}=\left(\frac{(4)(3)}{2}\right)\begin{bmatrix}1 & -1\\ -1 & 1\end{bmatrix} \quad \text{A1}$$

$$[S_c^e]=\begin{bmatrix}6 & -6\\ -6 & 6\end{bmatrix}\frac{W}{^oC} \quad \text{A2}$$

and the element convection matrix becomes:

$$[S_c^e]=\left(\frac{h\rho L}{6}\right)\begin{bmatrix}2 & 1\\ 1 & 2\end{bmatrix} \quad \text{A3}$$

$$[S_c^e]=\begin{bmatrix}0.667 & 0.333\\ 0.333 & 0.667\end{bmatrix}\frac{W}{^oC} \quad \text{A4}$$

The end element (4) must have an added convection term for the exposed end

$$[S_c^e]=\begin{bmatrix}0 & 0\\ 0 & hA\end{bmatrix}=\begin{bmatrix}01 & 0\\ 0 & (0.1)(4)\end{bmatrix}=\begin{bmatrix}0 & 0\\ 0 & 0.4\end{bmatrix}\frac{W}{^oC} \quad \text{A5}$$

Now, each elements conduction and convection matrices are summed resulting in:

$$[S_c^e]_1=\begin{bmatrix}6.667 & -5.333\\ -5.333 & 6.667\end{bmatrix}\frac{W}{^oC}=[S^e]_2=[S^e]_3 \quad \text{A6}$$

$$[S_c^e]_4=\begin{bmatrix}6.667 & -5.333\\ -5.333 & 7.0667\end{bmatrix}\frac{W}{^oC} \quad \text{A7}$$

When these four matrices are summed the result is:

$$[S_c^e]=\begin{bmatrix}6.667 & -5.333 & 0 & 0 & 0\\ -5.333 & 13.333 & -5.333 & 0 & 0\\ 0 & -5.333 & 13.333 & -5.333 & 0\\ 0 & 0 & -5.333 & 13.333 & -5.333\\ 0 & 0 & 0 & -5.333 & 7.066\end{bmatrix}\frac{W}{^oC} \quad \text{A8}$$

The force vector for each element, $\{F^e\}$, may be computed by:

$$\{F^e\} = -\int [N]^T Q\, dv + \int [N]^T q\, ds \ -\int [N]^T T_a\, h\, ds \qquad A9$$

$$= \frac{-QAL}{2}\begin{Bmatrix}1\\1\end{Bmatrix} + \frac{pLq}{2}\begin{Bmatrix}1\\1\end{Bmatrix} - \frac{hpLT_a}{2}\begin{Bmatrix}1\\1\end{Bmatrix} \qquad A10$$

where,

Q = the quantity of heat generated within the body per second per unit volume .

q = heat flux = the quantity of heat per second per unit area.

h = the convection coefficient = the quantity of heat per second per unit area per unit temperature difference between surface area and heat.

It is important to note that heat flux and convection (the second and third terms) cannot occur over the same boundary area at the same time.

From this it may be shown that,

$$\{F^e\}_1 = \{F^e\}_2 = \{F^e\}_3 = \begin{Bmatrix}20\\20\end{Bmatrix} W \qquad A11$$

$$\{F^e\}_4 = \begin{Bmatrix}20\\28\end{Bmatrix} W \qquad A12$$

and that the final $\{F^e\}$ matrix becomes,

$$\{F^e\} = \{20\ \ 40\ \ 40\ \ 40\ \ 28\ \}^T\ W \qquad A13$$

now,

$$[S_c^e]\ \{T\} = \{F^e\} \qquad A14$$

Since it is known that $T_1 = 80°C$, eq. 3.2 may be reduced to,

$$\begin{bmatrix} -5.333 & 13.333 & -5.333 & 0 & 0 \\ 0 & -5.333 & 13.333 & -5.333 & 0 \\ 0 & 0 & -5.333 & 13.333 & -5.333 \\ 0 & 0 & 0 & -5.333 & 7.066 \end{bmatrix} \frac{W}{°C} \begin{Bmatrix} T_2 \\ T_3 \\ T_4 \\ T_5 \end{Bmatrix} = \begin{Bmatrix} 493.333 \\ 40 \\ 40 \\ 28 \end{Bmatrix} W \qquad A15$$

which may be solved to obtain:

$$\{\ T\ \} = \{\ 80,\ \ 53.95,\ \ 39.87,\ \ 32.81,\ \ 30.27\ \}°C \qquad A16$$

This example may be re-worked with two elements and three nodes instead of four elements and five nodes, see Figure 3.2, which results in,

$$\{ T \} = \{ 80,\ 38.6,\ 29.18 \}^{\circ}C \qquad A17$$

Note that with half the number of nodes and elements a satisfactory level of accuracy is still obtained. In addition, this example may be re-worked using different shape functions. However, after using second and third order equations and even exponential functions, the linear shape function still gives the best results.

To model a bridge cross section, the computer program FETAB uses an assemblage of quadrilateral and/or triangular elements, see Figure 3.3. Hence, the conduction matrix must be determined in both x and y directions. Again, the convection matrix is determined for each boundary surface and added to the conduction matrix. In order to illustrate this procedure the previous example will again be presented. For ease of computation, two rectangular elements will be used to model the steel bar, see Figure 3.4.

The conduction matrix for each element is the same,

$$\left[S_c^{\,e}\right]_x = \frac{k_x t k c_l}{6b_l}\begin{bmatrix} 2 & -2 & -1 & 1 \\ -2 & 2 & 1 & -1 \\ -1 & 1 & 2 & -2 \\ 1 & -1 & -2 & 2 \end{bmatrix} = \begin{bmatrix} 1 & -1 & -0.5 & 0.5 \\ -1 & 1 & 0.5 & -0.5 \\ -0.5 & 0.5 & 1 & -1 \\ 0.5 & -0.5 & -1 & 1 \end{bmatrix} \qquad A18$$

$$\left[S_c^{\,e}\right]_y = \frac{k_y t k b_l}{6c_l}\begin{bmatrix} 2 & 1 & -1 & -2 \\ 1 & 2 & -2 & -1 \\ -1 & -2 & 2 & 1 \\ -2 & -1 & 1 & 2 \end{bmatrix} = \begin{bmatrix} 16 & 8 & -8 & -16 \\ -8 & 16 & -16 & -8 \\ -8 & -16 & 16 & 8 \\ -16 & -8 & 8 & 16 \end{bmatrix} \qquad A19$$

Therefore, the conduction matrix for each element becomes,

$$\left[S_c^{\,e}\right] = \begin{bmatrix} 17 & 7 & -8.5 & -15.5 \\ -7 & 17 & -15.5 & -7 \\ -8.5 & -15.5 & 17 & 7 \\ -15.5 & -8.5 & 7 & 17 \end{bmatrix} \qquad A20$$

Summing the two matrices results in the structures conduction matrix,

$$[S_c^e]=\begin{bmatrix} 17 & 7 & 0 & 0 & -8.5 & -15.5 \\ 7 & 34 & 7 & -8.5 & -31 & -8.5 \\ 0 & 7 & 17 & -15.5 & -8.5 & 0 \\ 0 & -8.5 & -15.5 & 17 & 7 & 0 \\ -8.5 & -31 & -8.5 & 7 & 34 & 7 \\ -15.5 & -8.5 & 0 & 0 & 7 & 17 \end{bmatrix} \qquad \text{A21}$$

This conduction matrix must now be modified for the boundary surfaces around each element by a convection matrix. The convection matrix which accounts for the boundary surfaces depends on the shape function selected and may be determined by equation 3.4. Integrating this equation over the surface of each element will result in six matrices, one for each surface. The first element, 1256, has four surfaces exposed to the air while the second, 2345, has five surfaces. The resulting convection for each element is as follows:

$$[S_c^e]_1=\begin{bmatrix} 0.6222 & 0.3111 & 0.0222 & 0.0444 \\ 0.3111 & 0.6222 & 0.0444 & 0.0222 \\ 0.0222 & 0.0444 & 0.6222 & 0.3111 \\ 0.0444 & 0.0222 & 0.3111 & 0.6222 \end{bmatrix} \qquad \text{A22}$$

$$[S_c^e]_2=\begin{bmatrix} 0.6222 & 0.3111 & 0.0222 & 0.0444 \\ 0.3111 & 0.7555 & 0.1111 & 0.0222 \\ 0.0222 & 0.1111 & 0.7555 & 0.3111 \\ 0.0444 & 0.0222 & 0.3111 & 0.6222 \end{bmatrix} \qquad \text{A23}$$

Once these two matrices are added, the conduction matrix becomes:

$$[S_c^e]=\begin{bmatrix} 17.6222 & 7.3111 & 0 & 0 & -8.4777 & -15.4555 \\ 7.3111 & 35.2444 & 7.3111 & -8.7777 & -30.9111 & -8.4777 \\ 0 & 7.3111 & 17.7555 & -15.3888 & -8.4777 & 0 \\ 0 & -8.4777 & -15.3888 & 17.7555 & 7.3111 & 0 \\ -8.4777 & -30.9111 & -8.4777 & 7.3111 & 35.2444 & 7.3111 \\ -15.4555 & -8.4777 & 0 & 0 & 7.3111 & 17.6222 \end{bmatrix} \qquad \text{A24}$$

The loading vector is determined in a similar manner. Going back to equation 3.6:

$$\{F^e\} = -\int [N]^T Q \, dv + \int [N]^T q \, ds \; - \int [N]^T T_a \, h \, ds \qquad \text{A9}$$

Here, the first two terms are zero. After integrating the third term six vectors are obtained, one for each surface. As with the convection matrices there are four surfaces for element one and five for element two. The resulting load vector becomes:

$$\{F^e\} = \{ 20, 40, 24, 24, 40, 20\}^{T}\,{}^{o}C \qquad \text{A25}$$

now equation 3.7 may be solved,

$$[S_c^e]\,\{T\} = \{F^e\} \qquad \text{A14}$$

knowing that $T_1 = T_2 = 80^oC$ the equation 3.7 may be reduced and solved:

$$\{T\} = \{ 80, 38.62, 29.18, 29.18, 38.62, 80 \}^{T}\,{}^{o}C \qquad \text{A26}$$

which is the same as the result for two bar elements.